A common European approach to the regulatory testing of nanomaterials

# NANoREG

Grant Agreement Number 310584

## Deliverable D 5.2

### Report on the development of a solubility testing procedure

**Due date of deliverable: M30, August 2015**

**Actual submission date:** *2015/10/30*

| | |
|---|---|
| Author(s) and company: | NIA; David Carlander<br>KI; Hanna Karlsson<br>UNamur; Julie Laloy<br>IIT: Stefania Sabella<br>DLO-RIKILT: Meike van der Zande<br>Udl-LEG: Carlos Rey-Castro<br>NPL: Ratna Tantra |
| Work package/task: | WP5/Task 5.2 |
| Document status: | Draft / **Final** |
| Confidentiality: | Confidential / Restricted / **Public** |
| Key words: | Solubility |

DOCUMENT HISTORY

| *Version* | *Date* | *Reason of change* |
|---|---|---|
| 1 | 2015/05/14 | First version. Not all chapters included. Editing of chapter title numbering needed. |
| 2 | 2015/10/07 | Second version. More chapters included, still some missing. Editing of chapter title numbering needed. |
| 3 | 2015/10/23 | Third version. All chapters included. Editing of references needed. |
| 4 | 2015/10/30 | Final document |
| 5 | 2017/03/08 | Project Office harmonized lay-out |



*This project has received funding from the European Union Seventh Framework Programme (FP7/2007-2013) under grant agreement no 310584*

**Lead beneficiary for this deliverable: NIA, partner 12 (main contact: David Carlander)**

| Owner(s) of this document | |
|---|---|
| Owner of the content | NIA, partner 12 |
| Co-Owner 6 | KI, partner 15 |
| Co-Owner 5 | UNamur, partner 22 |
| Co-Owner 3 | IIT, partner 28 |
| Co-Owner 1 | DLO-RIKILT, partner 30 |
| Co-Owner 2 | Udl-LEG, partner 43 |
| Co-Owner 7 | NPL, partner 46 |

# Table of Content

# 1 Description of task

The description of task 5.2 is taken from the description of work (DoW) and is included below for convenience.

**From DoW: Develop solubility testing procedures**

This task will evaluate the applicability of solubility testing, as used in drug development, and review similar results achieved in other projects, with a view to developing a solubility testing procedure to be applied in rapid MNM screening as part of the risk assessment decision tree (Task 5.7) and the regulatory framework/toolbox (Task 1.4). This Task will also make a link to WP4, by characterising external and internal exposure and evaluating the relationship between external exposure and internal dose.

The main limiting factor for solubility testing are the analytical methods to detect nanoparticles (or differentiate between NP and non nano (i.e. ionic forms). This task will therefore use FFF- ICPMS and or HDC- ICP-MS and Single Particle-ICP-ms, confirmed by EM and/or ion exchange and electrochemical techniques to include microchip capillary electrophoresis with conduction detection.

Step 1: Evaluation of the applicability of solubility testing, as used in drug development, though in a broader context, as well as data already available from other EU, National or ongoing FP7 projects and other disciplines (e.g., nanomedicine) from the perspective of 'regulatory toxicity testing'.

Step 2: Develop additional requirements for the solubility testing of nanoparticles, so that they will cover not only the degree of solubilisation from the moment of exposure/administration, but also in the different biological and environmental matrices where the particles might end up. This step may include in vitro digestion, studying the impact of the conditions within the human digestive tract on the fate of nanoparticles, and the study of the stability in cell culture media (and other media used in toxicological studies) and environmental waters ("pre-kinetics").

Step 3: Devise a suitable rapid solubility testing procedure.

# 2 Description of work & main achievements

## 2.1 Summary *[DLO-RIKILT (lead); Meike van der Zande, UNamur; Julie Laloy, IIT: Stefania Sabella, Udl-LEG: Carlos Rey-Castro, NPL: Ratna Tantra]*

Presently, it is generally acknowledged that toxicological *in vitro* and *in vivo* studies on NPs should be supported by thorough physical chemical characterization of NPs. More specifically, by characterization in relevant exposure conditions and media. In order to do this, suitable methods should be identified and standard procedures developed and validated, which is the scope of the NANoREG framework. Task 5.2 focuses on measurement of dissolution of NPs in complex biological media, with the final goal to devise a suitable rapid solubility testing procedure.

The work in WP 5.2 started with an extensive review on the "state of the art" concerning dissolution measurement methods. In this review, all possible methods for dissolution measurement were identified and thoroughly discussed (*1*). The review process was followed by experimental work. To improve comparability of the experimental work, and thus the methods investigated, all partners used *in vitro* digestion juices or cell culture media as complex media model systems. Several of the core NANoREG materials were selected for testing. We tested three ICP-MS/AES based methods, one was based on single particle (SP) ICP-MS measurement, and the other two consisted of a combination with ultrafiltration (UF) or ultracentrifugation (UC). UF-ICP-MS was demonstrated to be a robust technique, although interactions of the nanomaterial with the matrix and/or filter were a limiting factor to this technique. These interactions resulted in an underestimation of the "total" amount of material dissolution, as only the free dissolved species could be measured. In-depth knowledge of the nanomaterial and the matrix is essential when selecting this technique. UC-ICP-MS was shown to be applicable as well, although results indicated that the supernatant should always be tested for remnants of materials, as it was shown that not all material could always be properly pelleted. Also for this technique in-depth knowledge on the material and the matrix is of importance. Ion-salt/protein complexes could be pelleted leading to an underestimation of the "total" amount of dissolution; it is essential to determine an optimal centrifugation speed. Finally, SP-ICP-MS was also demonstrated very suitable for the evaluation of the dissolution of nanomaterials. This technique is especially interesting for evaluation of nanomaterials that are known to form complexes with the matrix, as this technique does not depend on separation of the particulate material from the dissolved species. However, the size detection limit of the technique is the limiting factor of the technique. Future research is currently focussing on lowering the size detection limits of SP-ICP-MS. Besides ICP-MS/AES based methods also colorimetry methods were tested. They have the advantage to be cheaper and they work well with certain materials/metals. However,

the choice of materials that work well with colorimetry is limiting and complex matrices can interfere with the technique. Finally, theoretical modelling of dissolution was evaluated, which was shown very helpful to provide insight in the dissolution behaviour of nanomaterials. However, in-depth knowledge on the material and matrix is essential and as the technique is no detection technique the actual behaviour of the nanomaterials is not confirmed by measurement.

Taken together, measuring dissolution in a complex matrix is highly challenging. At present it is not possible to device one universal robust, rapid test method for regulatory testing that is applicable for all types of nanomaterials in all types of matrices. However, several methods have been identified for future use (*e.g.* UF-ICP-MS/AES, UC-ICP-MS/AES, SP-ICP-MS, and colorimetry). A relative easy and highly robust method that can be used for a rather broad range of nanomaterials appeared to be UF-ICP-MS/AES, given that no nanomaterial-matrix interactions take place. If these interactions do take place SP-ICP-MS would be a good choice for measurement, given that the material is not below the size detection limits. Nevertheless, to select the best suitable method, knowledge of physical-chemical properties of the nanomaterials is crucial and it is recommended to use a combination of techniques. Furthermore, processing protocols (*i.e.* sonication, elemental detection method and procedures *etc*.) were shown to influence nanomaterial dissolution and it is therefore recommended to further standardize these procedures. When reporting dissolution analysis, the used protocol must be reported in detail, including all experimental conditions in which the data were collected. Finally, methods should be validated by conducting appropriate round robin studies and suitable reference materials should be available in order to obtain good quality results.

### 2.2 Introduction *[NIA; David Carlander]*

In the NANoREG report 'Report on a Virtual Workshop to identify, formulate and prioritize issues/questions' (Deliverable D1.1) a number of regulatory issues and questions in the area of regulatory toxicology and risk assessment of nanomaterials have been compiled. These questions are to be addressed by the NANoREG project. In table 5[1] of D1.1 all 16 key questions from a regulatory perspective are presented. To ensure that all questions are addressed by NANoREG each work package has assessed the relevance of the 16 questions for various tasks. For Task 5.2 question 3 (Characterisation/Transformation) is considered to be the main relevant question, whereas questions 1, 2, 4, 5, 6, 7, 8, 9, 11, 12 and 13 are related to the task.

[1] Deliverable 1.1: table 5 on page 15 of the document 'NANoREG D1.1 2013-07-15 JRS plus annexes.pdf' in CIRCABC (Library > C-Consortium > 03 Deliverables uploaded to EC)

**Table 1. Questions relevant for Task 5.2 (taken from D1.1[1])**

| Q | Question with main relevance for Task 5.2 |
|---|---|
| 3 | ***Characterisation/Transformation:*** What testing should be performed to identify surface modifications that occur once a MNM has been released into the environment or taken up into the body? How can transformation, including agglomeration surface modification, dissolution and incineration, be determined and considered in the exposure and hazard assessment and how do they change the intrinsic toxic properties and biodistribution Do we need to know the details of such surface modifications or of what is bound, or do we need some simple test systems that actually determine the behaviour and transformation of MNM in relevant media throughout all life cycle stages? Is a nano-derived material still nano when it becomes agglomerated? Take into account relationship with questions 7-9. |
| | **Questions related to Task 5.2** |
| 1 | **Measurement and characterization - Identification**: How can MNMs be identified according to the EC recommendation for a definition of MNMs and for regulatory purposes (i.e. the implementation of the EC definition in e.g. REACH, CLP, cosmetics, novel food, etc.), including other jurisdictions (global harmonisation)? Can we develop robust measurement protocols which enable assessment of whether a NM falls under, or not, the EC definition? Are there robust measurement protocols available (and for which matrices) that enable identification? |
| 2 | **Measurement and characterization**: Could an "intelligent characterisation strategy" be defined? What is a minimal set of physical (and/or chemical) characteristics that should be available for risk assessors within the context of regulatory toxicology? What are the relevant features to characterise MNMs, e.g. size, form, aspect ratio, rigidity, flexibility and coating? What methods (SOPs) should be developed / used to determine the physical chemical characteristics of MNMs throughout their different life cycle stages within the context of regulatory toxicology?<br><br>These questions (closely related to Q1) refer to developing cost effective standard methods, detailed protocols and reference materials both for calibration and analysis of both pristine materials and materials in relevant media or complex matrices throughout the complete life cycle of the nanomaterial. they also refer to whether different categories of characterisation methods (varying e.g. in precision and accuracy) can be defined: Could an "intelligent characterisation strategy" be defined? |
| 4 | **Metrology and dose metrics:** Which metrics (metrology) should be used for MNMs in regulatory toxicology? As recommended by several committees and guidance, notwithstanding e.g. the OECD GSPD, NANoREG should use mass, particle numbers and surface area (as far as possible) to characterise dose. The data generated within the project will contribute to the development of a body of comparative data (e.g. shape and aspect ratio should be examined when appropriate for the MNM). Using this comparative data, NANoREG should examine which metrics are the most appropriate depending on the different types of materials and media involved, as well as the (eco)toxicological effects and exposure to be assessed in the Risk Assessment process. |
| 5 | ***Extrapolation and grouping***: What guidance can be provided on how to decide when information from different forms of MNMs (or from the bulk material) can be "re-used" in the sense of read-across, categorisation and grouping? Should / could guidance be based exclusively on physical-chemical properties or could exposure related (eco)toxicological and mechanistic information (as Mode of Action) be used as well and how? Take into account the relation with the following questions. |
| 6 | ***Fate, persistence and long-term effects:*** Can effective in vitro and alternative models to understand long-term effects be developed? Will MNMs accumulate in humans, the environment, environmental species and the food chain and what are the driving forces? Is this mechanistically different from bulk materials? Will nanomaterials present long-term and/or cause deferred effects? How will coatings or surface modifications or the bio-based nature of the MNM affect biopersistence / biodegradability rates? |
| 7 | **Kinetics and fate, determination:** How and when should information on absorption from the various routes of exposure, on deposition (e.g. lung burden), on biodistribution, on potential persistence and bioaccumulation, and on internal exposure (taking into account dose, duration, coating and interaction with biological systems) be generated and used? Relate the information with, for instance, the following objectives:<br>• To perform more accurate risk assessment<br>• To decrease uncertainty (safety factors),<br>• To select, if needed, a second route for acute toxicity testing,<br>• To design additional tests – that are 'affordable' – or to relate to studies that involve exposed workers, such as in the silica industry,<br>• To decide on a strategy for further testing (carcinogenicity, reproductive toxicity, etc.). |
| 8 | **Kinetics and fate, extrapolation:** How and when can information on kinetics and fate be used to justify grouping / read across or testing triggering / waiving and for building knowledge on the relationship between physical-chemical properties and toxicity? In other words: to what extent are the kinetics and fate of MNMs (e.g. environmental distribution or deposition and biodistribution in the lung) different from the bulk material? Are there ways to extrapolate this information from the bulk material or from several forms (size, shape, coating, etc.) of the same chemical and how should this extrapolation be made? |
| 9 | **Mode of action:** What are the physical and chemical properties driving exposure and (eco)toxicity of MNMs at all stages of their life cycle? How is MNM interaction with biological systems affected? What are critical characteristics of MNMs that need to be considered and included / excluded when developing MNMs to ensure they are safe and which materials have a known increased toxicity in the nanoform vs. the bulk form, |

| | |
|---|---|
| | and why? How will this facilitate the regulatory safety assessment of new nanomaterials? |
| 11 | **Exposure:** What are the main determinants for occupational and consumer exposure to MNM and what are the duration and type of exposure? |
| 12 | ***Exposure:*** How should human and environmental exposure be assessed in practice (determining exposure scenario, quantify input parameters for models, assumptions and use of proxy indicators, background and uncertainty estimation)? Consider both measuring and specific modelling for nanomaterials and evaluate the needs for standardisation and validation. |
| 13 | ***Exposure and life cycle analysis:*** Which scenarios could denote potential exposure and what information do we have on them? Can we develop standardized and efficient testing procedures for estimating release of nanoparticles (NP) from powders and NPs in matrices? What are situations in which MNM exposure is expected to be negligible / high? Are the amount and the nature of releases of MNM similar to regular chemicals, when common recycling and end-of-pipe techniques are used?<br><br>How to minimise and structure LCA to avoid ending up with a '1:1 model of the world'?<br><br>In other words: what is the exposure probability throughout the different life cycle stages of the MNM: production process of the NM itself, releases during the production process of products in which MNM are used, waste treatment, consumer articles, wearing, abrasion, etc.? Do waste treatment / recycling processes lead to exposure to NMs that can be hazardous to health and environment? If so, are additional risk management measures required? Do the recycled product / residues loose some value /usefulness due to undesired characteristics? |

The partners in Task 5.2 have aimed to address the issues raised in the 11 questions in order to discuss how to '**Develop solubility testing procedures'** for nanomaterials. Based on discussions among Task 5.2 partners on the DoW description and the relevance of the 11 questions, this report has been prepared.

### 2.2.1 Readership *[NIA; David Carlander]*

Following the NANoREG DoW, this report is for restricted use. It will have to be discussed with the Consortium Management if a public version will be made available.

### 2.2.2 Scope of report *[DLO-RIKILT; Meike van der Zande]*

In this report, an overview of the "state-of-the-art" concerning dissolution measurement methods is given. The following part of the report consists of experimental data of the most promising methods for nanomaterial dissolution measurement methods in complex matrices. The experimental data are discussed in detail and provide an extensive overview of the applicability and limitations of the tested methods. Finally, several recommendations concerning the use of these methods in a regulatory context are given.

### 2.2.3 Applicability of tested/used procedures *[DLO-RIKILT; Meike van der Zande]*

All methods tested were shown to be applicable for nanomaterial dissolution measurement in complex matrices, but all methods also had some limitations. Therefore, we concluded that it is not possible to device one universal robust, rapid test method for regulatory testing that is applicable for all types of nanomaterials in all types of matrices at present. A relative easy and highly robust method that can be used for a rather broad range of nanomaterials appeared to be UF-ICP-MS/AES, given that no nanomaterial-matrix interactions take place. If these interactions do take place SP-ICP-MS would be a good choice for measurement, given that the material is not below the size detection limits. However, in order to select the best suitable method, knowledge of physical-chemical properties of the nanomaterials is crucial and it is recommended to use a combination of techniques. Furthermore, the methods and pre-processing protocols should be further standardised and validated in the future in order to obtain good quality results.

## 2.3 State of the art *[NPL (lead); Ratna Tantra, K.N. Robinson, DLO-RIKILT; M. van der Zande, H. Bouwmeester, A.K. Undas, UdL; C. Rey-Castro, C.A. David, UNamur; J. Laloy, J.M. Dogné, J. Jarman, University of Zaragoza; E. Bolea, F. Laborda]*

Solubility is an important physicochemical parameter, of relevance in various nano-applications. From a risk assessment point of view, if nanomaterial is shown to be completely soluble then nanomaterials will be absent. From this point of view, its disposal can be treated much in the same way as "ordinary" chemicals, which will simplify testing and characterisation regimes. Undoubtedly, the need to have methods to measure the solubility of nanomaterial is needed and in this section, a review on state of the art will be given. This purpose of this here is three-fold. First, terminology of relevance will be presented; this is important, as it avoids misunderstandings. Second, sources of potential errors measurements in general, will be given. Third, an overview of different methods that can potentially be employed will be discussed. The methods presented can be broadly divided into 4 categories: a) methods involving separation b) quantification of free ions c) quantification of total dissolved species d) theoretical modelling/predictions.

### 2.3.1 Terminology

#### *2.3.1.1 Nanomaterial*

Nanomaterial is a *"natural, incidental or manufactured material containing particles, in an unbound state or as an aggregate or as agglomerate and where, for 50% or more of the particles in the number size distribution, one or more external dimensions is in the size range 1nm-100nm. ……. In specific cases and where warranted by concerns for the environment, health, safety or competitiveness the number size distribution threshold of 50% may be replaced by a threshold between 1 and 50%".* This definition is in accordance to the recently published European Commission (EC) Recommendation (2011/696/EU).

#### *2.3.1.2 Solubility*

The term solubility has been previously defined by Organisation for Economic Co-operation and Development (OECD), in relation to chemical solubility: "*the degree to which material (the solute) can be dissolved in another material (the solvent) so that a single homogeneous phase results …*" with water solubility being "*the saturation mass concentration of the substance at a given temperature. Water solubility is expressed in mass of solute per volume of solution. The SI unit is kg/m$^3$ but g/l is commonly used*" (*2*). The term solubility has also been defined by International Organization for Standardization (ISO), as *"…the maximum mass or concentration of the solute that can be dissolved in a unit mass or volume of the solvent at specified (or standard) temperature and pressure, unit [kg/kg] or [kg/m3] or mole/mole]*" (*3*).

In addition to solubility, there are also other terms that require clarification. It is important to differentiate three terms: solubility, dissolution and dispersibility. Out of the three, the terms solubility and dissolution are used interchangeably. They share similarities but are differentiated on the basis that solubility is assumed to be at equilibrium, whereas dissolution is considered as a kinetic process (*4*). Dispersibility however, has an entirely different meaning and has been defined as *"the degree to which a particulate material can be uniformly distributed in another material (the dispersing medium or continuous phase)"* (*4*).

### 2.3.2 Measurement Issue: Dynamics of Solubility Equilibria

The measurement of solubility for nanomaterial is not trivial, as one must consider the dynamic nature of solubility equilibria, which complicates the measurement. For example, an increase in temperature can result in an unstable suspension, which leads to agglomeration and sedimentation of the nanomaterial. Potentially, this can lead to changes in solubility due to changes in particle size of the particles exposed. Another factor affecting dissolution is the presence of dissolved species (at different concentrations) e.g. "free" (hydrated) metal ions, soluble inorganic complexes (e.g. chlorides, hydroxides), soluble organic complexes (e.g. amino acids, proteins). In the case of ZnO nanomaterial, dissolution/solubility will be dependent on pH. (*5, 6*), at low pH, dissolved zinc is likely to exist as free ions (*7*):

$ZnO + 2H_3O^+ \rightarrow Zn^{2+} + 3\ H_2O$ [Equation 1]

Although, $Zn^{2+}$ [Equation 1] is labelled as "free", strictly speaking these ions will exist in hydrated forms, with chemical formula of $[Zn(H_2O)_n]^{2+}$. At moderately to highly alkaline pH, the following reactions are likely to occur (*8*, *9*):

$Zn^{2+} + OH^- \rightarrow Zn(OH)^+$ [Equations 2-4]

$Zn^{2+} + 2OH^- \rightarrow Zn(OH)_{2(aq)}$

$Zn^{2+} + 3OH^- \rightarrow Zn(OH)_3^-$

etc.

leading to formation of soluble hydroxo-complexes such as $Zn(OH)_3^-$ or $Zn(OH)_4^{2-}$ (*7*).

The presence of different species in the sample, implies the need to identify what to measure. According to Equations 1 – 4, dissolved Zn can be in various forms: $Zn^{2+}$, $Zn(OH)_{3-}$, $Zn(OH)_4^{2-}$, etc. The question as to which of the dissolved species to measure will be dependent on the testing requirements. For example, according to the OECD/ISO solubility definition (that support (Registration, Evaluation, Authorisation and Restriction of CHemicals (REACH)), solubility should be focused on measuring total dissolved nanomaterial, without taking into account species differentiation. However, it may be argued that this definition may not be entirely supportive of nanoregulation. In 2008, European Chemicals Agency (ECHA) has released guidance, recognising the need to measure speciation (i.e. the distribution of an element amongst dissolved species) (*4*). In fact, nanotoxicology studies have shown that it is often the free ions that are correlated to toxicity.(*10*) Furthermore, both Biotic Ligand Model (BLM) and Free Ion Activity Model (FIAM) have been used to explain and predict the effect of free ion concentration on toxicity to organisms (*11, 12*). The important role that free ions play in governing toxicity indicates that the measurement of solubility should not only report the total dissolved species but also that of free ion concentrations.

### 2.3.3 Overview of Methods

#### *2.3.3.1 Separation Methods*

One of the important requirements to measure nanomaterial solubility is the need for a technique to be highly selective, in particular in the presence of particulates. Ideally, the complete removal of nanoparticulate matter from the analytical sample prior to quantification of dissolved species is needed. Note that separation methods presented here, do not measure solubility by themselves and are often integrated with a detection method in order to achieve this.

*OECD guideline, filtration and centrifugation*

According to an OECD guideline (*2*), two types of methods should be considered for measuring solubility (even though this guideline is specific for conventional chemicals and, in particular, *pure substances which are stable in water and not volatile)*. The two methods are: column and the flask method. The column method involves packing a column with a "support material" and test substance, after which the column is connected to a series of pumps (allowing liquid to flow through). A piece of glass wool inserted at the end of the column acts as a plug to ensure that any liquid flowing through is free from particulate matter. In the case of the flask method, the test substance (in a liquid medium) is placed inside a flask and shaken for a certain time period. The solution is then filtered separately in order to remove particulates. In both cases, the sample, which is assumed to be free from particulate matter, can then be subsequently analysed using an appropriate detection/quantification technique. To date, no work has been published that compares the two methods. Hence, future work is needed to evaluate:

a) drawbacks of the methods e.g. potential clogging of column outlet (in the column method), in which blockages with the nanomaterial can occur.

b) efficiency of the two methods , in the removal of the particulates (especially the nanomaterial) from the final sample for analysis.

Although these methods have not been rigorously tested with nanomaterials, a similar approach to remove particulates from a dispersion of nanomaterial has already been adopted amongst the nanotoxicology community. The use of physical filters (as in the flask method) has been used in the characterisation of nanomaterial solubility (*13, 14*).

Undoubtedly, the main advantage of methods mentioned so far is that they are extremely affordable and accessible. However, these methods are deemed to be unreliable as particulates in the nano-scale can easily end up in the sample for analysis e.g. by passing through the pores of the filters. In the case of the centrifugation method, an assumption is made that the operator has extracted the resultant supernatant without disturbing the pellet that has been formed. In fact, Xu and co-workers have reported the incomplete removal of nanomaterial from the supernatant after exhaustive centrifugation (*15*).

*Dialysis and ultrafiltration*

In an effort to improve the reliability of the separation process, alternative ways to remove particulates, such as dialysis and ultrafiltration, should be considered. The basic principle of (equilibrium) dialysis is that it relies on the diffusion across a semi-permeable membrane. The use of equilibrium dialysis has been reported by past workers in the measurement of nanomaterial solubility (*13, 16*). The dialysis method however can take a long time and a quicker method of ultrafiltration (UF) can be used to speed up the process. UF is different from dialysis in that this is a pressure-driven process (through the use of a vacuum/centrifugal force), which leads to the separation across a semi-permeable membrane (*17*). The use of UF has been extensively applied to nanomaterials, and membranes with pore size in the range of 3 – 100 kDa (smaller than 1 nm) have been used to study the solubility/dissolution of (for example): silver (*13, 18-22*), zinc oxide (*6, 13, 23, 24*), cerium oxide (*13, 22, 25*), titanium dioxide (*13*), copper oxide (*26*), quantum dots (*18*) and gold (*13*). One limitation in UF relates to potential interactions of the membrane not only with the nanomaterial but also with the dissolved species. The choice of membrane is thus crucial.

Although UF has better reliability in removing particulate matter in comparison to normal filters and centrifugation, this method may not be considered to be sufficiently reliable in satisfying the requirements of cosmetic regulation. When using such methods, an assumption is being made that particulates cannot have size smaller than that of the pores of the membranes. Even though pore sizes as low smaller than 1 nm are currently available, a complete removal of all particles may prove difficult to achieve in some cases because of sub-nanometer particles that may potentially pass through the pores of such membranes. Clearly methods that offer better reliability of the separation process are sought for and such methods will be discussed in the remainder of this sub-section.

*Ion exchange*

Another technique that offers promising separation performance is the ion exchange technology (IET), with the most common being based on ion exchange resins. This method is mainly applicable in the separation of free metal ions and involves the equilibration of a known mass of resin column with a given volume of sample (*27, 28*). Separation is based on the assumption that the resin/aqueous partition coefficient for the metal is constant with respect to the free ion concentration. The IET requires a careful control of pH and percolation time to ensure that equilibrium conditions are attained. Once equilibrium is reached, steps of washing and elution follow. The metal ion contained in the eluted sample can then be quantified using a suitable analytical technique. The IET has several advantages:

a) it can not only separate but also pre-concentrate samples.
b) it has been shown to be reliable (through cross validation with electrochemical techniques) (*29*).
c) although the technique allows primarily the quantification of the free ion, potentially it can be used for the simultaneous evaluation of free and total dissolved metal concentrations, as achieved through certain resin titration schemes (*30*).

Despite the promising features of this IET, only a few studies have been carried out in relation to the measurement of nanomaterial dissolution/solubility (*21, 31*).

Another technique involving ion exchange resins is Diffusion Gradients in Thin Films (DGT) (*32*). The DGT device is a commercially available passive sampler consisting of a three-layer assembly encased in a cylindrical plastic holder with a circular window that allows contact with the aqueous sample. The three layer assembly is composed of: a) a membrane filter (0.45 μm pore size) that is in contact with the sample solution b) a second hydrogel layer of a known thickness (the *diffusion* layer, usually 800 μm thick) c) a thin hydrogel layer (400 μm thick) containing embedded beads of a strong chelating ion exchange resin. The ion exchange resin is typically Chelex®100 for most metal cations, but other binding resins are also available for inorganic anions e.g. titanium dioxide or ferrihydrite (*33*). The concentration of analyte measured by DGT is usually regarded as a *labile fraction* of the dissolved element. This operationally defined fraction depends on the concentration, diffusion coefficient and dissociation rate constant of the different dissolved metal species (hydrated ions, complexes with inorganic and small organic ligands, colloidal species, etc.). Further theoretical details on DGT will not be covered here and can be found elsewhere (*33-35*). In relation to nanomaterial and the measurement of solubility, past studies have used DGT in the context of ecotoxicological studies of several nanomaterials, for example: silver (*19, 36-40*), copper oxide (*37, 41, 42*) and zinc oxide (*37*).

DGT shares many of the advantages that IET has, in that it is: simple, robust, can be used over a wide range of pH, capable of multielement analysis, has good reproducibility, and has high elemental selectivity and high sensitivity. In addition, large pre-concentration factors and consequently low detection limits can be achieved in combination with ICP-MS analysis for the analysis of the eluted samples. DGT devices, however, are relatively non-expensive, easy to use and can be deployed directly *in situ* . A disadvantage of both DGT and IET is associated with the large sample volume needed for analysis i.e. in the order of hundreds of mLs. For the particular case of nanomaterial dispersions, several issues associated with IET and DGT still exist. In DGT, the effect of partial penetration of nanoparticles into the diffusion gel is still not well understood. In IET, the direct contact of the exchange resin with the sample means that adsorption of particles can take place on the resin beads.

*High Performance Liquid Chromatography*

In HPLC, a chromatography column (stationary phase) is used to separate different components in a sample. When the sample enters the column, the sample interacts with the stationary phase. A solvent (eluent) is then added to the column, which is the (flowing) mobile phase. Separation is achieved on the basis of differences in partitioning behaviour between the flowing mobile phase and the stationary (reverse) phase. Subsequent to the separation step, the separated components are often transported for detection/quantification. In relation to nanomaterial characterisation, HPLC based techniques have been employed to determine particle size/concentration of gold nanoparticles (*43*) and fullerenes (*44, 45*). To date, HPLC has not been used in the measurement of nanomaterial solubility.

*Capillary Zone Electrophoresis and Field Flow Fractionation*

Another technique that is capable of reliable separation is capillary zone electrophoresis (CZE). This electrokinetic separation based method is particularly powerful and widely used in separation science. In CZE, high voltages are applied in order to separate molecules when moving in an electric field. The CZE set up typically consists of a buffer filled capillary (small diameter tubes) placed between two buffer reservoirs, with a potential field being applied across the capillary. The velocity of a given analyte in the capillary is governed by the electrophoretic mobility as dictated by charge to mass ratio of the analyte. In addition, the velocity is also affected by electroosmotic flow (EOF) (as governed by zeta-potential of the surface of the capillary wall). The EOF is an induced bulk liquid flow (that is moving with the same velocity as the counter ions i.e. these being the cations in the diffuse layer at the walls of the capillary). The electrophoretically separated species are often detected near the outlet end of the capillary, in which various detection schemes exists: fluorescence, absorbance, electrochemical and refractive index. The choice of detection will be dependent on the analytical criteria (e.g. selectivity, sensitivity, etc.) and the type of sample under analysis.

The use of electrophoretic separation techniques have been developed and refined over decades and are now widely used for the separation of different analytes in complex mixtures. In relation to nanomaterial characterisation, electrophoresis has been shown to be able to separate nanomaterial of different, size, shape and compositions (*46-51*). In addition, CZE has been shown to be particularly useful in the study of nanoparticle-protein interactions (*52-54*). Although these studies have shown the potential on the use of CZE in relation to nanomaterial, much fundamental work is still required. Unlike molecules, the theoretical understanding of the separation mechanism and electrokinetic behaviour of nanomaterials is not completely understood. For example, electrophoretic motion can no longer be estimated by considering molecular weight and expected charge as particles possess "electrophoretic heterogeneity" i.e. exhibiting a wide distribution of charge, size and shape, all of which can vary with experimental conditions and time. In relation to using CZE based methods to measure the solubility of nanomaterial, its use is limited. Recently, Tantra et al have shown the applicability of the CZE (with conductivity detection) in a microchip format in relation to dissolution measurement of zinc oxide nanomaterial when dispersed in ecotoxicological media (*55*). To prevent potential interaction and clogging of nanomaterial within the CZE microchannels, the authors have reported the need to remove most of the nanomaterial using a filter prior to injecting into the microchannels.

Lastly, a reliable separation method to consider is Field Flow Fractionation (FFF). FFF is a family of techniques designed to separate analytes with different physicochemical properties. The separation principle is based on the differential movement of analytes in a fluid flowing in laminar regime inside a flow chamber or channel, generally directed towards a detector. Separation is not directly caused by the flow itself, but by a generated field perpendicular to the direction of this flow. The applied field determines the properties on which the analytes will be separated. The field may be generated by sedimentation, electrical, or magnetic forces, thermal gradients, or a crossflow (*56*). The latter, called flow FFF, is the most commonly used FFF technique in which the crossflow carries the analytes to an accumulation wall. This wall consists of a semipermeable membrane lying on top of a supporting frit. The lower size limit of this technique is set by the molecular weight- or size cut off of the membrane. The most critical factor for flow FFF is the choice of membrane, since interactions of nanomaterial with the membrane could occur, depending on the type of membrane (*57*). Separation in flow FFF is driven by differences in diffusion of the analytes, which is inversely correlated with the hydrodynamic diameter of the analyte i.e. the lower the diameter the larger the diffusion. Smaller analytes have higher diffusion rates and will therefore be transported at a higher flow speed in the parabolic flow profile than larger ones. The original flow FFF design includes two permeable walls, but the more recent asymmetrical design with one permeable wall, known as asymmetrical flow FFF or AF4, is the most commonly used design (*58*). A variety of detectors may be coupled to FFF dependent on the type of analyte to be detected. Commonly used detectors for the detection of nanomaterial include: multiangle light scattering (MALS), UV absorbance, and elemental detectors like inductively coupled plasma mass spectroscopy (ICP-MS) or optical emission spectrometry (ICP-OES) (*56, 58*).

AF4 has several advantages over other separation techniques for the separation and detection of nanomaterial. Firstly, it does not comprise a stationary phase in contrast to traditional liquid chromatography techniques such as size exclusion-, and ion exchange chromatography. A stationary phase is often not desirable for the separation of nanomaterial, since unpredictable interactions between the stationary phase and the nanomaterials could occur possibly resulting in very strong interactions or even irreversible binding of the nanomaterial to the stationary phase. Secondly, the carrier solution may be changed with respect to pH and ionic strength in order to match the carrier solution with the sample composition, and finally, the outcome of AF4 is easy to interpret. Separation is driven only by size, so the retention time is directly proportional to the nanoparticle physical properties, whereas techniques like ion exchange chromatography and capillary zone electrophoresis are driven by both size and charge. AF4 is also particularly advantageous in dealing with when nanomaterial is dispersed in complex biological matrices and applicable to the analysis of heterogeneous samples (containing a broad mass/size range from ~1 nm up to 100 µm), thus reduces the need for sample pre-processing (*59*). The selectivity and speed of the technique is also tuneable. Furthermore, the low shear rates provide the possibility to handle samples in which weak forces prevail and thus the "soft" fractionation of this technique compared to other techniques. Compared to capillary zone electrophoresis AF4 has a greater sensitivity due to larger injection volumes that can be used. Nevertheless, the AF4 channel can easily be overloaded, requiring dilution of the sample and a sensitive detection system. Over the last decades asymmetrical flow FFF or AF4 has been extensively refined with respect to separation and characterization of various nanomaterial, such as gold (*60-64*), silver (*65-69*), silica (*70*), titanium (*71, 72*) nanomaterial, carbon nanotubes (*73-76*), etc. Most of these studies however have been in relation to characterisation of nanomaterial such as size and mass. However, in relation to solubility, information on

using AF4 as a method is limited. This is mainly due to the fact that soluble (dissolved) material will mostly be transported through the membrane by the cross-flow. The cross-flow is used as a means to separate the nanomaterial and is collected separately, often regarded as waste. Therefore, this flow is typically not on-line and not connected to a detection system. Nevertheless, the cross-flow may be collected and measured as a separate fraction, theoretically rendering this technique to be suitable for solubility measurements (*77*). In that case, it should be pointed out that although possible, the high dilution of the species collected would make its detection challenging.

A large advantage of AF4 is the fact that this technique can separate very small particles over a wide size range with high resolution. This implicates that AF4 can separate original particles from particulate that were newly formed after dissolution, providing information not only on the fraction of original particles and the dissolved soluble fraction, but also on the fraction of newly formed particulate complexes. The latter fraction contributes to the dissolved fraction, but could be missed using other solubility testing separation techniques like ultrafiltration or ultracentrifugation.

#### *2.3.3.2 Methods: quantification of free ions (and labile fractions)*

As previously discussed in the introduction, the need to have techniques that can quantify free ions is important, from the point of view of speciation characterization.

*Electrochemical methods*

Electrochemical methods in particular are suited for the measurement of free ions. Perhaps the simplest and cheapest is by measuring electrical conductivity i.e. a solution's ability to carry a current and conducts electricity. The measurement of conductivity has several advantages in that it is rugged, easy to use, with quick analysis time. Measurement of conductivity has been widely accepted and has been shown to be particularly useful for the assessment of water quality (*78, 79*). One limitation in conductivity measurement is that it is unspecific and without the addition of a separation technique, the conductivity signal can be easily masked by background ions. Hence in relation to their use for nanomaterial characterisation, in particular solubility measurement, a reliable separation method is needed e.g. integration with CE, as previously discussed (*55*). Electrochemical methods that offer better selectivity are thus needed (*80-82*), such as ion selective electrodes.

In potentiometric ion selective electrodes (ISE) measurement, the set-up involves an electrochemical cell that consists of a reference electrode (with an electric potential independent of the measuring conditions) and an ISE. The ISE is a membrane-based electrochemical sensor that responds specifically to the activity of a particular ionic species. When the electrodes are immersed in solution, an electric potential is created across the electrodes and measured by a millivolt meter under (ideally) zero-current conditions (*81, 82*). ISE potentiometry has several advantages. The ISE is considered to: be a non-destructive technique, show fast response (often below 1 min), not be affected by sample colour or turbidity, be relatively inexpensive, and not entail extensive operator training. Furthermore, relatively small amount of sample (in the order of 10 mL) is required for analysis and specially designed flow cells can be used with much smaller volumes (*82*). Several limitations, however, are associated with ISEs. First, the detection/quantification limit is not much lower than $10^{-6}$ M, although in well-buffered systems (with excess of a metal binding ligand) values as low as $10^{-14}$ M have been reported by some authors (*83, 84*). Second, they are potentially sensitive to certain interferences/contaminations, with most ISEs showing a response for other ions in solution apart from the target ion, to a greater or lesser extent (*85*). Interference effects are mainly due to the presence of other ions of the same charge as the target ion. Furthermore, commercial ISEs offer only a limited variety of the ions that can be analysed (to include: $Ca^{2+}$, $Cd^{2+}$, $Cu^{2+}$, $Ag^{+}$ and $Pb^{2+}$). To date, the vast majority of past studies surrounding the use of ISE to measure dissolution/solubility has been associated with ecotoxicology investigations using different nanomaterials, for example silver (*13, 19, 83, 84, 86-88*) and copper (*89*).

Like ISE, voltammetric methods have primarily been used for the measurement of free ions. Promising voltammetric methods are those based on some kind of preconcentration step, such as: anodic stripping, adsorptive cathodic stripping voltammetry and absence of gradients and Nernstian equilibrium stripping (AGNES). Anodic stripping voltammetry (ASV) consists of two stages. In the first stage, a small amount of electroactive metal species (negligible in comparison with the total content of the sample) is reduced and

pre-concentrated at an electrode under controlled conditions of time, stirring and deposition potential. This is what is referred to as an accumulation step. The second stage is what is referred to as the "stripping stage" i.e. where the accumulated metal is reoxidized (or "stripped") as the potential is scanned anodically (towards more positive potentials) either in a linear way or, usually, in a pulse waveform (such as the Differential Pulse mode, DPASV) (*82*). The resulting signal measured is a peak current, whose profile is dependent on characteristics of the metal ion (e.g. diffusion coefficient, charge number), the geometry of the electrode, the hydrodynamic conditions during the deposition step, etc. and the medium composition (due to possible contributions from the dissociation of metal complexes during deposition). In adsorptive cathodic stripping voltammetry (AdCSV), an indirect method of determination of dissolved metal concentrations is employed. This is based on the competitive ligand complexation with a suitable chelating agent (*27, 90*) thus forming a surface-active, electroactive metal complex. The metal complex is then accumulated by adsorption on the electrode surface at a controlled potential (during the accumulation step). In the stripping step, a negative-going potential scan is applied, and the current due to the reduction of the adsorbed metal complex (which is proportional to its electrode surface concentration) is recorded.

AGNES is also a stripping based technique implemented with mercury working electrodes. The fundamental difference in AGNES (in relation to other stripping methods) is that the accumulation stage lasts until a special equilibrium state is reached where (a) there is no concentration gradient of any species within the mercury electrode or the surrounding solution, and (b) the redox couple is in Nernstian equilibrium at the mercury interphase (*91*). Under these conditions, the applied deposition potential determines the gain or preconcentration factor in the amalgam, with respect to the free ion concentration in solution, through Nernst equation. The stripping stage in AGNES allows the quantification of the metal accumulated in the amalgam by measuring the current under diffusion limited conditions or the charge as the response functions (*92, 93*).

Stripping based methods can potentially have remarkably high sensitivities, mostly due to the large preconcentration factors (of the order of $10^2$-$10^3$) achieved prior to stripping. These methods are usually able to reach sub-ppb detection limits (as low as $10^{-10}$ - $10^{-12}$ mol/L), which compares favourably with other techniques like Inductively Coupled Plasma detection techniques. Time of analysis is short (typically, a few minutes) and relies on relatively inexpensive equipment. Moreover, in many cases these techniques do not require a solid-liquid separation step, but there is potential adsorption of dissolved organic matter and particles on the working electrode, which may interfere with the measurement. Although they can be used for the measurement of free ions, voltammetric methods are often sensitive to other dissolved species. A disadvantage in voltammetric methods is the need for some level of expertise in the operators. However, AGNES avoids typical complications in the interpretation of dissociation kinetics and mass transport of metal complexes, etc., so that the results are much simpler to interpret. In relation to the measurement of nanomaterial solubility/ dissolution, ASV has been used in solubility measurements such as quantum dots (*94*), silver (*95, 96*) and gold (*97*). The use of AdCSV has been limited so far to the study solubility/dissolution of titanium dioxide nanoparticles (*98, 99*). AGNES has been used for the solubility measurement in relation various nanomaterials (for example): latex (*100*), zinc oxide (*101-104*), quantum dots (*105*) and clays (*106*).

*Colorimetry and fluorimetric methods*

In addition to electrochemical based methods, colorimetric and fluorimetric assays in, can also be used to measure metal ions (*107, 108*). These methods rely on the interaction of the metal with the complexing agent to result in a coloured complex, which can be monitored using appropriate spectrometers e.g. through measuring a change in absorbance or fluorescence signal. As with electrochemical based methods, these methods are inexpensive (*109*) and does not require extensive sample preparation. However, one disadvantage of these dyes is that they may not be exclusive to one type of ion. Furthermore, other species may interfere or mask the ions of interest. For example, it Nitroso-PSAP is affected by bilirubin (*110*).

In relation to nanomaterial analysis, it is important to ensure that the presence of the nanomaterial do not interfere with the analysis. A recent document reported on the use membrane filters to remove the nanomaterial prior to analysing the supernatant to quantify free zinc ions as a result of ZnO nanomaterial dissolution using Zincon colorimetric dye (*111*).

#### 2.3.3.3 Methods: quantification of total dissolved species

Although the techniques in the previous section are mainly suitable for the measurement of free (hydrated) ions, rather than total concentration of dissolved species, it is important to note that the total dissolved species can be sometimes estimated indirectly by means of titration experiments. For example, consider the dissolution of ZnO in a test solution (with a mixture of different inorganic and organic compounds). The total solubility will be the sum of the free $Zn^{2+}$ concentration plus the concentration of all complexes containing Zn:

$$S = c_{Zn^{2+}} + c_{Zn(OH)^{+}} + c_{ZnL^{2+}} + \cdots \qquad \text{[Equation 5]}$$

where $Zn(OH)^{+}$ and $ZnL^{2+}$ are examples of the inorganic and organic soluble complexes (L is a representative organic ligand), respectively. The concentrations of each complex can be calculated from the free ligand concentrations, using the corresponding conditional stability constants $K_i^{cond}$, which are referred to the actual background conditions (pH, ionic strength, temperature, etc.):

$$S = c_{Zn^{2+}}\left(1 + K_1^{cond} c_{(OH)^{-}} + K_2^{cond} c_L + \cdots\right) \qquad \text{[Equation 6]}$$

The value between brackets is characteristic of the medium composition, and represents the ratio between the total solubility and the free metal concentration:

$$S = c_{Zn^{2+}} K_{medium} \qquad \text{[Equation 7]}$$

In those cases where pH is constant, and the concentration of dissolved zinc is very low (so that the concentrations of free ligand are much larger than those of the metal complexes), the value of $K_{medium}$ is approximately constant with respect to the free metal ion concentration. In this case, it can be calculated from independent experiments where the test medium (in absence of ZnO) is titrated against known additions of a soluble Zn standard solution. This allows the estimation of the total solubility of ZnO from measurements of the free ion concentration.

Although the possibility of measuring total dissolved species indirectly is an option worthy of note, a direct measurement for multi-elemental analysis can yield far more accurate results. Atomic spectrometry techniques such as Inductively Coupled Plasma/Optical Emission Spectrometry (ICP-OES), Inductively Coupled Plasma Mass Spectrometry (ICP-MS) and Atomic Absorption Spectrometry (AAS) are appropriate here.

*Atomic spectrometry*

Both ICP-OES and ICP-MS use inductively coupled plasmas (ICP). An ICP is a discharge maintained by the interaction of a radiofrequency field and a partially ionized gas, usually argon. These plasmas can reach temperatures as high as 10,000 K, allowing the atomization and ionization of the elements in a sample and minimizing potential chemical interferences. In the case of ICP-OES, the plasma works as an excitation source for atoms and ions, whereas in ICP-MS it is a source of ions. Samples are introduced as solutions or suspensions through a nebulization system, consisting of a nebulizer and a spray chamber, which produces an aerosol of droplets. Once the droplets are into plasma, solvent evaporates, forming solid particles, which in turn are vaporized and their elements atomized and ionized. In ICP-OES, the UV-visible radiation emitted by excited atoms and ions is collected by an optical spectrometer, which is used to separate the individual wavelengths of radiation and focus them onto a detector. In ICP-MS, ions are extracted through an interface into a mass spectrometer, where they are separated according to their mass/charge ratio and detected.

A promising use of ICP-MS is when the technique is being used in single particle mode. Single particle ICP-MS (SP-ICP-MS) is increasingly being used in nanomaterial analysis, primarily as it provides a means to detect individual nanoparticles. The SP-ICP-MS technique is mainly employed for the determination of particle size and number concentrations (*68, 112-115*), although it has been shown to be able to differentiate

directly the dissolved and particulate forms of the analyte (*21, 115*). The technique works by acquiring thousands of individual intensity readings with a very short dwell time (*i.e.* 1-10 ms) and at very low nanoparticle concentrations (i.e., thousands of nanoparticles per mL, or ng/L). Dwell times and concentrations are chosen to detect just one nanoparticle per reading. Intensity readings are collected as a function of time and the number of pulses above the continuous background is proportional to the number concentration of nanoparticles. The intensity of each pulse is proportional to the mass of analyte in the particle, from which the particle size can be calculated (if the composition, shape and density are known). This method requires limited sample preparation and no separation before measurement. Current limitations of this technique are that only one element can be measured at a time and the relatively large size limit of detection attainable (*i.e.* ~20 nm or larger). On the other hand, no distinction can be made between pristine and surface modified nanoparticles because just the inorganic core is detected. The use of SP-ICP-MS for solubility testing is based on the constant signal produced by the dissolved analyte, which induces a shift of the continuous background to higher values, maintaining the pulses due to the particles. By plotting the number of readings for each intensity, two distributions are obtained: the first one, at lower intensities, is due to the dissolved analyte, whereas the second one due to the nanoparticles. By integrating the distributions and using dissolved standards, the mass concentration of analyte in the dissolved and nanoparticle forms can be obtained (*21, 68, 115*). It should be noted that the presence of dissolved species in SP-ICP-MS measurements, and its accompanying increase in background intensity, has a direct effect on the nanomaterial size detection limit of the technique, which will increase with increasing concentrations of the dissolved fraction (*115*).

As in the ICP techniques, atomic absorption spectrometry (AAS) is a quantitative technique for the determination of the total element content in a sample. The technique involves the atomization of the analyte, in which atoms (in the ground state) are promoted to a higher excitation states by absorption of radiation at specific wavelengths. The amount of absorbed radiation is thus a quantitative measure for the concentration of the element analysed. There are two commonly used atomizers: flame and graphite furnace (GF) atomizers. Flame atomizers are suitable for liquid and less sensitive than furnace atomizers. Graphite furnace atomic absorption spectrometry (GF-AAS) are used are used in order to quantify elements when in solutions or in solid samples; gas samples are uncommon in GF-AAS.

Most atomic spectrometry techniques often require the need to undergo conventional acid digestion as part of the sample preparation step. In the case of suspensions, this is usually carried out to prevent nebulizer blockage and coating of the spray chamber. For example, Fabricius et al. (*13*) have recommended the use of microwave assisted acid digestions as the optimal strategy for reliable routine analysis of any kind of metallic nanoparticles.

The choice of ICP-OES, ICP-MS or AAS for determining the total element content depends on the sample concentration level. ICP-MS is the most sensitive, with limits of detection below 1 ng $L^{-1}$, whereas in ICP-OES detection limits are 2-3 orders of magnitude higher. Detection limit of AAS vary enormously, with GF-AAS being in between ICP-OES and ICP-MS but flame-AAS being 3- 4 orders of magnitude higher (worse) compared to ICP-MS. The fact that the most sensitive method out the three is ICP-MS has resulted in its wide use for the analysis of inorganic nanomaterials in various types of matrices, varying from in vitro cell culture media (*116-118*) to cells (*119, 120*) and tissues (*121, 122*). Atomic spectrometry techniques measure total element content and thus cannot distinguish between different forms of an element i.e. particulate *vs.* dissolved forms; this is true apart from when ICP-MS is used in a single particle mode. Hence, these techniques are often coupled to separation techniques like FFF, hydrodynamic chromatography, HPLC, ultracentrifugation, dialysis or ultrafiltration.

#### *2.3.3.4 Methods: Theoretical modelling*

Although not a measurement tool, predictive analytical models should be considered, as simulated data can lead towards a better understanding of the solubility/dissolution process. An important theoretical calculation to consider surrounds the equilibrium concentration of the different chemical species formed as a result of the dissolution of a bulk solid material. This can be easily carried out using a thermodynamic speciation software such as Visual MINTEQ (v. 3.0, downloadable from http://vminteq.lwr.kth.se/), MINEQL+ (v. 4.6, see http://www.mineql.com/), or WHAM (v. 7, see http://www.ceh.ac.uk/products/software /wham/). All these programs have been originally designed for geochemistry and environmental chemistry applications. They combine a built-in thermodynamic database (with values of e.g. equilibrium stability constants of complexes,

standard redox potential values etc.) with a numerical algorithm for solving the set of non-linear equations associated to simultaneous multiple equilibria in aqueous solution. In many cases, they also integrate models for the description of ion adsorption on surfaces or binding to natural colloids. Some of them also allow implementing mass transport and kinetic models, like ORCHESTRA (see http://www.macaulay.ac.uk/ORCHESTRA/) or PHREEQC (v. 3, see http://wwwbrr.cr.usgs.gov/projects/GWC_coupled/ phreeqc/index.html).

In the case of nanomaterial dispersions, these models can be very useful to calculate e.g. the expected values of solubility and free ion concentrations. Most of the studies reported have centred around the assessment of exposure and fate of nanomaterials in ecotoxicity and *in vitro* testing, with particular reference to several nanomaterials, such as silver (*19, 123-127*), zinc oxide (*23, 101-103, 128*), copper oxide (*37, 89*). Although of immense potential, users must be aware of several limitations that exist: a) an assumption of the existence of an equilibrium situation is made; b) results are strongly dependent on the reliability and accuracy of the reference thermodynamic data included in the software; c) calculations rely on thermodynamic data available from bulk materials (unless the database is updated manually by the user).

### 2.3.4 Which method?

The selection of appropriate methods to measure solubility is not trivial, as the selection of the technique is highly dependent of various factors e.g. the type of nanomaterial (and corresponding matrix). However, whatever analytical method chosen, an assessment must be made in relation to whether it fulfils analytical requirements being set. Eurochem, states that "*analytical measurements should be made to satisfy an agreed requirement i.e. to a defined objective and should be made using methods and equipment which have been tested to ensure that they are fit for purpose*". "Fit for purpose" implies that the technique/method must be sufficiently reliable (in relation to the level of: specificity or selectivity, accuracy, precision, detectability and sensitivity) and robust.

In order to satisfy the analytical requirements, researchers should look into the integration of various methods, in particular combining separation methods with detection/quantification methods. This is particular needed if an elemental spectroscopy based method is used in order to deduce the total dissolved material. For example, ICP-MS is a popular detection technique that has been coupled with AF4, ultracentrifugation (*129, 130*) and ultrafiltration (for Ag (*13, 19, 21, 22, 122, 127, 131, 132*), $CeO_2$ (*13, 22, 25*), Be (*133*), Au, ZnO and $TiO_2$ (*13*). Unlike the popularity of ICP-MS as a detection technique, only several studies have employed ICP-OES to study dissolution of different nanomaterial. They are often coupled to ultrafiltration (for separation) and UF-ICP-OES has been used to study: Ag (*134*) and ZnO (*6, 18, 23, 24*). The use of AAS to study nanomaterial solubility has been reported but this has been somewhat limited. AAS has been used (in conjunction with ultrafiltration) to determine the solubility of ZnO (*135*), Ag (*136, 137*) and CuO (*26*).

## 2.4 Experience from partners on solubility testing of nanomaterials

### 2.4.1 *In vitro* digestion *[UNamur; Julie Laloy]*

#### *2.4.1.1 Introduction*

The *in vitro* digestion model was used as a model to mimic the digestion process of nanoparticles after ingestion. It is a simply acellular model, which aims to be closer to the *in vivo* digestion. It is the first step in the determination of solubilisation of nanoparticles after ingestion. This model takes not into consideration the different status of stomach (empty or field with food).

#### *2.4.1.2 Procedure*

The fed *in vitro* digestion model is based on the model described by Walczak et al. (*138*). The different juices composing the *in vitro* digestion model are prepared on day 1. The pH are measured and adjusted after total dissolution of all components as indicated in Table 2. The solutions are stored overnight at room temperature in the incubator. About 2 h prior to the experiments, the incubator is switched on and set at 37 ± 2°C. The *in vitro* digestion model under fed conditions is applied on day 2. The total digestion model is composed of 1 ml saliva, 2 ml gastric juice, 2 ml duodenal juice, 1 ml bile juice and 333 µl $NaHCO_3$ added step by step. The pH of the total digestion juice is checked to be at 6.5 ± 0.5. If the pH is not comprised in this range, the digestion should not be started and the juices should be prepared again.

#### 2.4.1.3 Recommendations

We recommended the use of this model as a first screening test to assess the solubility of nanoparticles after potential ingestion.

*Table 2. Preparation of the juices for the fed in vitro digestion model*

| **Saliva** | | **Gastric** | | **Duodenal** | | **Bile** | |
|---|---|---|---|---|---|---|---|
| *Inorganic stock (RIKILT)* | Total 1 L | *Inorganic stock (RIKILT)* | Total 1 L | *Inorganic stock (RIKILT)* | Total 1 L | *Inorganic stock (RIKILT)* | Total 1 L |
| KCl (89.6 g/l) | 10 ml | NaCl (175.3 g/l) | 15.7 ml | NaCl (175.3 g/l) | 40 ml | NaCl (175.3 g/l) | 30 ml |
| KSCN (20 g/l) | 10 ml | $NaH_2PO_4 \cdot H_2O$ (102.1 g/l) | 3 ml | $NaHCO_3$ (84.7 g/L) | 40 ml | $NaHCO_3$ (84.7 g/L) | 68.3 ml |
| $NaH_2PO_4 \cdot H_2O$ (102.1 g/l) | 10 ml | KCl (89.6 g/l) | 9.2 ml | $KH_2PO_4$ (8 g/l) | 10 ml | KCl (89.6 g/l) | 4.2 ml |
| $Na_2SO_4$ (57 g/l) | 10 ml | $CaCl_2$ (30.2 g/l) | 10 ml | KCl (89.6 g/l) | 6.3 ml | HCl (37%) | 150 µl |
| NaCl (175.3 g/l) | 1.7 ml | $NH_4Cl$ (30.6 g/l) | 10 ml | $MgCl_2 \cdot 6H_2O$ (5 g/l) | 10 ml | $CaCl_2$ (30.2 g/l) | 5.5 ml |
| $NaHCO_3$ (84.7 g/L) | 20 ml | 37% HCl | 6.5 ml | HCl (37%) | 180 µl | | |
| | | | | $CaCl_2$ (30.2 g/l) | 5 ml | | |
| *Organic stock (RIKILT)* | | *Organic stock (RIKILT)* | | *Organic stock (RIKILT)* | | *Organic stock (RIKILT)* | |
| urea (25 g/l) | 8 ml | glucose (65 g/l) | 10 ml | urea (25 g/l) | 4 ml | urea (25 g/l) | 10 ml |
| | | glucuronic acid (2 g/l) | 10 ml | | | | |
| | | urea (25 g/l) | 3.4 ml | | | | |
| | | glucosamine-hydrochloride (33 g/l) | 10 ml | | | | |
| *Add to mixture* | | *Add to mixture* | | *Add to mixture* | | *Add to mixture* | |
| Amylase | 290 mg | BSA | 1000 mg | BSA | 1000 mg | BSA | 1800 mg |
| uric acid | 15 mg | pepsin | 2500 mg | pancreatin | 9000 mg | bile | 30 000 mg |
| Mucin | 25 mg | mucin | 3000 mg | lipase | 1500 mg | milli-Q water | fill to 1 L |
| milli-Q water | fill to 1 L | milli-Q water | fill to 1 L | milli-Q water | fill to 1 L | | |
| Measure the pH, it should be 6.8 ± 0.1. Adjust to the correct pH with NaOH (1 M) or HCl (37%) | | Measure the pH, it should be 1.3 ± 0.1 Adjust to the correct pH with NaOH (1 M) or HCl (37%). | | Measure the pH, it should be 8.1 ± 0.1. Adjust to the correct pH with NaOH (1 M) or HCl (37%). | | Measure the pH, it should be 8.2 ± 0.1. Adjust to the correct pH with NaOH (1 M) or HCl (37%). | |
| In addition the pH of the total digestion juice is measured (1 ml saliva, 2 ml gastric juice, 2 ml duodenal juice, 1 ml bile juice and 28 mg (26.5-29.5 mg) $NaHCO_3$). The pH has to be 6.5 ± 0.5. | | | | | | | |

### 2.4.2 Hydrodynamic chromatography (HDC) and Field Flow Fractionation (FFF) *[DLO-RIKILT; Meike van der Zande]*

#### 2.4.2.1 Introduction

In order to measure dissolution of nanomaterials several methods rely on separation of the particulate from the free ionic fraction before measurement, as measurement methods (*e.g.* ICPMS, ICP-OES, AAS, etc.) are often not able to distinguish between the two fractions. Hydrodynamic chromatography (HDC) and Field Flow Fractionation (FFF) are two separation methods worth considering. HDC is a solution-phase separation

method (*139*), the method may be employed in an open tube (capillary) or in a column packed with nonporous inert particles (Figure 1A). When flowing an eluens through the capillary or column different flow profiles are created and nanoparticles can be separated in these varying flow streams in a size dependent manner. Using either a capillary or column separation arises from the parabolic flow profiles that develop. The flow is fastest in the centre and slowest near the walls and larger nanoparticles will remain in or near the centre of the flow whereas smaller particles will be located on the sides of the parabolic flow. Therefore, the largest particles will be first to elute followed by the smaller particles.

The principle of Field Flow Fractionation (FFF) has been described in detail in the second chapter (*i.e.* state-of-the-art) of this report. Asymetrical flow FFF or AF4 has been most refined over the last decades with respect to separation and characterization of various nanomaterials. Briefly, with AF4 nanoparticles are loaded into a parabolic fluid flow inside a flow chamber (Figure 1B). Separation is caused by a cross-flow perpendicular to the direction of this flow. The cross-flow will direct the nanoparticles to an accumulation wall (*i.e.* a semipermeable membrane lying on top of a supporting frit) and separation is driven by differences in diffusion of the nanoparticles. Smaller nanoparticles have higher diffusion rates and will therefore be transported at a higher flow speed in the parabolic flow profile than larger ones.

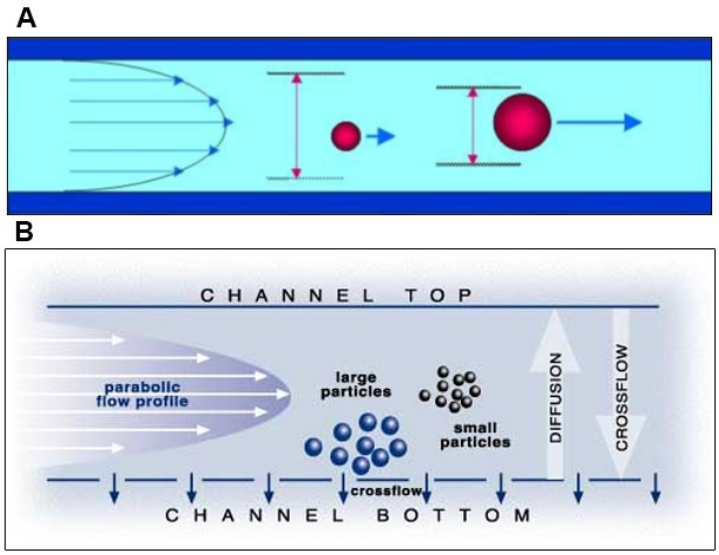


*Figure 1: Principle of NP separation by A) hydrodynamic chromatography and B) field-flow fractionation.*

#### *2.4.2.1 Discussion and conclusions*

The advantage of HDC is that the method is robust, relatively cheap, and often easy accessible. Furthermore, as separation is driven only by size making the outcome easier to interpret and calculation models have been described in literature. However, the disadvantage of HDC is that the separation resolution is rather low. As a consequence, it will not be possible to separate very small particles from the ionic fraction, what deemed this technique not suitable to study dissolution of nanoparticles. Therefore, in this project this technique was not pursued any further.

FFF has several advantages over other separation techniques for the separation of nanomaterials, as also described in detail in the second chapter of this report. In brief, one of the biggest advantages of this technique is the high separation resolution in comparison to other size separation techniques like HDC. Because of this high separation power particulate matter could be separated from the dissolved fraction, but also original particles could possibly be separated from particulate matter that was newly formed after dissolution. The latter fraction contributes to the dissolved fraction, but could be missed using other solubility testing separation techniques. Furthermore, FFF does not comprise a stationary phase so there is no risk of interactions (possibly very strong or even irreversible) between the nanoparticles and the stationary phase. As separation is only driven by size, the outcome is easy to interpret and FFF is applicable for analysis of heterogeneous samples (*e.g.* complex biological matrices), thereby reducing the need for sample pre-processing. Finally, due to the use of low shear rates the method is a very “soft” fractionation method compared to other methods. The downside of FFF however is that it requires dedicated expensive equipment which is often not easily accessible. The soluble (dissolved) fraction will be transported through the membrane by the cross-flow, which may be collected and measured as a separate fraction. The first consideration is the choice of membrane, which should have a sufficiently low pore size, not allowing

passage of small particles. Secondly, the FFF channel can easily be overloaded and often requires dilution of the sample, the cross-flow will even further dilute the sample, which could make detection very challenging. Therefore, a very sensitive detector is required and a relatively high concentration of the sample. In this project we strived to develop and evaluate techniques that are broadly applicable (*i.e.* including measurement in samples with low concentrations and with low dissolution values) and easy accessible, therefore it was decided not to continue with this technique.

### 2.4.3 Single particle inductively coupled plasma mass spectrometry (spICP-MS) *[DLO-RIKILT; Meike van der Zande]*

#### *2.4.3.1 Introduction*

Inductively coupled plasma mass spectrometry (ICP-MS) or atomic emission spectrometry (ICP-AES) is used to identify the amount and type of elements in a sample. Both techniques are described in detail in chapter 2. In summary, a sample is introduced into an ICP where it is ionized or atomized creating atoms and ions as a source for AES and ions as a source for MS. In ICP-AES, the optical spectrometer collects the UV-visible radiation emitted by excited atoms and ions and separates the individual wavelengths of radiation and focuses them onto a detector. In ICP-MS, ions are extracted through an interface into a mass spectrometer, where they are separated according to their mass/charge ratio followed by detection.

ICP-MS may be used to detect the amount and type of elements in a sample, but it can also be used to specifically detect metallic nanoparticles when used in single particle mode. In nanomaterial research single particle ICP-MS (SP-ICP-MS) is increasingly being used for the detection and quantification of individual nanoparticles. By acquiring a high number of individual intensity readings with a very short dwell time at very low nanoparticle concentrations individual nanoparticles can detected as high intensity peaks as a function of the time. The intensity of the peaks is proportional to the mass of the nanoparticle and the number of the peaks is proportional to the number of particles in the solution (see chapter 2 for more in-depth information). At present, SP-ICP-MS is mainly employed for the determination of particle size and number concentrations, but it has been shown to be applicable for dissolution measurements.

This method requires relatively easy accessible equipment, limited sample preparation, and no separation before measurement. DLO-RIKILT evaluated the suitability this method for solubility testing in a complex matrix.

#### *2.4.3.2 Materials and methods*

As a model for a complex matrix the *in vitro* human digestion model, as described in chapter 2.4.1, was used. The model consists of three phases mimicking the mouth, stomach and intestines and samples for ICP-MS (*i.e.* to measure the “total” elemental amount) and SP-ICP-MS measurement (*i.e.* to measure only the amount of NPs) were taken at the end of the complete digestion process (Figure 2). Two nanomaterials were selected for measurement (*i.e.* NM-300K and NM-101). The materials were dispersed according to the NANoREG guidance document and measured with DLS according to the NANoREG SOP. For ICP-MS measurement, the samples were pre-processed with the appropriate destruction process for the element of interest and the total amount (*i.e*. particulate matter and ions) of the element was measured. Ag samples were destructed by addition of 0.5 ml $HNO_3$ (70 vol%) and 1.5 ml HCl (37 vol%) to 1 ml sample and incubation in a water bath at 60°C for 30 minutes. $TiO_2$ samples were destructed by addition of 2 ml $H_2O_2$ (40 vol%), 2 ml HF (30 vol%), and 6 ml $HNO_3$ (70 vol%) to 1 ml sample, followed by a microwave treatment. For SP-ICP-MS measurement, the samples were diluted to the appropriate concentration for measurement and the mass, number and concentration of the particles in the dispersion were measured in single particle ICP-MS mode. The data from the total ICP-MS and SP-ICP-MS measurement was used to calculate the percentage of dissolution as follows:

([element ICP-MS] - [element SP-ICP-MS] / [element ICP-MS])*100 = % dissolution

Both materials were analysed as a dilution series in order to evaluate whether the nanomaterial concentration had an impact on the dissolution results. Concentrations used were: 0.5, 2.5, 5, 10, and 50 µg/ml in the final digestive juice (*i.e.* after completion of the whole digestion process) and six replicates (each

separately digested) for each concentration were used. In order to evaluate the efficacy of this method DLO-RIKILT used the exact same study setup (*i.e.* the same materials at the same concentrations, *in vitro* digested), but now instead of using SP-ICP-MS to measure the amount of NPs, ultrafiltration was used to separate the particulate matter from the dissolved fraction followed by ICP-MS measurement (which then only measures the free ionic dissolved fraction). These results are discussed in more detail in chapter 2.4.4, but in this chapter they are shown for comparison.

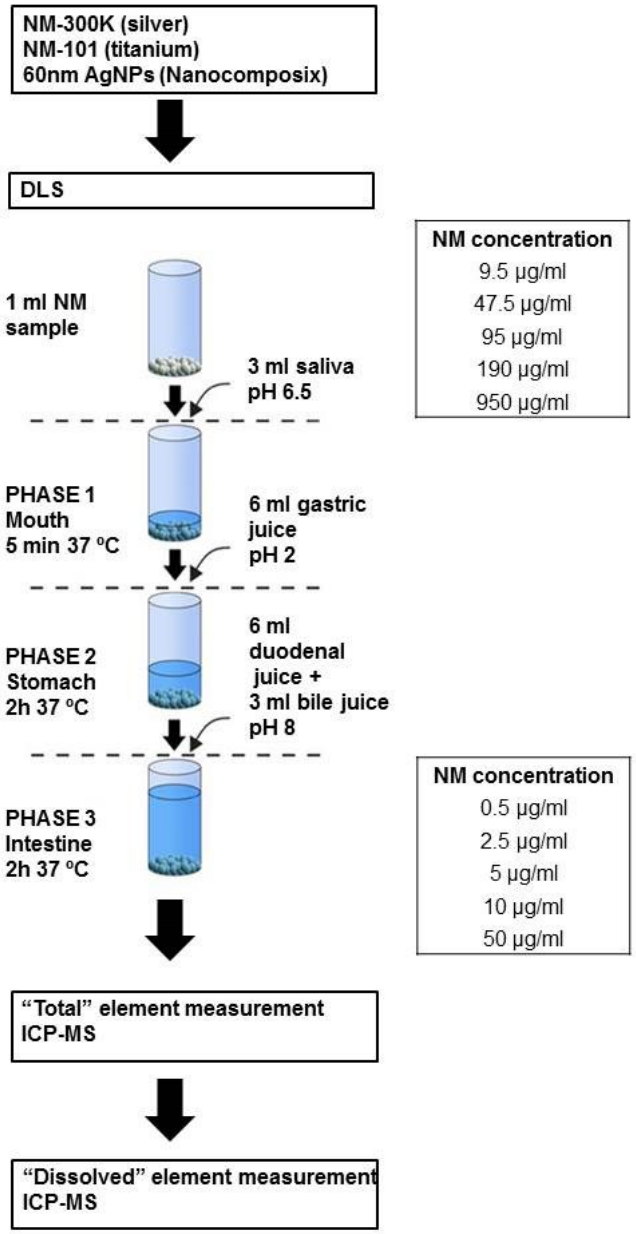


*Figure 2: Schematic depiction of the study design for dissolution measurement of NM-300K and NM-101 in a complex matrix, consisting of digestion juices from the in vitro digestion model, using (sp)ICP-MS.*

### *2.4.3.3 Results and discussion*

Using SP-ICP-MS measurement the silver NM-300K material showed dissolution of the material in the range of 70-90% of the total mass (Figure 3 A and B). Dissolution appeared to not to be concentration dependent. Silver nanomaterials are known to dissolve, although this percentage of dissolution appears to be rather high, especially when comparing the results of SP-ICP-MS measurement with those of UF-ICP-MS measurement (discussed in the following chapter). The reason for this high amount of measured dissolved silver is most likely due to the type of material that was measured. The NM-300K material contains particles

with an average size of ~15 nm and > 99 % number of particles <20 nm (by TEM measurement). The size detection limit of SP-ICP-MS measurement lays around 20 nm. Measurement of the materials in ultrapure water indicated that a large fraction of the material could not be detected; assuming that the material was not dissolved to a high extend in water. Therefore, it is very likely that a large fraction of the NM-300K NPs was not detected by SP-ICP-MS, and that the calculated fraction of dissolved silver is in fact an overestimation. Comparison with literature is complicated as highly variable dissolution of AgNPs has been reported, strongly depending on the material, the type of matrix, and the type of separation and detection technique.

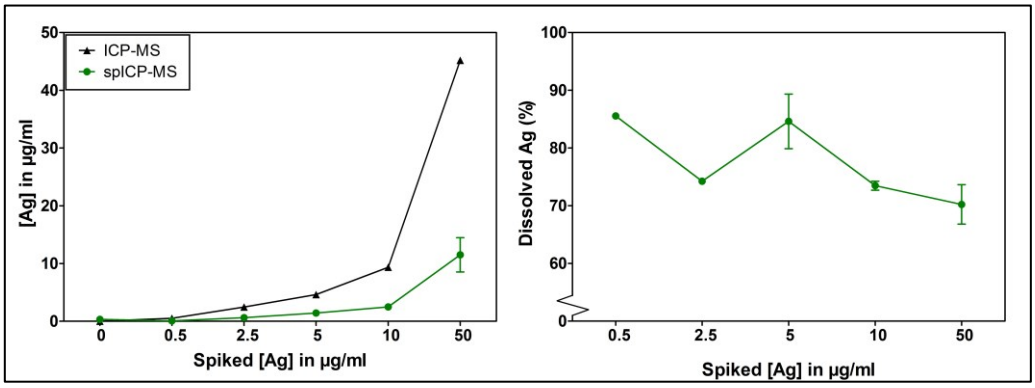


*Figure 3: A) ICP-MS and SP-ICP-MS Ag measurements after complete in vitro digestion in µg/ml ± SEM, B) calculated dissolution rate of NM-300K as a percentage ± SEM of the total mass.*

For the $TiO_2$ NM-101 material we also observed considerable dissolution of the material with SP-ICP-MS measurement, namely in the range of 30-50% (Fig 4A and B). However, only limited to no dissolution was expected as described in most available literature and as also seen in the UF-ICP-MS results that are discussed in the next chapter. Again, the high percentage of dissolution, observed by SP-ICP-MS, is likely caused by the size limit of detection of the SP-ICP-MS technique, which lies around 50 nm for $TiO_2$ NPs. NM-101 consists of aggregates ranging from 10 to 170 nm of which 77.3% is <50 nm (by TEM measurement). Measurements with SP-ICP-MS of NM-101 in water indicated that indeed a fraction of approximately 10% would be missed by SP--ICP-MS, but this does not account for the observed 30-50%. However, it could be possible that the harsh environment in the digestion juices caused larger aggregates to break up into smaller aggregates below the size detection limit.

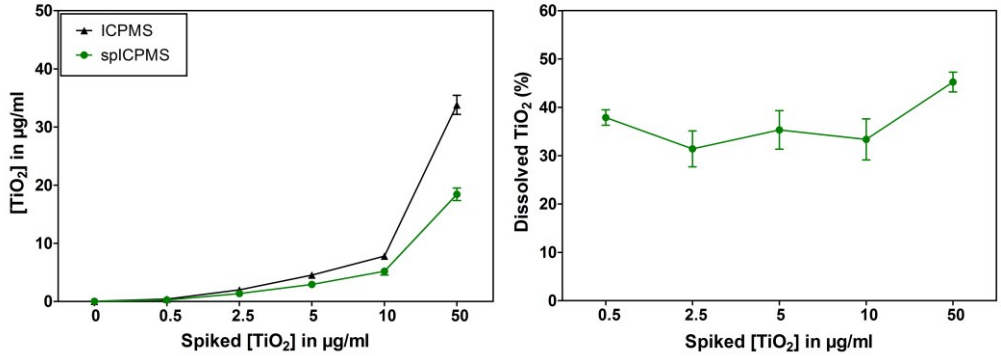


*Figure 4: A) ICP-MS and spICP-MS $TiO_2$ measurements after complete in vitro digestion in µg/ml ± SEM, B) calculated dissolution rate of NM-101 as a percentage ± SEM of the total mass.*

As the material properties of the selected NANoREG core materials were not ideal for testing this method (*i.e.* NM sizes were partly below the detection limit) DLO-RIKILT also performed the same experiment on 60 nm AgNPs purchased from Nanocomposix as a proof-of principle. As the size of the AgNPs were well above the detection limit, all particles could be detected with certainty. Dissolution was shown to lie between 24% and 55% of the total amount of silver and it appeared to be concentration independent (Table 3). Comparison with the UF-ICP-MS results (*i.e.* dissolution <0.1%; as discussed in the next chapter) shows a significantly higher dissolution values when using spICP-MS. These differences lie in the fact that silver ions can form complexes with components of the matrix which, when using UF, may be filtered from the solution (for more detailed information see next chapter). This clearly indicates that spICP-MS is likely more suitable

for dissolution measurements in biological matrices when the material is known to interact with the matrix. However, the size detection limit of the technique should be taken into account.

*Table 3: (sp)ICP-MS Ag measurements of DLO-RIKILT after complete in vitro digestion of 60 nm AgNPs (Nanocomposix). The total amount of silver in the dispersion was measured with ICP-MS and the amount of NPs in the dispersion was measured with SP-ICP-MS and given in µg/ml ± SEM. From these results the dissolution of the AgNPs was calculated as a percentage of the total mass.*

| | |
|---|---|
| Total concentration Ag ICP-MS | 0.00 µg/ml<br>0.37 µg/ml<br>2.43 µg/ml<br>5.26 µg/ml<br>9.98 µg/ml |
| Concentration of AgNPs and calculated percentage of dissolution SP-ICP-MS | 0.00 µg/ml<br>0.17 µg/ml (55%)<br>1.38 µg/ml (43%)<br>4.01 µg/ml (24%)<br>6.58 µg/ml (34%) |

#### *2.4.3.4 Conclusion and recommendations*

These results illustrate very clearly that in depth knowledge of the size of the material and its behaviour in the matrix is essential for choosing the best suitable detection method for solubility measurements. SP-ICP-MS could be a promising technique to study the total dissolution of nanomaterials, especially when the materials are known to have a high affinity to salts and/or proteins in the matrix, but the size detection limit may be limiting. Future research is currently focussing on lowering the size detection limits of SP-ICP-MS what would make this technique very promising for future applications.

### 2.4.4 Ultrafiltration - ICP-MS/ICP-AES *[DLO-RIKILT (lead); Meike van der Zande, IIT Stefania Sabella, UdL; Carlos Rey-Castro]*

#### *2.4.4.1 Introduction*

Several separation techniques that may be used to separate particulate matter from the dissolved fraction before detection have been discussed in the previous paragraphs and in chapter 2.3 (state-of-the-art). One of these methods is the use of filters in the form of ultrafiltration (UF). UF filters consist of semipermeable filters in a centrifugation tube; filtration is driven by pressure caused by centrifugal forces. UF filters are available with pore sizes in the range of 1 – 100 kDa (1-3 kDa is smaller than 1 nm) and have been used to study the solubility/dissolution of nanomaterials in the past. UF can be coupled to various elemental detection techniques like ICP-MS, ICP-AES and AAS.

UF is an affordable and easily accessible technique and does not require in-depth nanomaterial knowledge for measurement. Furthermore, once the material is separated and destructed for analysis it does not require immediate analysis, which adds flexibility to the technique. Therefore, these techniques are regarded as some of the most promising techniques and were further evaluated by DLO-RIKILT, IIT, and UdL for its applicability in solubility testing in a complex matrix.

#### *2.4.4.2 Materials and methods*

The model that was used as a complex matrix was an *in vitro* digestion model (as discussed in chapter 2.4.1) for which the experimental procedure, stock solutions, and order numbers for the additional enzymes were distributed by DLO-RIKILT. A schematic depiction of the general study design is given in Figure 5, the concentrations and processing methods used by each partner are given in Table 4. To separate the particulate fraction from the dissolved fraction UF AmiconUltra ultrafiltration tubes containing a cellulose membrane with a 3 kDa cut-off value were used. For this, 4 ml sample was ultra-filtered at 4000g for 40 min at RT. After UF 1 mL (DLO-RIKILT, UdL) or 4 mL (IIT) was taken from the filtrate and destructed for "dissolved" element measurement (*i.e.* measurement of free dissolved fraction). The data from the "total" and "dissolved" element measurements were used to calculate the percentage of dissolution as follows:

(["dissolved" element] / ["total" element])*100 = % dissolution (DLO-RIKILT, IIT)

Several nanomaterials were selected for measurement (Figure 5). The materials were dispersed according to the NANoREG guidance document and measured with DLS according to the NANoREG SOP. All materials were analysed at several concentrations (Table 4) and either 6 (DLO-RIKILT) or 3 (IIT, UdL) replicates per concentration were used.

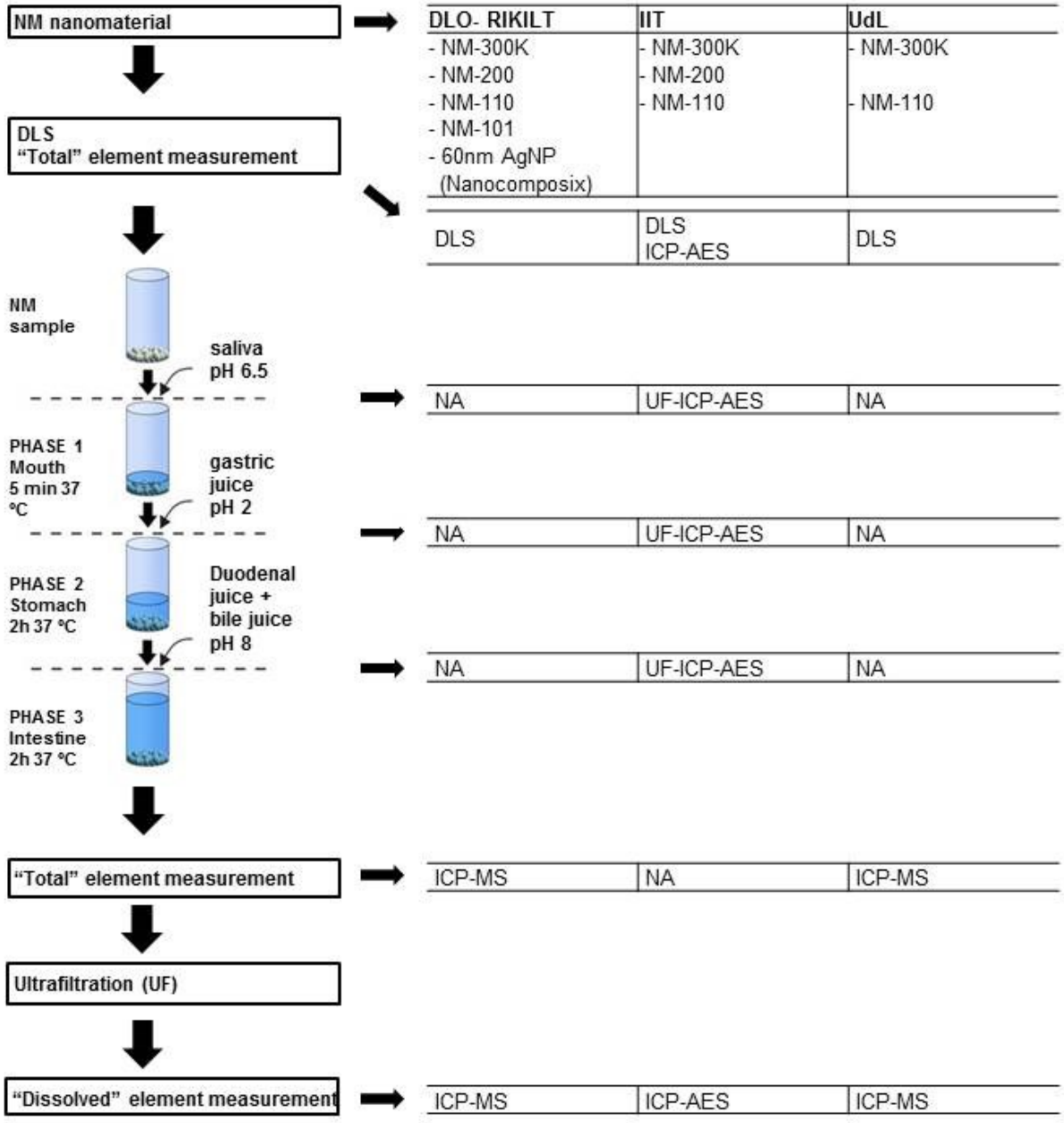


*Figure 5: Schematic depiction of the study design for dissolution measurement of nanomaterials in a complex matrix consisting of digestion juices using UF-ICP-MS/AES.*

*Table 4: Overview of study setup used by the different partners (i.e. DLO-RIKILT, IIT, UdL).*

| | DLO- RIKILT | IIT | UdL | |
|---|---|---|---|---|
| | **all NM materials** | **all NM materials** | **NM-300K** | **NM-110** |
| **Concentration nanomaterial at start of *in vitro* digestion (theoretical)** | 9.5 µg/ml<br>47.5 µg/ml<br>95.0 µg/ml<br>190.0 µg/ml<br>950.0 µg/ml | 47.5 µg/ml<br>950.0 µg/ml | 1.29 mg/ml<br>12.99 mg/ml<br>26.01 mg/ml | 9.75 µg/ml<br>97.5 µg/ml<br>195.0 µg/ml |
| **Concentration nanomaterial after *in vitro* digestion (theoretical)** | 0.50 µg/ml<br>2.50 µg/ml<br>5.00 µg/ml<br>10.0 µg/ml<br>50.0 µg/ml | 1.28 µg/ml<br>25.7 µg/ml | 33.0 µg/ml<br>333.0 µg/ml<br>667.0 µg/ml | 0.25 µg/ml<br>2.50 µg/ml<br>5.00 µg/ml |
| **Total volume at end of *in vitro* digestion** | 19 ml (scaled down model) | 37 ml (standard model) | 39 ml (standard model with addition of 2 ml $NaHCO_3$) | |
| **Destruction process Ag** | 0.5 ml $HNO_3$ (70 vol%) + 1.5 ml HCl (37 vol%), 60°C water bath for 30 minutes | 0.5 mL $HNO_3$ (70%) room temperature over night | 0.5 ml $HNO_3$ (70 vol%) + 1.5 ml HCl (37 vol%), 60°C water bath for 30 minutes | |
| **Destruction process $SiO_2$/$TiO_2$** | 2 ml $H_2O_2$ (40 vol%) + 2 ml HF (30 vol%) + 6 ml $HNO_3$ (70 vol%), microwave treatment | 0.5 mL aqua regia | | |
| **Destruction process ZnO** | 10 ml of $HNO_3$ (70 vol%), microwave treatment | 0.5 mL aqua regia | 9 mL $HNO_3$ (2%) | |

*This project has received funding from the European Union Seventh Framework Programme (FP7/2007-2013) under grant agreement no 310584*

### 2.4.4.3 Results and discussion

**DLS and TEM.** The hydrodynamic size of the materials after dispersion was measured with DLS and the results are given in Table 5. The materials were also evaluated in the different phases of the *in vitro* digestion model by IIT using DLS and TEM and the results of the TEM data of NM-300K, NM-200, and NM-110 are shown in Figure 6. DLS and TEM analysis showed that aggregation of NM-300K and NM-200 occurred already in the gastric phase and more pronounced in the intestinal phase. Higher concentrations also seemed to induce more aggregation of the materials than lower concentrations. For NM-110, DLS and TEM data reported huge aggregation. One should take into account that DLS data obtained from the digestive juices should be interpreted with caution as the high ionic strength and the high concentration of proteins in the digestive juices, as well as the high concentrations of NPs have been described in literature to affect the measurement.

*Table 5: DLS measurement results for the NM materials after dispersion according to the NANoREG guidance document.*

| | **RIKILT-DLO** | | **IIT** | | **UdL** | |
|---|---|---|---|---|---|---|
| | size | PDI | size | PDI | size | PDI |
| **NM-300K** | 178 nm | 0.26 | 154 nm | 0.22 | 61.7 | 0.35 |
| **NM-200** | 258 nm | 0.32 | 201 nm | 0.27 | | |
| **NM-101** | 549 nm | 0.33 | | | | |
| **NM-110** | 2044 nm | 0.27 | 1216 nm | 0.37 | 213.2 | 0.14 |
| **10nm PVP-AgNP (Nanocomposix)** | | | | | | |
| **60nm AgNP (Nanocomposix)** | 62.1 nm | 0.24 | | | | |

*This project has received funding from the European Union Seventh Framework Programme (FP7/2007-2013) under grant agreement no 310584*

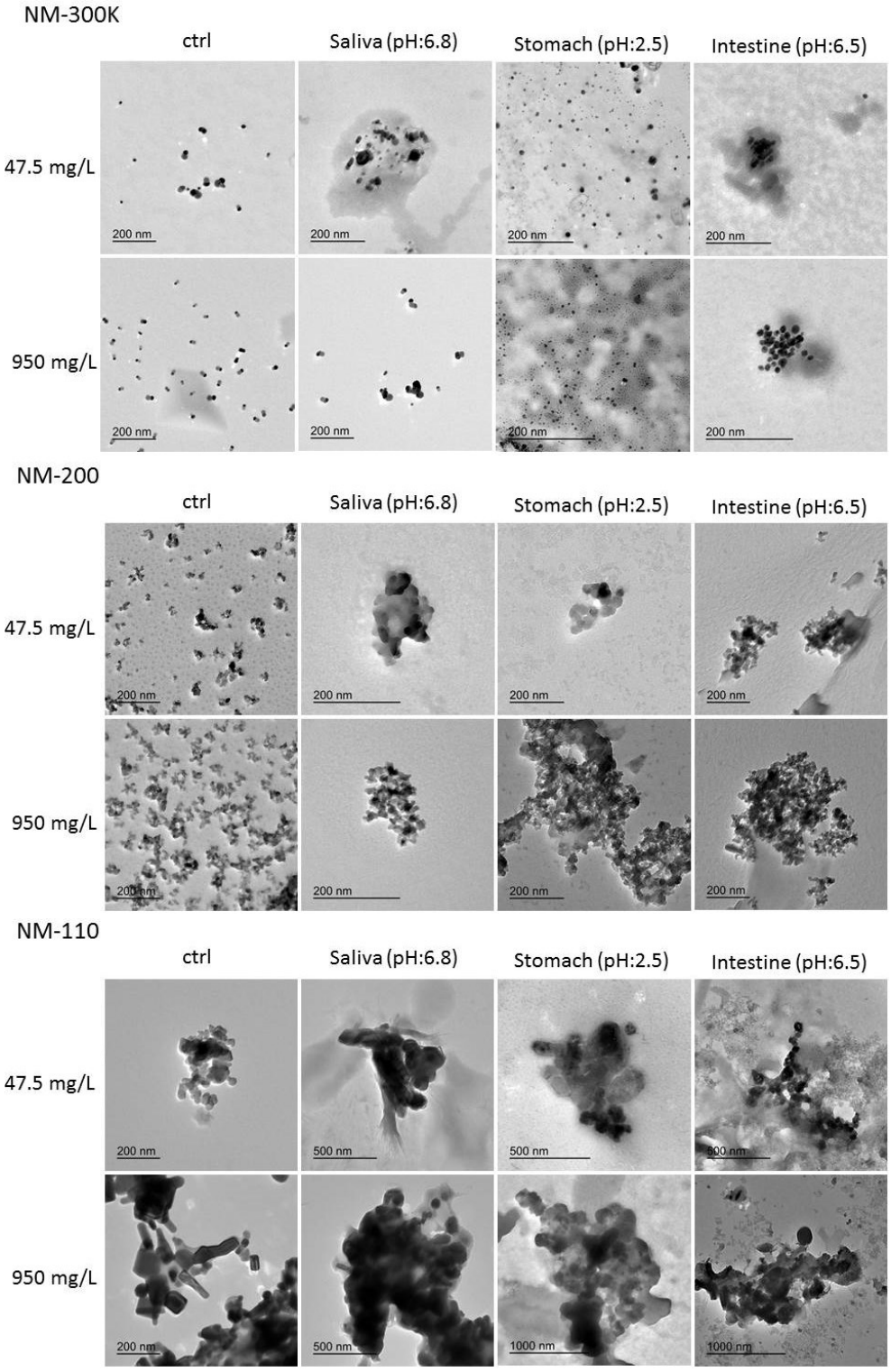


*Figure 6: TEM images from IIT of NM-300K, NM-200, and NM-110 in suspension (control), in saliva, in the stomach phase, and in the intestinal phase.*

**Elemental ICP-MS/AES analysis.** Evaluation of the "total" element concentration in all dispersions showed in general a good correlation between the spiked (theoretical) concentrations and the measured concentrations with the exception of the $SiO_2$ (NM-200) materials (Table 6, 7, 8). At DLO-RIKILT, NM-200 showed a high concentration of $SiO_2$ (*i.e.* ~30-40 µg/ml) for the theoretical 0.5, 2.5, 5, and 10 µg/ml concentrations without a concentration dependent increase (Table 6). The reason for these deviating results in the $SiO_2$ samples likely lies in the fact that $SiO_2$ is an element that is abundantly present in nature, meaning that it could have been present in the digestion mixture, but it could have also been caused by the presence of $N_2$ and CO (which have elemental masses equal to Si) in the mixture, which interferes with the measurement resulting in high background noise.

*Table 6: ICP-MS results (i.e."total" element analysis) from DLO-RIKILT for different types of NM materials after in vitro digestion.*

| NPs | Spiked (theoretical) concentration Ag, $SiO_2$, $TiO_2$, ZnO in mg/L | Concentrations Ag, $SiO_2$, $TiO_2$ and ZnO measured by ICP-MS in mg/L |
|---|---|---|
| NM-300K | 0.5 | 0.51 ± 0.05 |
| | 2.5 | 2.47 ± 0.22 |
| | 5 | 4.63 ± 0.17 |
| | 10 | 9.35 ± 0.21 |
| | 50 | 45.2 ± 0.51 |
| NM-200 | 0.5 | 25.0 ± 2.59 |
| | 2.5 | 39.0 ± 3.6 |
| | 5 | 41.2 ± 6.3 |
| | 10 | 42.7 ± 1.8 |
| | 50 | 68.7 ± 5.2 |
| NM-110 | 0.5 | 0.91 ± 0.04 |
| | 2.5 | 2.51 ± 0.41 |
| | 5 | 4.01 ± 0.34 |
| | 10 | 7.80 ± 0.13 |
| | 50 | 39.50 ± 0.54 |
| NM-101 | 0.5 | 0.42 ± 0.04 |
| | 2.5 | 1.99 ± 0.16 |
| | 5 | 4.54 ± 0.13 |
| | 10 | 7.79 ± 0.43 |
| | 50 | 33.8 ± 3.66 |
| 60nm AgNPs (Nanocomposix) | 0.5 | 0.37 ± 0.01 |
| | 2.5 | 2.43 ± 0.03 |
| | 5 | 5.08 ± 0.38 |
| | 10 | 9.90 ± 0.39 |

*Table 7: ICP-AES results (i.e."total" element analysis) from IIT for different types of NM materials before in vitro digestion.*

| NPs | Theoretical [NP] in mg/L | [batch element] measured by ICP-AES in mg/L |
|---|---|---|
| NM-300K | 950<br>47,5 | 783<br>44.5 |
| NM-200 | 950<br>47,5 | 325<br>16.5 |
| NM-110 | 950<br>47,5 | 617<br>39 |

*Table 8: ICP-MS results (i.e."total" element analysis) from UdL for different types of NM materials after in vitro digestion.*

| | | |
|---|---|---|
| | | |
| | | |

**Dissolution of NM-300K.** The silver NM-300K material was evaluated by DLO-RIKILT, IIT, and UdL. Results from DLO-RIKILT are given in Table 9. ICP-MS measurements (before and after UF) showed that free soluble ions were almost absent after complete *in vitro* digestion (*i.e.* with a highest percentage of 0.85%). DLO-RIKILT also tested 60 nm AgNPs (Nanocomposix) that were used as proof-of-principle material for spICP-MS measurements. Also this material showed very low dissolution with a maximum of 0.08% dissolution. Results from IIT are given in Figure 8. ICP-AES measurements (before and after UF) showed that dissolution of AgNPs primarily occurred in the gastric compartment. Partial aggregation of released ions in the stomach/intestine/bile fluid was also observed. After complete digestion 1.6% and 0.8% Ag dissolution was measured for the lowest (47.5 µg/mL) and highest (950 µg/mL) concentrations respectively. The reduced dissolution at the highest concentration could have been caused by a progressive aggregation that indeed appears more pronounced at these values (as indicated also by the DLS and TEM data), which in part may cause filter clogging. Results from UdL are given in Table 10. The data suggest that 0-3% of NM300K (Ag) is "dissolved", in the range of concentrations studied. Differences between filtered and non-filtered blanks were as high as 0.03-0.70 µg/mL (Ag).

*Table 9: ICP-MS Ag measurements of DLO-RIKILT after complete in vitro digestion before and after UF in µg/ml ± SEM, and the calculated dissolution of NM-300K as a percentage of the total mass.*

| **NM-300K** | |
|---|---|
| Total concentration Ag | 0.51 µg/ml<br>2.47 µg/ml<br>4.63 µg/ml<br>9.35 µg/ml<br>45.2 µg/ml |
| Dissolved concentration Ag | 0.00008 µg/ml (0.02%)<br>0.00117 µg/ml (0.05%)<br>0.00000 µg/ml (0.00%)<br>0.00905 µg/ml (0.10%)<br>0.38550 µg/ml (0.85%) |
| **60 nm AgNP (Nanocomposix)** | |
| Total concentration Ag | 0.37 µg/ml<br>2.43 µg/ml<br>5.08 µg/ml<br>9.90 µg/ml |
| Dissolved concentration Ag | 0.00008 µg/ml (0.02%)<br>0.00202 µg/ml (0.08%)<br>0.00384 µg/ml (0.08%)<br>0.00735 µg/ml (0.07%) |

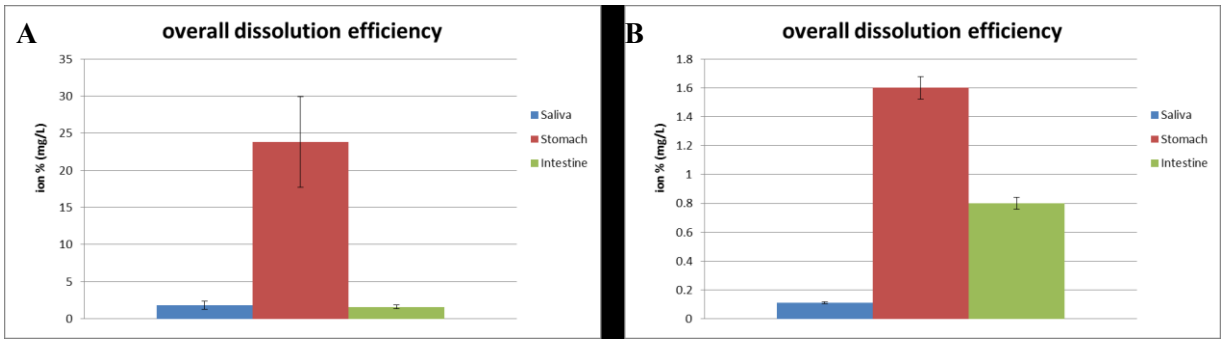


*Figure 8: Calculated dissolution rate of NM-300K in each phase of the in vitro digestion as a percentage of the total mass measured with ICP-AES by IIT. A) Spiked at a concentration of 47.5 mg/L, and B) spiked at a concentration of 950 mg/L*

*Table 10: ICP-MS Ag measurements of UdL after complete in vitro digestion before and after UF and the calculated dissolution rate of NM-300K as a percentage of the total mass.*

| | |
|---|---|
| Total concentration Ag | 31.3 µg/ml<br>337.5 µg/ml<br>695.0 µg/ml |
| Dissolved concentration Ag | 0.0 µg/ml (0%)<br>4.8 µg/ml (1.4%)<br>21.7 µg/ml (3.1%) |

Comparison of the dissolution behaviour of NM-300K as analysed by DLO-RIKILT, IIT, and UdL shows that there only minor differences in the outcomes, all indicating very low (<5%) dissolution of NM-300K. Furthermore, the results did not indicate a clear correlation between the NM-300K concentration and the percentage of dissolution. The IIT measurements in the different phases of digestion indicate that dissolution of AgNPs primarily occurred in the gastric compartment, whereas in the intestinal phase the amount of free $Ag^+$ appeared to decrease. It must be pointed out that, in this context, "dissolved" means that the NM is transformed into chemical species not retained by a 3kDa ultrafiltration membrane, which does not mean that the remaining silver of the initial NM should necessarily persist as such nanomaterial after the digestion procedure. Silver ions are known to form silver salts with for instance chloride and sulphur, they have also been described to have a high affinity to thiol groups in proteins. In the digestive juices a high concentration of salts and proteins containing thiol groups are present, so it is therefore possible that not all dissolved silver will be present as "free" $Ag^+$ in the mixture and was filtered out or of the mixture pelleted during UF. Another limitation of UF relates to potential interactions of the membrane with the nanomaterial and the dissolved free $Ag^+$ although previous results by DLO-RIKILT with NM-300K and the same UF tubes indicated that this did not occur (van der Zande et al., ACSNano, 2012).

**Dissolution of NM-110.** The ZnO NM-110 material was evaluated by DLO-RIKILT, IIT, and UdL. The results from DLO-RIKILT are shown in Table 11. NM-110 clearly dissolved, although dissolution proved to be variable between 25-65%. The results from IIT are shown in Figure 10. Data indicate that complete dissolution of NM-110 occurred in the gastric compartment corresponding to the 100% of dissolution. Partial aggregation of a small amount of released ions in the intestine/bile fluid was also observed. The data obtained by UdL suggest that 50-67% of NM110 (ZnO) is "dissolved", in the range of concentrations studied (Table 12).

*Table 11: ICP-MS ZnO measurements of DLO-RIKILT after complete in vitro digestion before and after UF in µg/ml ± SEM, and the calculated dissolution of NM-110 as a percentage of the total mass.*

| | |
|---|---|
| Total concentration ZnO | 0.91 µg/ml<br>2.51 µg/ml<br>4.01 µg/ml<br>7.8 µg/ml<br>39.5 µg/ml |
| Dissolved concentration ZnO | 0.56 µg/ml (62%)<br>1.16 µg/ml (48%)<br>1.88 µg/ml (47%)<br>5.14 µg/ml (66%)<br>9.96 µg/ml (25%) |

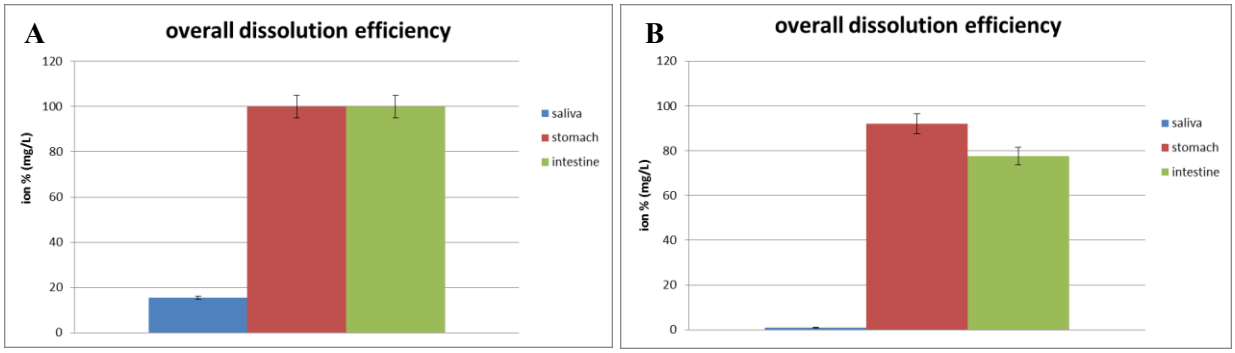


*Figure 10: Calculated dissolution rate of NM-110 in each phase of the in vitro digestion as a percentage of the total mass measured with ICP-AES by IIT. A) Spiked at a concentration of 47.5 mg/L, and B) spiked at a concentration of 950 mg/L*

*Table 12: ICP-MS ZnO measurements of UdL after complete in vitro digestion before and after UF and the calculated dissolution rate of NM-110 as a percentage of the total mass.*

| | |
|---|---|
| Total concentration ZnO | 0.26 µg/ml<br>2.23 µg/ml<br>5.09 µg/ml |
| Dissolved concentration ZnO | 0.13 µg/ml (50%)<br>1.4 µg/ml (63%)<br>3.39 µg/ml (67%) |

Clearly, NM-110 dissolved to a high extend as shown by all partners, which is in correlation with the literature were a high level of dissolution has frequently been reported. ZnO NPs are highly soluble at low pH, like during the stomach phase. In support of this, IIT also investigated the dissolution of similar ZnO NPs (NM-111) using a simplified model (*i.e.* water at pH 4,5) finding a total dissolution also at these conditions. The results from IIT indicated aggregation of a small amount of released ions in the intestinal/bile fluid, which also supports the somewhat lower dissolution values observed by DLO-RIKILT and UdL in the intestinal phase. As with silver, free $Zn^{2+}$ could interact with components of the digestion juices or with the UF membrane leading to an underestimation of the total dissolution that takes place.

**Dissolution of NM-200.** The $SiO_2$ NM-200 material was evaluated by DLO-RIKILT and IIT. The results of DLO-RIKILT are shown in Table 13. However, due to the high background noise during detection of the NM-200 samples it was unclear what fraction of the detected signal was caused by the NM-200 material or by the background (as discussed above). Therefore, it was decided to further disregard the NM-200 samples for evaluation of the dissolution.

The results from IIT are shown in Figure 11. IIT was able to measure lower $SiO_2$ concentrations than DLO-RIKILT, which is likely due to differences in the detection technique (*i.e.* MS vs. AES). Data indicate that dissolution of NM-200 primarily occurs in saliva and intestine compartments. A progressive aggregation of NPs was observed at both concentration values (as also shown by DLS and TEM data discussed above). It seems that parameters primarily influencing dissolution of NM-200 are matrix composition and mean residence time in each compartments. Acidic pH seems not to have a specific effect.

*Table 13: ICP-MS $SiO_2$ measurements of DLO-RIKILT after complete in vitro digestion before and after UF in µg/ml ± SEM, and the calculated dissolution of NM-200 as a percentage of the total mass.*

| | |
|---|---|
| Total concentration $SiO_2$ | 25.0 µg/ml<br>39.0 µg/ml<br>41.3 µg/ml<br>42.7 µg/ml<br>68.7 µg/ml |
| Dissolved concentration $SiO_2$ | 10.4 µg/ml (42%) |

| | |
|---|---|
| | 20.0 µg/ml (52%)<br>20.5 µg/ml (50%)<br>21.5 µg/ml (51%)<br>18.1 µg/ml (29%) |

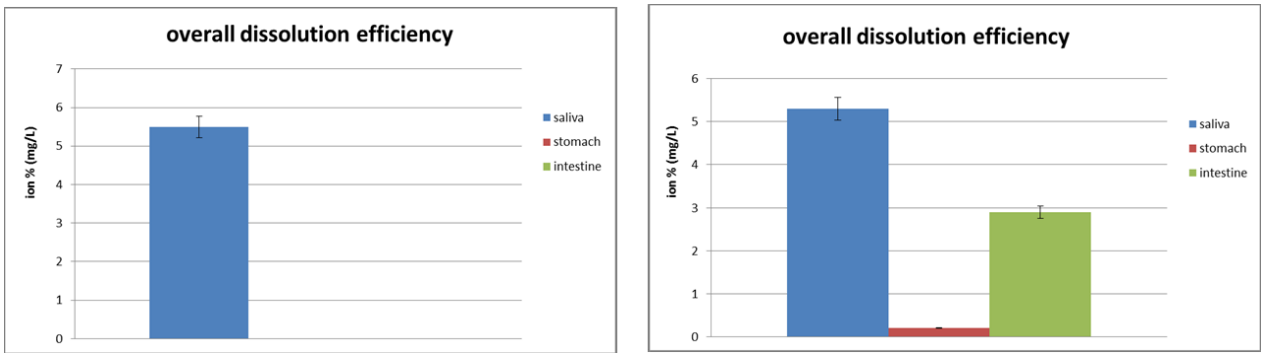


*Figure 11: Calculated dissolution rate of NM-200 in each phase of the in vitro digestion as a percentage of the total mass measured with ICP-AES by IIT. A) Spiked at a concentration of 47.5 mg/L, and B) spiked at a concentration of 950 mg/L*

**Dissolution of NM-101.** $TiO_2$ NM-110 material was evaluated by DLO-RIKILT, the results are shown in Figure 12. For the $TiO_2$ NM-101 material no dissolution was observed after UF, which is in line with most available literature describing the dissolution of $TiO_2$ NPs.

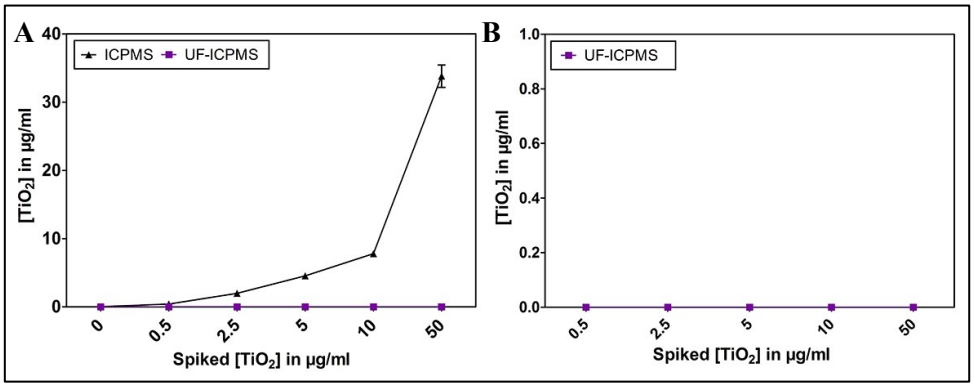


*Figure 12: A) ICP-MS and UF-ICP-MS $TiO_2$ measurements of DLO-RIKILT after complete in vitro digestion in µg/ml ± SEM, B) calculated dissolution rate of NM-101 as a percentage ± SEM of the total mass.*

### *2.4.4.4 Conclusion and recommendations*

Measurement in a complex matrix appeared to be more complicated than initially thought. Using UF-ICP-MS/AES, some variations in results were observed between institutes likely due to small differences in study design or pre-analytical procedures. It is recommended for future analysis to standardize these procedures to a further extend, in order to allow direct comparisons.

Although the reproducibility of UF-ICP-MS/AES looks promising, the technique is clearly not suitable for analysis of the "total" amount of dissolution of all types of materials. Materials that interact with the matrix (*e.g.* $Ag^+$ and $Zn^{2+}$) and/or filter membrane were removed from the mixture during UF, which highly influenced the detected amount of "dissolved" species. Quantification of the "total" amount of dissolution was therefore not possible using this technique. Although, from a regulatory point of view, it is questionable whether information on the "total" amount of dissolution is most important. Knowledge of the amount of "free" dissolved species (which are usually most reactive) might be more important than knowledge of the "total" amount of dissolution.

In conclusion, for selection of the best suitable technique for "total" dissolution measurement, in-depth knowledge of the nanomaterial and the matrix is essential and it is recommended to use a combination of measurement techniques.

### 2.4.5 Ultracentrifugation - Atomic Absorption Spectrometry (AAS) *[Unamur (lead); Julie Laloy, KI; Hanna Karlsson]*

#### *2.4.5.1 Introduction*

Different methods can be used to measure nanomaterial solubility and determine the presence of a specific element in a solution of NPs. One of these elemental detection techniques is atomic absorption spectrometry (AAS). AAS is suitable to assess the concentration of an analyte in a sample. It is based on the fact that metal atoms absorb strongly at characteristic wavelengths, which coincide with the emission spectra lines of the particular metal (*140*). Briefly, electrons of the atoms in the atomizer can be excited for a short period of time by absorbing a defined quantity of energy. This amount of energy (wavelength) is specific to only one element (Figure 13).

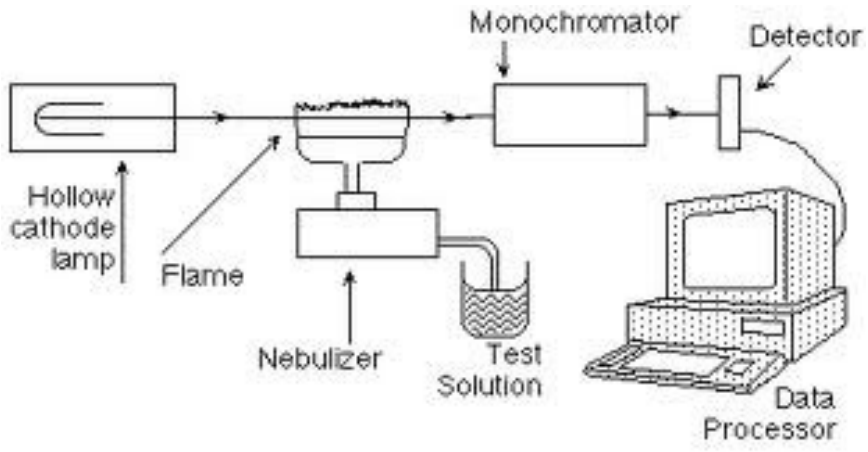


*Figure 13. Principle of Atomic Absorption Spectrometry*

AAS requires standards with a known analyte concentration to establish a relation between the measured absorbance and the analyte concentration. A separation method that is often used to separate nanomaterials from their dissolved species is ultracentrifugation (UC). Here, the particulate matter is pelleted using high centrifugal forces, whereas the dissolved fraction remains in the supernatant.

#### *2.4.5.2 Materials and methods*

Both KI and UNamur used AAS with a flame atomizer was used to investigate the fate of ZnO and Ag NPs in the GI-tract by using the previously described *in vitro* digestion model. The nanomaterials included in the study were the NANoREG NPs NM-110 (ZnO, UNamur), NM-300K (KI and UNamur) and NM-302 (UNamur), as well as 10 nm PVP coated Ag nanoparticles (OECD reference material) from NanoComposix (KI). The materials were dispersed according to the NANoREG guidance document and measured with DLS according to the NANoREG SOP. The digestive juices were prepared according to the protocol sent by DLO-RIKILT (as discussed in chapter 3.1), using the stock solutions sent by DLO-RIKILT and the indicated additional chemicals/proteins. After complete *in vitro* digestion the particulate matter was separated from the soluble fraction using UC. Before UC (Unamur) and after UC (KI, UNamur) a sample was taken from the supernatant and destructed for “total” and “dissolved” element measurement. This data was used to calculate the percentage of dissolution as follows:

([“dissolved” element] / [theoretical “total” element])*100 = % dissolution (KI)
([“dissolved” element] / [“total” element])*100 = % dissolution (UNamur)

**KI.** Part of the 10 nm PVP coated AgNP suspension was removed before sonication in order to test the role of the sonication process for the Ag ion release. The 10-nm PVP coated Ag nanoparticles were obtained as a 1 mg/mL suspension and therefore, the same sonication procedure could not be used. Due to the limited amount of these particles, KI used bath sonication (15 min) after dilution 1:1 in water with 0.05% BSA. 1 mL

of 19.5, 195 and 390 μg/mL was then prepared (dilution in water with 0.05% BSA) that give the final concentrations of 0.5, 5 and 10 μg/mL in final digestion volume. After this, the Falcon tubes were centrifuged for 2,000 rpm for 10 min in order to remove large aggregates. 8 mL of the supernatant was then transferred to 4×2 mL Eppendorf tubes and these were then centrifuged again at 13,000 rpm for 30 min in a cold room. 1.5 mL of the clear supernatant was then transferred from each Eppendorf-tube for Ag analysis.

The total Ag concentration in solution was determined using Atomic Absorption Spectroscopy AAS in the graphite furnace mode (Perkin Elmer Analyst 800). The samples were first acidified to a pH <2 with 65% HNO3, followed by digestion (4.5 mL sample + 1 mL 30 wt% H2O2, 100 µL 30 wt% HCl, 4.4 mL MilliQ water) via UV treatment (Metrohm 705 UV digestor, 95°C for 1 h). The digestion ensured that the total amount of Ag in the samples was measured using AAS. This was verified by analyzing digested samples spiked with known amounts of AgNPs. These samples yielded acceptable recoveries of the spiked Ag amount (±15% deviations). The determination limit was estimated to 5 µg/L. Triplicate readings were analyzed for each sample and control samples of known Ag concentration were analyzed in parallel generating data with the standard deviation of three independent samples and the blank value (matrix effect), if >0, subtracted.

KI also analyzed the samples using ICP-MS. For this analysis, KI did not use any $H_2O_2$+UV-treatment. The samples were spiked with Indium and Rhodium as internal controls and the samples were analyzed diluted in 1% $HNO_3$.

**UNamur.** Solubility of the prepared-ZnO/Ag NPs used in the *in vitro* digestion model was measured after centrifugation (Centrifuge 5804 R; Eppendorf, Hamburg, Germany), 5 minutes at 3,600g, to remove most of the large aggregates or after ultracentrifugation (Optima™ LE80K, used with 70.1 Ti type rotor; Beckman Coulter, Pasadena, USA), 90 minutes at 100,000g, to eliminate nanoparticles from the solution in order to measure ions only. The samples were then analyzed by AAS (AA-7000 F model; Shimadzu Atomic, Kyoto, Japan). AAS analyses were performed in three measurements of both stirred-NP and sonicated-NP samples. The AAS analysis program had rejected automatically the abnormal data. An AAS standardization curve was realized using standards of zinc or silver ions (Fluka Analytical, Sigma-Aldrich, St.-Louis, USA) to calculate the zinc or silver concentration and sterile-filtered 0.05% w/v BSA (99% purity) as blank in the different individualized gastrointestinal juices.

To verify the absence of nanoparticles and agglomerates in the supernatant, centrifugal liquid sedimentation technique (CLS) used. CLS technique measures the fraction of individualised particles and agglomerates migrating under centrifugal force in a quasi-liquid density gradient. For particles having same density, sedimentation time depends on particle size and morphology, influenced by the frictional force. Supernatant of agitated and sonicated ZnO NPs were conducted in a sucrose gradient at 24,000 rpm (maximum speed) using a CPS Disc centrifuge 24000 (accuracy ≥ 0,5nm; CPS Instruments Inc., USA). The sucrose gradient was prepared with the BSA suspending agent. CPS standardization was determined using ZnO NPs NM-110 dispersed in water. Centrifuged particles were detected by laser intensity variation recording continuously at 405nm and measured wavelengths were transformed by the analysis software into zinc concentration of the samples.

#### *2.4.5.3 Results and discussion*

**KI.** For the Ag (NM-300K) material, the Ag AAS analysis showed 0.213, 1.455 and 2.998 μg/mL for the final concentrations 0.5, 5 and 10 μg/mL, respectively. When calculated as % mass of released Ag these values correspond to 42.6%, 29.1% and 30.0%, see Figure 14 below. The sample that was not sonicated showed substantially less Ag release, 9.1% for the 10 μg/mL. For the 10 nm PVP-coated Ag nanoparticles, the values were 0.084, 0.858 and 1.576 μg/mL i.e. 16.7%, 17.2% and 15.8% of the mass was found in the "released fraction".

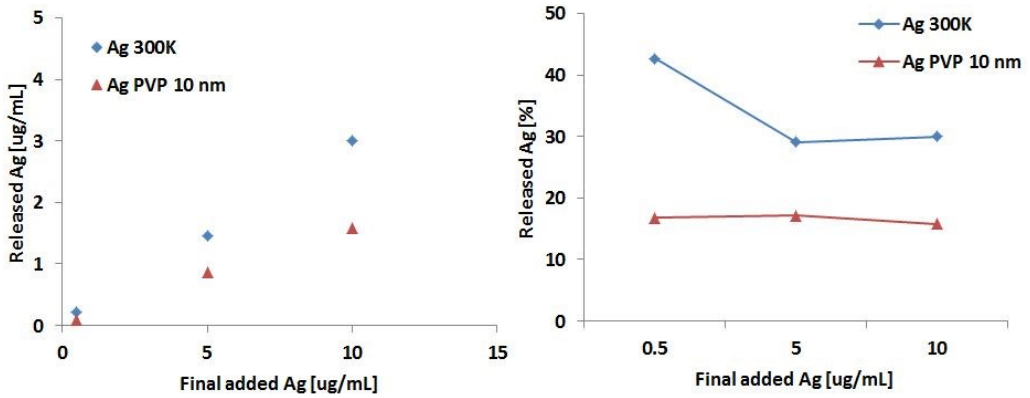


*Figure 14. Ag release from NM-300K and 10 nm PVP coated Ag nanoparticles following in vitro digestion under fed conditions.*

When the same analysis was performed in a scale-down version of the digestion model, KI found very different results. The % released Ag from NM-300K was 2.8%, 3.0% and 3.4%, for the three concentrations 0.5, 5 and 10 μg/mL, and 3.3% for the non-sonicated sample (10 μg/mL). For the PVP coated 10 nm particles the values were 16.0%, 2.8% and 3.0% and for the non-sonicated sample 2.5%. Next KI analyzed the samples using ICP-MS. For this analysis the difference between the "normal" and the "scale-down" version was not as pronounced. In the ICP-MS analysis the % release was consistently around 2-6% of total added mass and higher in the lowest concentration tested (12 and 18% for the NM-300K and 6 and 8% for the Ag 10 PVP). All results are compiled in Table 14.

*Table 14. The % of released Ag from NM300K and PVP-coated Ag 10 (OECD material from NanoComposix) following the digestion model. NS=non-sonicated particles.*

| μg/mL | Normal version (% released) | | Scale-down (% released) | |
|---|---|---|---|---|
| | AAS | ICP | AAS | ICP |
| **NM300 K** | | | | |
| 0.5 | 42.6 | 11.7 | 2.7 | 18.4 |
| 5 | 29.1 | 5.2 | 3.0 | 5.1 |
| 10 | 30.0 | 6.0 | 3.4 | 3.3 |
| 10 (NS) | 9.1 | 4.4 | 3.3 | 2.6 |
| **Ag 10 (PVP)** | | | | |
| 0.5 | 16.7 | 6.2 | 16.0 | 8.1 |
| 5 | 17.2 | 3.2 | 2.8 | 2.5 |
| 10 | 15.8 | 6.1 | 3.0 | 2.3 |
| 10 (NS) | 5.2 | 1.2 | 2.5 | 1.8 |

**UNamur.** The results obtained after centrifugation 5 minutes at 3600g showed dissolution of NM-110 and NM-300K NPs in the supernatant of the digestion model mixture with the detection of ions by AAS (Figure 15). The presence of Zn or Ag was partially due to the presence of nanoparticles in the supernatant as it has been demonstrated by CLS measurements (Figure 16). With ultracentrifugation, UNamur was able to remove all the NPs present in the supernatant for NM-110 and partially for Ag (NM-300K). In these conditions, in the *in vitro* digestion model, dissolution of NPs was observed only for ZnO NPs. A dissolution of 24% was observed after ultracentrifugation. Without ultracentrifugation, the dissolution percentage was 59%, with part of ZnO NPs measured. No dissolution of NM-300K was clearly observed.

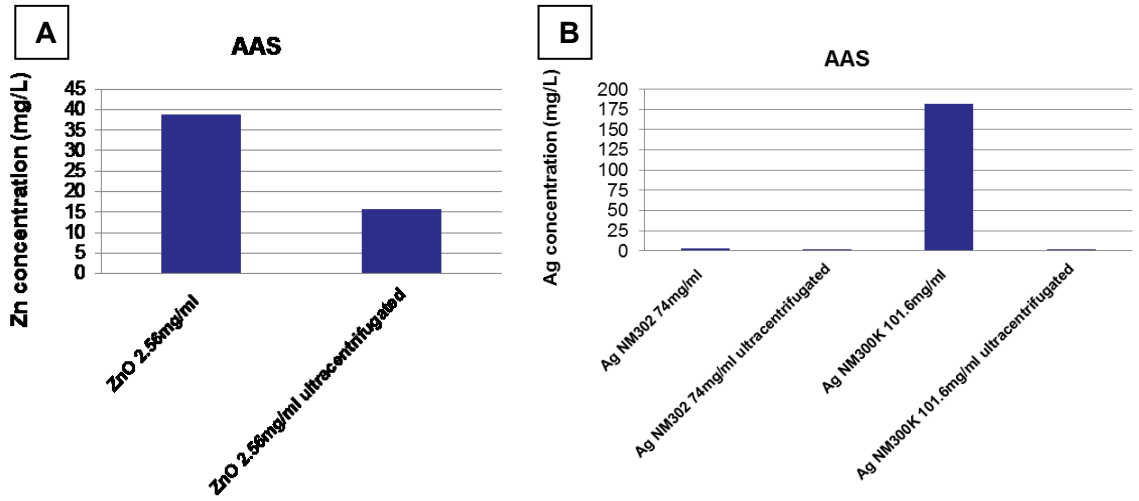


*Figure 15. Determination by AAS of Zn (A) and Ag (B) concentration in supernatant of digestion model mixture after centrifugation 5 minutes at 3600g or after ultracentrifugation 90 minutes at 100 000g. ZnO NM-110 was incubated at 2.56 mg/mL initial concentration, Ag NM-302 and Ag NM-300K was incubated at 74 mg/mL and at 101.6 mg/mL respectively.*

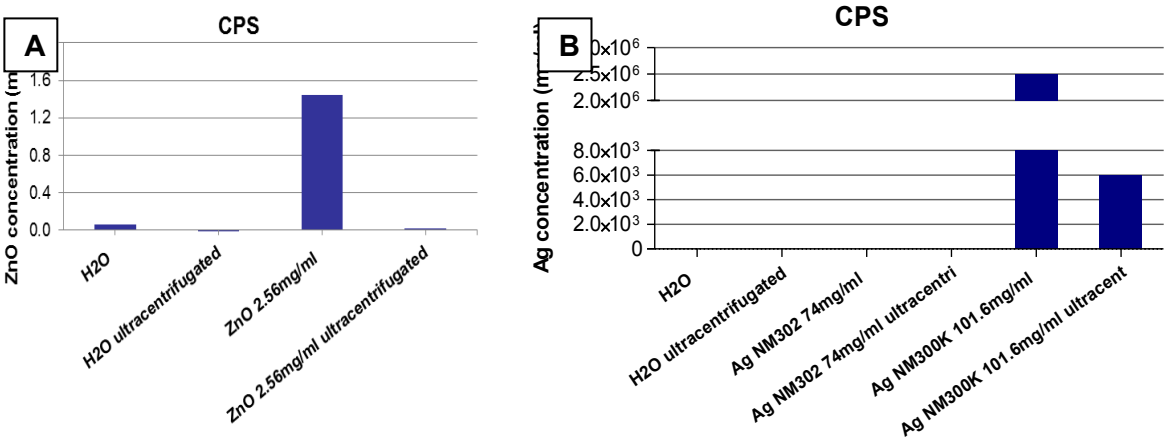


*Figure 16. Determination by CLS of of ZnO (A) and Ag (B) nanoparticles concentration in supernatant of digestion model mixture after centrifugation 5 minutes at 3600 g or after ultracentrifugation 90 minutes at 100 000g. ZnO NM-110 was incubated at 2.56 mg/mL initial concentration, Ag NM-302 and Ag NM-300K was incubated at 74 mg/mL and at 101.6 mg/mL respectively.*

#### *2.4.5.4 Conclusion and recommendations*

Based on the results obtained by KI, the NANoREG material Ag NM-300K released Ag species in the *in vitro* digestion model under fed conditions that corresponded to 42.6%, 29.1% and 30.0% of the added mass. Thus, at lower concentration somewhat more Ag was released. These results couldn't be confirmed by UNamur due to the presence of large amounts of Ag NPs in the supernatant after UC. Therefore, it is recommended that when using UC the supernatant is always tested for the presence of NPs.

UNamur could determine dissolution of the Nanoreg ZnO NPs (NM-110) in the *in vitro* digestion model using UC-AAS. This dissolution was proven by the absence of NPs in the supernatant as observed in CPS. However, the results need to be confirmed by further investigations with more research groups using the same pre-analytical protocol, an important step in regard to the presence of NPs in the supernatant after low speed centrifugation.

Sonication (probe *vs* bath) seemed to affect the Ag release to a significant extent and thus, the comparison of NM-300K with the 10 nm PVP coated material (OECD material) was difficult since the same sonication protocol could not be used. Taking this into account, the Ag release was somewhat higher for the NM-300K material compared to the PVP-coated Ag. Also, the volume used during digestion (normal *vs* scale-down

version) seemed to affect the amount of Ag release, as well as the elemental detection method used (AAS *vs* ICP-MS). In all, the analysis of Ag in complex matrixes seems to be quite challenging.

### 2.4.6 Theoretical modelling *[UdL; Carlos Rey-Castro]*

**Dissolution of NM-300K.**

UdL carried out thermodynamic calculations in simulated solutions reproducing the conditions of two phases of the in vitro digestion model (stomach and final intestine solutions) using the speciation software Visual Minteq v.3.1 (*141*) with the default standard database. This database is relatively limited regarding the information of binding constants with organic compounds and, therefore, only the major inorganic components have been accounted for (see Table 15). Some exceptions to this will be considered in the case of NM-110 (see below).

*Table 15: Composition of major inorganic components in two different steps of the standard digestion model (excluding the NM). Phase 2 (Stomach mixture, pH 2.5): 1 mL of sample + 6 mL of artificial saliva + 12 mL of gastric juice; Phase 3(a) (Intestine mixture, pH 6.5): 1 mL of sample + 6 mL of artificial saliva + 12 mL of gastric juice + 12 mL duodenal juice + 6 mL bile; Phase 3(b): same mixture as Phase3(a) + 2 mL $NaHCO_3$ 84.7 g/L. In all cases volumes are considered additive.*

| Phase 2 | mol/L |
|---|---|
| $K^+$ | 0.01143 |
| $Cl^-$ | 0.09084 |
| $NH_4^+$ | 0.00361 |
| $PO_4^{-3}$ | 0.00234 |
| $Na^+$ | 0.04399 |
| $Ca^{+2}$ | 0.00172 |
| $SCN^-$ | 0.00065 |
| $SO_4^{-2}$ | 0.00127 |
| $HCO_3^-$ | 0.00637 |

| Phase 3 (a) | mol/L |
|---|---|
| $K^+$ | 0.00933 |
| $Cl^-$ | 0.1058 |
| $NH_4^+$ | 0.00186 |
| $PO_4^{-3}$ | 0.00139 |
| $Na^+$ | 0.10034 |
| $Ca^{+2}$ | 0.00157 |
| $SCN^-$ | 0.00033 |
| $SO_4^{-2}$ | 0.00065 |
| $HCO_3^-$ | 0.02752 |
| $Mg^{+2}$ | 0.00008 |

| Phase 3 (b) | mol/L |
|---|---|
| $K^+$ | 0.00885 |
| $Cl^-$ | 0.10037 |
| $NH_4^+$ | 0.00176 |
| $PO_4^{-3}$ | 0.00132 |
| $Na^+$ | 0.1469 |
| $Ca^{+2}$ | 0.00149 |
| $SCN^-$ | 0.00032 |
| $SO_4^{-2}$ | 0.00062 |
| $HCO_3^-$ | 0.07781 |
| $Mg^{+2}$ | 0.00008 |

In these systems, solubility of elemental Ag is mainly determined by two reactions:

$$Ag \rightleftharpoons Ag^+ + e^- \quad (1.1)$$

$$AgCl_{(s)} \rightleftharpoons Ag^+ + Cl^- \quad (1.2)$$

The first reaction is the oxidation of metallic silver, which is determined by the standard redox potential of the couple $Ag^+/Ag^0$, $E^0$=0.799V (at 25ºC). This value corresponds to the bulk (macroscopic) $Ag^0$ phase, and it is the one used in subsequent calculations. However, oxidation reactions are thermodynamically enhanced as silver particle size decreases. In fact, the standard redox potential is inversely proportional to the particle's radius of curvature. Recent works have reported a shift of ca. 60 mV towards negative values between Ag-NPs of 45 and 20nm (which corresponds approximately to the diameter of NM-300K). Therefore, very small Ag-NPs are expected to be more susceptible to oxidation than bulk silver because of lower redox potentials. There is a much larger uncertainty, though, on the actual value of the redox potential (here expressed as Eh) in the test samples, which can depend on a number of environmental variables (concentration of dissolved $O_2$, presence of traces of oxidizing/reducing agents, etc.). In these calculations, a range of Eh values has been considered, as representative of usual redox conditions described in literature for different body fluid types (*142*): 100<Eh<500 mV for gastric fluids at pH 2.5, and -200<Eh<200 mV for intestinal fluids at pH 6.5. We must point out that redox conditions have not been experimentally assessed in the actual in vitro digestion test samples, so the results of these calculations must be considered with caution. Moreover, equilibrium conditions are assumed throughout this section, although very little is known about the kinetics of oxidation of AgNPs in complex environments and, in particular, the effects of complex natural organic matter. Therefore, the actual rate of those transformations can significantly alter these predictions. For a more detailed analysis on the environmental variables influencing the oxidation and dissolution of Ag in natural media see *e.g.* Levard *et al.* (*143*).

The results of inorganic speciation calculations for the estimation of Ag solubility are shown in Figure 17, for three different NM initial concentrations (9.5, 47.5 and 950 µg/mL) corresponding to the lowest, medium and highest doses tested experimentally by DLO-RIKILT and IIT.

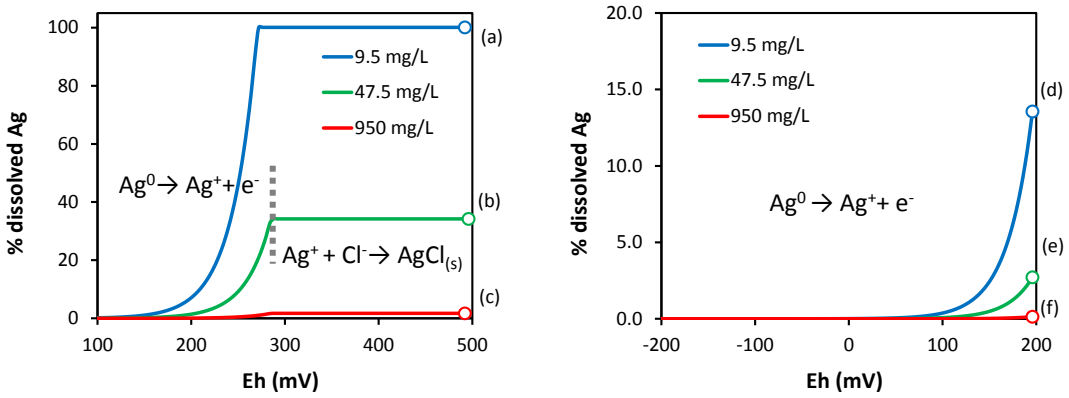


*Figure 17: Fraction of dissolved Ag calculated by UdL using Visual Minteq v.3.1 for two different steps of the digestion model (excluding organic components) at 37ºC, as a function of the redox potential (Eh) within the typical range of Eh values characteristic of each compartment (according to Plumlee and Ziegler[3]). Left) Phase 2 (Stomach mixture, pH 2.5). Right) Phase 3(b) (Intestine mixture, pH 6.5). Note the different scale of the y axis in each plot. The initial NM concentrations simulated are shown in the legend. The total dissolved Ag concentrations calculated for each sample at the most oxidizing conditions (depicted as open circles) are: $[Ag_{diss}]/(mgL^{-1})$= 0.50(a), 0.85(b,c), and 0.033(d,e,f), which represent a percentage over the total Ag amount of: 100% (a); 34%(b); 1.7%(c); 13%(d); 2.7%(e); and 0.1% (f), respectively. In samples (b) and (c), the solubility is limited by the formation of solid $AgCl_{(s)}$ (Cerargyrite).*

Note that under gastric conditions (Figure 17 left), complete dissolution at equilibrium is foreseen at the lowest concentration (9.5 µg/mL) above Eh=268 mV, whereas in the cases of medium and high doses, the maximum ***apparent*** solubility is 0.85 µg/mL ***due to the precipitation of solid AgCl***. This solubility corresponds to a fraction of ionic Ag species of 34% and 1.7%, respectively, which agrees reasonably with the experimental results obtained by IIT with NM-300K (see Figure 8 in section 2.4.4.3). The use of the word "apparent" in this context responds to the fact that, in these cases, Visual Minteq predicts the quantitative transformation of 100% of the original NM, which is oxidized and partially precipitated in the form of a different solid material ($AgCl_{(s)}$) and thus, leading to a concentration of dissolved Ag species that is representative of the solubility of $AgCl_{(s)}$ rather than that of the original NM.

The agreement of theoretical calculations and experimental results suggests the following conclusions: i) the non-deaerated synthetic gastric solutions might remain at a relatively high redox potential during digestion; ii) oxidative dissolution of Ag NM seems to proceed at a relatively high rate at gastric conditions, which is consistent with fast kinetics at low pH values described in literature (*123*); iii) the presence of organic matter such as glucose, BSA, pepsin, mucin etc. does not seem to exert a significant impact on the observed solubility at gastric conditions; and iv) ***the experimental solubility may be a misleading measure of the NM persistence, i.e.: the amount of NM remaining as such in the test solutions***.

Under intestinal conditions, however, the experimental overall dissolution efficiency of NM-300K is notably lower than in the gastric stage, as shown by IIT results (Figure 8 in section 2.4.4.3). The theoretical maximum solubility in equilibrium with $AgCl_{(s)}$ in the intestinal mixture is 0.88 µg Ag/mL, which corresponds to 72% and 3.6% of the total Ag concentration, in the case of the doses tested by IIT. These values are clearly much higher than the experimental results. ***This indicates that $AgCl_{(s)}$ does not seem to be the limiting phase for the solubility of NM-300K in the intestinal phase***. The speciation calculations plotted in Figure 17 (right) indicate that IIT's results may be consistent with Eh values close to 200mV, if equilibrium redox conditions are achieved. This, in turn, suggests that the ionic Ag species that previously dissolved in gastric conditions can be reduced back to $Ag^0$ in the intestinal solution, thus leading to a lower solubility in the final stage. Note that the reduction of silver ions in the intestine solution might lead to the formation of solid particles with completely different physical properties to the original NM-300K material.

Thermodynamic calculations also allow predicting the partitioning of the soluble Ag(I) ions into the different chemical species (see Figure 18). Taking into account that the contribution of low molecular weight organic ligands (such as urea, phospholipids and derivatives of cholic acids from bile) is disregarded in the calculations, the most abundant species in the dissolved fraction seems to be the $AgCl^-$ complexes.

Finally, it must be pointed out that calculations using Phase 3(a) and 3(b) recipes (Table 15) lead to almost exactly the same results (at the same values of Eh), so little differences are expected in the application of either version of the digestion protocol.

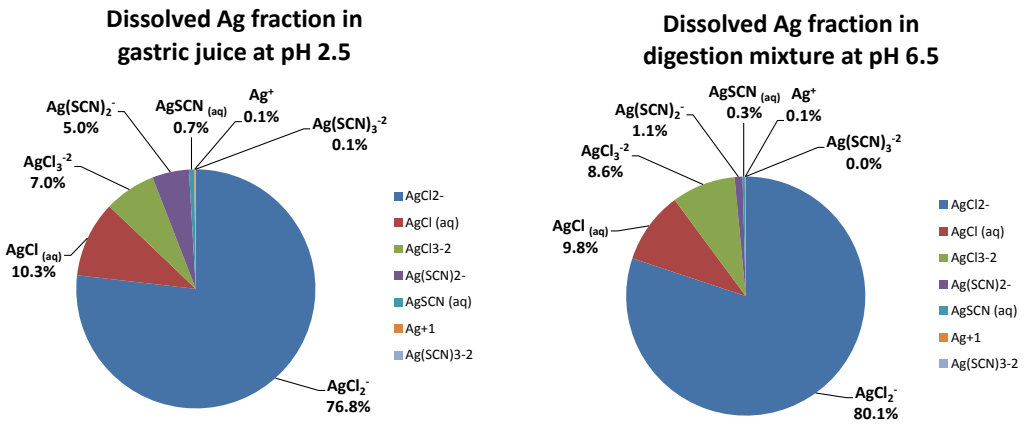


*Figure 18: Chemical composition of dissolved Ag fraction calculated by UdL using Visual Minteq v.3.1 for two different steps of the digestion model (excluding organic components) at 37ºC. Left) Phase 2 (Stomach mixture, pH 2.5, Eh=500mV). Right) Phase 3 (Intestine mixture, pH 6.5, Eh=200mV). Activity coefficients were calculated using the Davies model.*

**Dissolution of NM-110**.

In the case of ZnO, the dissolution of the solid NM is a result of the hydrolysis / ionization equilibrium

$$ZnO_{(s)} + H_2O \overset{K_{sp}}{\leftrightarrow} Zn^{2+} + 2OH^- \qquad (0.1)$$

which is described by the solubility product $K_{sp}$. The value of $K_{sp}$ for ZnO NMs is larger than for bulk material (as described by the Ostwald-Freundlich equation), but the differences have been found to be negligible above a primary particle size of 70 nm (*101*). Therefore, the thermodynamic value of the bulk material (zincite) is considered accurate enough for NM-110.

The same inorganic composition of the digestion systems as listed in Table 1 is used here. In these conditions, the overall solubility is conditioned mainly by pH. The concentration of bicarbonate and phosphate ions has also an important influence, due to the possible co-precipitation of solid zinc carbonate or phosphate phases concomitant to the dissolution of ZnO. Regarding the precipitation of carbonates, there is some degree of uncertainty in the calculations associated to the lack of control of the $CO_2$ partial pressure in the test conditions. Therefore, two limiting scenarios were considered for the speciation calculations: a) completely closed systems, where the total concentration of dissolved carbonate species is given by the recipe listed in Table 1 (*i.e.,* there is no stripping of $CO_2$ out of the liquid phase); and b) open systems, where the liquid samples are equilibrated with air at the conventional $CO_2$ partial pressure (which leads to a lower concentration of carbonates at equilibrium). With regard to the influence of phosphates, speciation calculations predict the precipitation of $Ca_5(PO_4)_3(OH)$ (hydroxyapatite) in the intestine mixture. The formation of solid calcium phosphate decreases the concentration of dissolved phosphates which, in turn, affects the speciation of Zn. However, the fact that no precipitate is observed in blank test tubes (with no NM) after the digestion protocol suggests that precipitation of hydroxyapatite in hindered, either due to a reduced activity of $Ca^{2+}$ ions (as a consequence of binding to the organic constituents of the digestion mixture) or due to kinetic reasons (oversaturated solutions in metastable situation). This scenario has also been considered in the thermodynamic calculations.

The results of Visual Minteq (in absence of organic ligands) indicate that ***100% of ZnO is dissolved in gastric conditions at pH 2.5 for any initial concentration of NM up to 950 µg/mL***. This is consistent with the experimental results obtained by IIT (Figure 10 in section 2.4.4.3), thus suggesting that dissolution kinetics is fast under these conditions. Previous results in the literature have also reported relatively high kinetic dissolution rates for similar NMs, where equilibrium situations where reached within *ca*. 1h in stirred systems at 25ºC[6]. In addition, the protonation of the acid/base groups of organic ligands is expected to hinder the formation of Zn complexes under these acidic conditions, which means that metal association to

macromolecular matter (see discussion below on the role of BSA in intestine solutions) is probably of little relevance. All these reasons support the reliability of thermodynamic predictions of the solubility of ZnO NMs in the synthetic stomach media.

On the other hand, the comparison of speciation predictions (see Figures 19 and 20) and experimental results after the complete digestion protocol seems to be far more complex. ***All the scenarios and ZnO doses explored lead to a complete dissolution of ZnO but, in some cases, the formation of a new solid phase is predicted***, leading to ***apparent*** solubilities below 100%. For instance, the results of the inorganic speciation model in a closed system (scenario 1) suggest the transformation of ZnO into solid $ZnCO_3$ (smithsonite) above a total concentration of 1mg ZnO per L (concentrations in the final digestion mixture), due to the relatively high concentration of carbonates (see Table 15). This leads to an overall ***apparent*** solubility of only 0.82 mg/L (expressed as ZnO). Scenarios 2 and 3 (open systems) assume that a significant amount of carbonate is removed from solution. In these situations, ***the concentration of dissolved phosphate is critical***, and saturation conditions for solid $Zn_3(PO_4)_2$ are reached above total ZnO concentrations of ca. 4 and 2 mg/L, depending on whether hydroxyapatite precipitation is allowed (scenario 3) or not (scenario 2), respectively. In these situations for) the overall NM ***apparent*** solubility is determined by that of $Zn_3(PO_4)_{2(s)}$, assuming equilibrium conditions are reached. For instance, *ca*. 50% of the total NM would remain in solution at ZnO concentrations of 4-5 mg/L (Figure 20).

Note that, when comparing with experimental results from DLO-RIKILT and UdL, all three scenarios of the inorganic speciation model tend to overestimate the total fraction of dissolved Zn at low ZnO concentrations (except the results of IIT at the lowest dose). Conversely, inorganic speciation results underestimate the experimental solubility data at high ZnO concentrations.

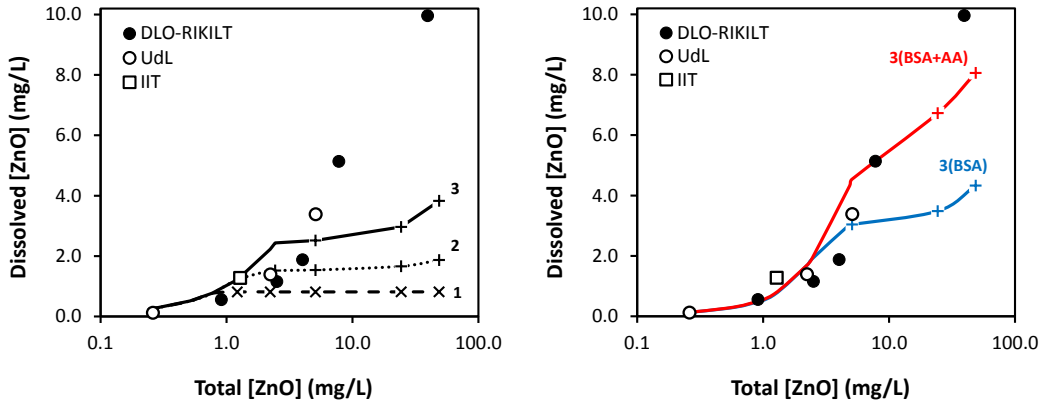


*Figure 19: Amount of dissolved Zn (expressed as ZnO) calculated by UdL using Visual Minteq v.3.1 at the final stage of the digestion model (Phase 3b) at 37ºC and pH 6.5, as a function of the total ZnO dose after in vitro digestion, for different fate scenarios. Left: Inorganic speciation (excluding all organic components). Scenario 1 (dashed line): closed system with hydroxyapatite precipitation; scenario 2 (dotted line): open system without hydroxyapatite precipitation; scenario 3 (continuous line): open system with hydroxyapatite precipitation. Right: Results of scenario 3 including BSA at 0.92 g/L (blue line) or BSA 0.92 g/L and acetic acid at 0.1 mol/L (red line) as models of high and low molecular weight organic ligands. 50% of the Zn bound to BSA is considered "not soluble" (retained by 3kDa filters in UF), whereas 100% of Zn complexes with acetic acid are included in the dissolved fraction. Symbols "x" and "+" indicate the conditions where Visual Minteq predicts precipitation of $ZnCO_{3(s)}$ (smithsonite) and $Zn_3(PO_4)_{2(s)}$, respectively. The experimental results obtained by DLO-RIKILT, UdL and IIT with NM-110 are included for comparison purposes.*

There are several possible causes of these discrepancies. The overerestimation of solubility at low concentrations should not be due to a hypothetical slow dissolution kinetics of ZnO, since 100% of the material was already dissolved during the gastric stage (as demonstrated experimentally by IIT, and supported by thermodynamic calculations). It could, rather, be a consequence of the formation of chemical species not accounted for in the inorganic speciation model. In particular, the formation of a significant amount of Zn complexes of large molecular weight (that would be retained by the 3 kDa membrane during UF step) could, in principle, account for most or all of the "non-soluble" fraction. To exemplify this, additional speciation calculations were carried out with the same system composition listed in Table 15 (Phase 3b) plus an organic ligand resembling BSA. The estimated concentration in the intestine stage (according to the protocol's recipe) is 0.92 g/L, and molecular weight was taken as 66kDa. The formation constant of the Zn-BSA complex was taken from bibliography (*144*) as logK=7.28 (reported at 4ºC and pH 7, so this value

should be regarded merely as an approximation). From the speciation calculation outcome, 50% of the Zn-BSA was considered "non-soluble". The results are shown in Figure 19 (blue line). This model still does not account for the relatively high solubility observed experimentally at high ZnO total concentrations. In this case, the deviations from theoretical calculations could be either due to slow precipitation kinetics and/or metastable situations (remember that Visual Minteq predicts formation of solid zinc carbonates or phosphates) or to the influence of a relatively large concentration of low molecular weight organic ligands with a relatively small binding constant towards $Zn^{2+}$ ions. These ligands could be, for instance, the cholic acid derivatives from bile. Unfortunately, no values of formation constants for Zn complexes have been found in literature, but binding constants of these ligands with $Ca^{2+}$ have been reported with values around 1-2 in log units (*145*). Therefore, and as a rough approximation, acetic acid 0.1 mol/L (with a binding constant value with $Zn^{2+}$ of LogK=1.57) was also included in the speciation model. The results are shown in Figures 19 and 20 (red line).

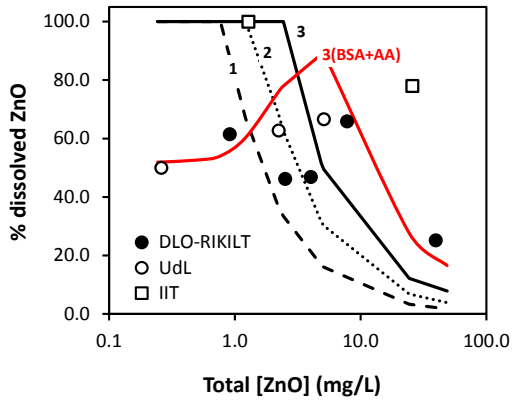


*Figure 20: Fraction of dissolved ZnO calculated by UdL using Visual Minteq v.3.1 at the final stage of the digestion model (Phase 3b) at 37ºC and pH 6.5, as a function of the total ZnO dose after in vitro digestion, for different fate scenarios. Scenario 1 (dashed line): closed system with hydroxyapatite precipitation; scenario 2 (dotted line): open system without hydroxyapatite precipitation; scenario 3 (continuous line): open system with hydroxyapatite precipitation; scenario 3(BSA+AA) (red line): including BSA at 0.92 g/L and acetic acid at 0.1 mol/L (red line) as models of high and low molecular weight organic ligands. 50% of the Zn bound to BSA is considered "not soluble" (retained by 3kDa filters in UF), whereas 100% of Zn complexes with acetic acid are included in the dissolved fraction. The conditions where Visual Minteq predicts precipitation of $ZnCO_{3(s)}$ (smithsonite) or $Zn_3(PO_4)_{2(s)}$ are not shown here for clarity reasons. The experimental results obtained by DLO-RIKILT, UdL and IIT with NM-110 are included for comparison purposes.*

As can be observed, the ***presence of low concentrations of high molecular weight ligands*** with large affinity for $Zn^{2+}$ might explain why, even though Visual Minteq predicts 100% dissolution of ZnO, the observed solubilities of NM-110 lie around 50% at low ZnO concentrations. In these conditions, speciation of Zn is dominated by the formation of complexes with BSA (see Figure 21, left), which are expected to be retained (to a lower or greater extent) in the membrane filters during UF. Conversely, the **presence of relatively large concentrations of low molecular weight and low affinity ligands** (such as acetic acid, taken here as a surrogate of bile acids) may increase the ***apparent*** solubility determined by the formation of solid zinc carbonates/phosphates, which might explain the observed experimental solubilities of 60-20% above 10 mgZnO/L. In these conditions, speciation of dissolved Zn is mainly dominated by the presence of free $Zn^{2+}$ ions and small molecular weight inorganic and organic complexes (Figure 21, right).

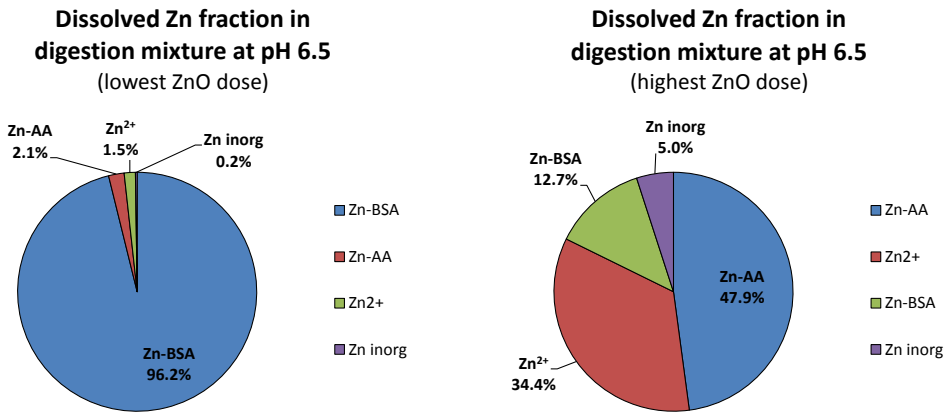


*Figure 21: Chemical composition of dissolved Zn fraction calculated by UdL using Visual Minteq v.3.1 for two different ZnO concentrations after in vivo digestion at 37ºC and pH 6.5. Left: 0.24 □g/mL. Right: 48.7 □g/mL (final concentrations). Here 100% of the Zn bound to BSA ("Zn-BSA") is considered as "dissolved" (even though, in principle, it would be retained by 3kDa filters). "Zn-AA" represents the organic Zn complexes with acetic acid. "Zn inorg" represents the total concentration of inorganic Zn complexes. Activity coefficients were calculated using the Davies model.*

Despite these results, the calculation results of the organic speciation model described here must be taken with great caution due to the limitations in the thermodynamic database. A more rigorous model should involve, for instance, the values of binding constants of BSA with other major cations (Mg and Ca) in order to account for metal competition, as well as the binding constants with other macromolecular (pancreatin, lipase, etc.) and small organic ligands (cholic acids, phospholipids, etc.). However, the development of such a model lies beyond the information currently available in the literature.

As a final comment, it must be pointed out that organic speciation is supposed to be less relevant in the case of dissolved Ag, due to the much smaller values of complexation constants (typical of +1 ions in comparison with +2 ions). For instance, the formation constants of Ag-BSA and Ag-acetic acid are just logK=3.60 (*146*) (i.e., almost 4 orders of magnitude lower than Zn-BSA), and logK=0.73, respectively.

### 2.4.7 Colorimetry assay to determine $Zn^{2+}$ from NM-110 after undergoing simulated digestion *[NPL; Ratna Tantra]*

#### *2.4.7.1 Introduction*

The main goal of the case study is to estimate using colorimetry the amount of dissolved free zinc ($Zn^{2+}$) from ZnO NM 110 nanomaterial when exposed to digestive juices. 5-Bromo-PAPS dye will be used to estimate the amount of free zinc arising from the NM 110 ZnO nanomaterial.

#### *2.4.7.2 Method*

**Common Protocols**

The following protocols were used; details found in CIRCB**:**

a) NanoGenetox Dispersion for Nanomaterial. In our case, a probe sonication was carried out for 8 minutes at 5% amplitude , using Misonix Sonicator 3000 (with a maximum power output of 400 W and operated at a frequency of 20 kHz). The diameter of the ultrasonication probe tip was 13 mm.
b) Dynamic Light Scattering. For digestive experiment, a temperature of 37 °C was applied.
c) Simulated digestive protocol (supplied from RIKILT).

Nanomaterial powders ZnO (NM-110) sealed under argon in small glass vials has been supplied by the European Commission Joint Research Centre, Institute for Health and Consumer Protection JRC (JRC-IHCP, Ispra, Italy) through FP7 NanoReg project. Stock digestive media has been supplied by RIKILT.

**Colorimetry analysis**

The following reagents were used in the colorimetric zinc determination; all chemicals were purchased from Sigma Aldrich, UK:

a) HEPES (4-(2-hydroxyethyl)-1-piperazineethanesulfonic acid ) buffer (1M), pH 8
b) 5-Br-PAPS solution (100 mg/L) in DI water
c) Zinc atomic spectroscopy standard stock concentrated diluted with DI water to give a final concentration of 10 g/L. Corresponding zinc standard concentration series solutions were made up by dilution with appropriate volume of DI water.

Prior to conducting the colorimetric assays, the samples from the digestion experiment were processed to remove particulate matter. This was achieved by centrifugation of the sample for 30 minutes at 1000 rcf and supernatant extracted using pipette. The supernatant was then filtered through a filter (pore size of 0.45µm) and the filtered solution was collected for colorimetric analysis.

For colorimetry assay, 1 mL of 5-Br-PAPS solution was thoroughly mixed with 0.3 mL of sample solution and allowed to stand for 5 minutes. 200 uL of this mixture was then diluted with 600 uL of HEPES buffer before being pipetted into a clean quartz UV cell (Hellma Analytics, UK). UV-visible absorbance spectrum was subsequently acquired using a Lambda 850 UV-Vis spectrometer supported by UV Winlab software [Version 5.1.5] (Perkin Elmer, USA). The instrument wavelength calibration was checked using a 15246-Ho Holmium glass standard (Serial # 9392, Starna Scientific, UK). For the reference channel of the spectrophotometer, a matched cell containing the corresponding dispersing media was used. Absorbance spectra were recorded from 350 - 700 nm using a slit width of 2 nm and a scan rate of 50 nm/min. 3 replicate measurements were carried out for each sample analysed.

### *2.4.7.3 Results and Interpretation*

Figure 22 shows the UV-vis absorption spectra when 5-Bromo PAPS was added to de-ionised water and blank digestive media. Results show that the spectra in both cases are very similar. When the dye was added to supernatant of NM110 (after exposure to digestive media), there is an apparent change in the UV-vis spectrum signature. The λmax= abs peak at 556 nm peak on top of blank indicates the presence of $[Zn^{2+}]$-dye complex in the supernatant.

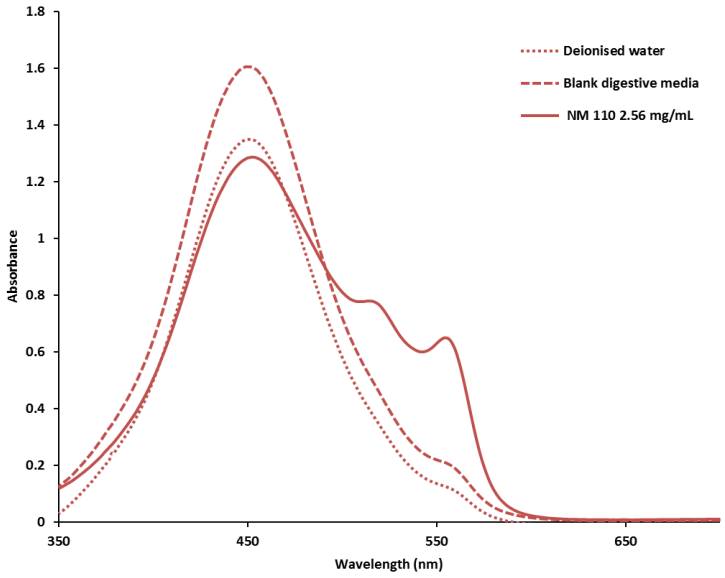


*Figure 22. UV-vis absorption spectra of 5-Bromo PAPS when: a) in de-ionised water b) blank digestive media c) supernatant after 2.56 mg/mL of NM 110 has been exposed to the digestive juices.*

Figure 23 shows a calibration plot, which shows how net absorbance signal changes w.r.t to [$Zn^{2+}$]. It is clear that the net response vs. concentration show a linear relationship within the region of 0 – 10 mg/L, which is expected. The plot displays the corresponding regression equation, which can be used to estimate the unknown [$Zn^{2+}$] concentrations arising from the digestive juice experiment.

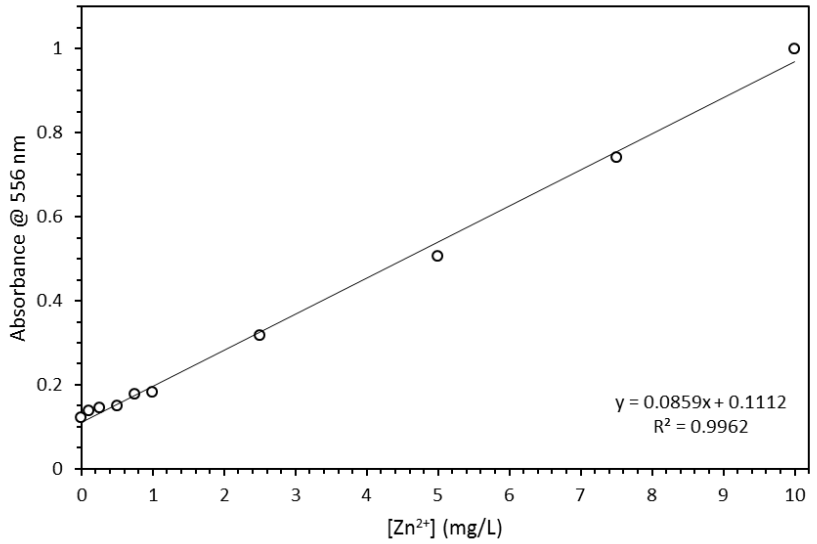


*Figure 23. [$Zn^{2+}$] concentration calibration plot using 5-Bromo-PAPS (λmax= abs peak at 556 nm, which corresponds to the maximum absorbance of the Zn- 5- Br-PAPS-complex). Each data point is the mean of triplicate measurements; standard deviation was too small to be shown. : $Zn^{2+}$ concentration calibration plot for 5-Br-PAPS.*

*Table 16. A summary of UV-vis absorbance signal (λmax= abs peak at 556 nm) and corresponding estimated [$Zn^{2+}$] found in the extracted supernatant from NM110 digestive juice experiment. The absorbance data reported are from corresponding 3 replicate measurements.*

| [NM110] (mg/mL) | 5-Br-PAPS | | |
|---|---|---|---|
| | A @ 556 nm (corrected) | | Estimated [$Zn^{2+}$] (µg/mL) |
| | Mean | RSD (%) | |
| 0 | 0 | 0 | 0 |
| 0.00001 | 0.0028 | 8.6078 | 0.0328 |
| 0.00256 | 0.0112 | 3.6284 | 0.1331 |
| 0.0256 | 0.0137 | 1.3362 | 0.1622 |
| 0.128 | 0.0420 | 0.6704 | 0.4979 |
| 0.256 | 0.0406 | 0.7436 | 0.4816 |
| 1.28 | 0.1377 | 0.2191 | 1.6335 |
| 2.56 | 0.4425 | 0.0809 | 5.2489 |

Table 16 shows the values associated with UV-vis Abs max associated with dye complex upon binding with [Zn2+]. The table also shows the corresponding concentration of [Zn2+], as estimated from the corresponding calibration plot. When the NM 110 particle concentration is plotted against the estimated [Zn2+], it is evident that there is a positive correlation between the two (Figure 24) i.e. increase in particle concentration resulted in an increase in dissolution and hence measured [Zn2+].

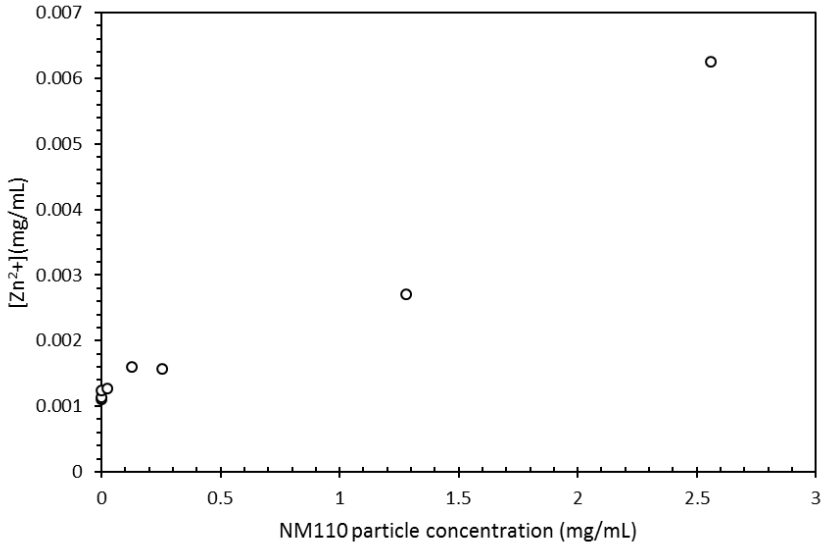


*Figure 24. Plot of estimated [Zn2+] as a function of NM110 particle concentration using 5-Br-PAPS colorimetry. The [Zn2+] arises from the dissolution of NM110 particle concentration as the result of digestive juice experiment.*

#### *2.4.7.4 Conclusion*

This report details NPL's contribution with regards to measurement of solubility using colorimetry. A method was developed that employs 5-Bromo-PAPS as the colorimetric reagent used for the zinc ion concentration determination. A range of particle concentration (NM 110, ZnO) was tested. Results showed a positive correlation between NM 110 particle concentration and [$Zn^{2+}$] released as a result of the digestive juice experiment.

## 2.5 Stability of nanomaterials in toxicological media *[IIT, S.Sabella, P. Bove; M. Malvindi; P. Valentini; A. Cassano]*

### 2.5.1 Introduction

While research community has suggested that characterization of NPs is key for risk assessment (*147, 148*), most of the present publications however show a detailed characterization of NPs in water or physiological buffer only at time zero, do not considering exposure conditions relevant for the assay such as the matrix composition and the exposure time.
It has been demonstrated that a proper *in situ* characterization of NPs (*149, 150*) may help a more accurate measure of the effective dose and a better correlation of the NP properties to the induced effect in relevant exposure conditions (e.g., ROS production, cytokines release, etc). Strictly connected to this argument are also the multiple interactions between NPs and matrix components (proteins, biomolecules, salts, etc.) that impact on NP colloidal stability and solubility inducing the formation of aggregates/agglomerates/secondary species (e.g. ions). Many literature examples discuss these aspects (*150-154*). For instance, due to different protein coronas (*151, 152*), same NPs dispersed in different cellular media (i.e., DMEM or RPMI) may have a different size pattern than nanoparticles dispersed in water (or in reference dispersant fluids) thus affecting NP cellular uptake, intracellular dose and toxicity (*153*). Positive or negative silica nanoparticles may become all negative when immersed in DMEM or RPMI, supplemented with a constant value of serum proteins (*154*). This surface charge "normalization" may be the cause of misleading data interpretation. Many other biophysical consequences may derive by these interactions such as formation of aggregates with different densities or presence of secondary substances (protein/NP complexes, ions, ion chelates, ion-protein complexes) (*151*) that will, in turn, undergo to interact with living systems.

Nascent recommendations to measure stability of NM dispersion in relevant exposure conditions are reported in the NANOREG Guidance document in which "*It is recommended to follow size distribution and sedimentation of NMs in the exposure medium during the test. (R) Sedimentation rates can be assessed from calculations, analytical centrifugation or tests using the DLS. By DLS one may analyze both*

*agglomeration and sedimentation. From experience, a time-resolution of 20 minutes after the first hour is a suitable time-resolution (e.g., 20 min.). Within the first hour a time-resolution of 10 minutes is normally suitable*. " These indications are however not considered mandatory yet and limited to NM size.

Within this framework, this Chapter aims at highlighting the importance of NP characterization in relevant exposure conditions by extending the need of characterization to a wider range of NM properties such as size, surface charge and dissolution and considering the matrices composition associated to the temporal exposure conditions (which may be reflective of the exposure in the assay). The Chapter provides some examples of this characterization approach focussing on cellular media and matrices relevant for the human digestive process and using a multi-technique based approach, which employs methods developed by and crosscutting to WP5 and WP2. The results based on experiments done on 3 case studies (3 NPs from the repository list) provide information on NP fate in the dispersant medium along with relative methodologies.

### 2.5.2 Scope and Results

Chapter 2.4 highlights the importance of NP characterization before an *in vitro* assay using matrix composition and temporal conditions, which are reflective of the exposure conditions. It also suggests a broader approach extending the characterization to surface charge and dissolution as these properties, together with size, being strictly linked to exposure, have been recently identified as physical descriptor key for NP risk assessment. They also may be informative of the NM fate in the dispersant medium. This in-depth characterization is fundamental to facilitate the data interpretation, to relate NP properties to the biological outcomes thus also improving data reliability for benchmarking.

This Chapter illustrates a multi-techniques based approach and the relative methods (in part also discussed and validated in 2.3 and WP2, T2.4) to provide a **pattern of NP physical properties** (size, surface charge and dissolution profiles) in cellular biological matrices that are typically employed for *in vitro* cellular tests (DMEM and RMPI). The characterization is performed at temporal conditions, which are reflective of cell exposure to NP treatments (0, 24 and 48 hours).

Moreover, the same approach is applied using synthetic biological matrices that simulate the human oral exposure (*e.g.*, saliva, stomach and intestine/bile juices) using temporal conditions reflective of the human food digestive process (5 minutes typical of saliva digestion, 2 hours typical of stomach digestion, etc.). This latter characterization may help not only to clarify the physical status of NPs at the phase of interaction with tracheal-gastro-intestinal epithelium, but also to provide structural information useful to standardize the NP dissolution test.

The Chapter illustrates experiments (and relative results) performed using NPs from the repository list of NANOREG (NM300K, NM200, NM110). These NPs were analysed by DLS, zeta-pot, TEM upon dispersion by Nanogenotox protocol (see details in experimental section) and selection of the aforementioned exposure conditions. Furthermore, dissolution of NPs at similar experimental conditions was performed by UF-ICP-OES and herein described

- Results indicate that the size profile of NPs already differed at time zero than size of primary NPs (as declared by the provider) in all the used synthetic biological media (DMEM, RPMI, saliva, stomach and intestine). Moreover, the size profile of each NP, and relative trend over time, appeared to be medium type- dependant.
- A progressive agglomeration/aggregation in the in vitro human digestive matrices was further confirmed by TEM analyses. In the specific case of NM300k, TEM also revealed a progressive dissolution of NPs in the stomach with an *ex-novo* creation of nanoparticles in the intestine (in line with current literature).
- By zeta potential analysis, we found that the employed dispersion protocol has altered the original charge values of primary NPs, leading to a "charge normalization" effect toward negative values ranging to about -20/-29 mV, values which are typical of amino acid charged groups. Hence, such effect can be explained by the protein coronas around NPs that are formed by albumin (present in the dispersant solution) and by sera within the media.
- In the case of in vitro human digestive compartments, the general trend of surface charge values are negative in saliva and intestine although more negative than in the Ctrl (NPs dispersed in 0.05% of BSA) and a tendency to charge neutralization in the stomach, possibly due to the increased concentration of hydrogen ions (pH 2,5).
- Dissolution profile of NPs in the cell culture media indicated that only NM200 dissolved, whereas silver and zinc NPs appeared quite stable at the experimental conditions used (neutral pH). Note that

amounts of released ions, the relative abundance and kinetics may be strongly affected by many experimental parameters (such as starting concentration, used media, techniques, filters, chemical coating of NPs, etc.) hence interlaboratory data comparison as well as application of more than one technique to follow the process is recommended for data validation.

- Dissolution of NPs in digestive juices is discussed in Chapter 2.4.

### 2.5.3 Materials and methods

#### *2.5.3.1 Dispersion of NMs and calibration of probe sonicator*

The NPs where dispersed according to the Nanogenotox dispersion protocol, which includes sonication of the NMs using a probe sonicator. The sonicator used was a Sonics Vibracell VC750, equipped with a 13mm probe. Before starting the experimental session, the probe sonicator was calibrated by using a calorimetric procedure, according to the NANoREG *"SOP for probe-sonicator calibration of delivered acoustic power and de-agglomeration efficiency for in vitro and in vivo toxicological testing"*, to the aim of ensuring inter-laboratory harmonization of the dispersion conditions. As resulting from the calorimetric calibration, the sonication parameters, necessary to deliver the same acoustic power as that used in the Nanogenotox protocol, were 20% amplitude and 8'30'' duration of sonication. These calculated parameters were confirmed by testing the de-agglomeration efficiency on reference material NM200, and analysing the dispersion efficiency by DLS, according to the "*SOP for measurement of hydrodynamic Size-Distribution and Dispersion Stability by Dynamic Light Scattering (DLS)*" provided by Nanoreg.

#### *2.5.3.2 DLS analysis and zeta potential characterization protocols*

Malvern Zetasizer Nano was used to measure the size and charge profiles of NPs dispersed in DMEM and RPMI, and in the synthetic digestive juices (*i.e.*: saliva, gastric and intestinal juices).

For biological media, size profiles of NPs were monitored at time zero ($t_0$), and after 24 and 48 hours, whereas NP size in the synthetic digestive juices were checked according to the timing of the employed *in vitro* digestion model, namely after 0, 5, 125 and 245 minutes for CTRL, saliva, stomach and intestine, respectively.

For the DLS analysis, about 50 µL of each sample from testing batch was diluted to 1 mL in MilliQ water and analysed using disposable polystyrene cuvettes at R.T. (10 repeated measurements). The optical parameters of the instrument were set for the selected NPs, as reported in the Table 17. Further technical details are discussed in WP2.

Table 17. $R_i$ and $R_{abs}$ indices

| | **NM 300K** | **NM 200** | **NM 110** |
|---|---|---|---|
| Ri | 0.180 | 1.544 | 2.020 |
| Rabs | 0.010 | 0.020 | 0.040 |

#### *2.5.3.3 TEM analysis: evaluation of nanoparticles size and morphology*

The nanoparticles size and morphology in cell culture medium and synthetic digestive juices were evaluated by TEM. The images were recorded by a JEOL JEM 1011 microscope operating at an accelerating voltage of 100 kV. TEM samples were prepared by dropping a dilute solution of nanoparticles in water on carbon-coated copper grids (Formvar/Carbon 300 Mesh Cu).

The performance of the TEM was evaluated using a calibration sample. TEM analysis evaluation criteria: From each TEM specimen, micrographs of ten regions on the grid are recorded and analysed. At least 500 particles have been analysed per specimen.

#### *2.5.3.4 NP dissolution by UF/ICPAES*

UF-ICPAES was used to quantify the amount of dissolved NPs in form of ions. This method consisted of a preliminary Ultrafiltration (UF) in which particulate component of testing batch was treated to separate the

complex organic part from the soluble saline fraction through the use of Amikon 3K cut-off filters. The 3K cut-off filters were centrifuged at 4000*g* for 40 minutes at R.T. Subsequently, the filtrated soluble fraction were dissolved *o.n.* in 0.5 mL of concentrated $HNO_3$ and diluted to 5 mL with MilliQ water. The resulting solution was then directly analysed by ICPAES.

To measure the amount of dissolved nanomaterial into both DMEM and RPMI, NPs were spiked at the final concentration of 6.8 µg/mL and incubated in 0.5 mL of biological medium, for 0, 24 and 48 hours. Dissolution into digestive juices was observed, using two starting concentration (47.5 µg/mL and 950 µg/mL) and after the incubation for 0, 5, 125, 245 minutes in the saliva, stomach and intestine, respectively. Experiments were carried out in triplicate. The performance of the ICP-AES was evaluated before each measurement using a Standard Tuning Solution to optimize the sensitivity of the instrument. ICP-AES analysis evaluation criteria: calibration standards were used to construct a multipoint standard curve covering the range of analyte concentrations possibly present in the samples. Data that fall in this concentration range were considered valid.

### 2.5.4 Apparatus and chemicals

#### *2.5.4.1 Equipment*

**Dynamic light scattering and Zeta potential**: A Zetasizer Nano ZSP (Malvern) equipped with a 10 mW He–Ne laser operating at 633 nm and an avalanche photodiode detector was used. Measurements were made at 25°C in water. Each sample was measured 10 times and the results were analyzed by Malvern Instruments Ltd software.

**ICP-AES**: Elemental analysis was carried out by inductively coupled plasma optical emission spectroscopy (ICP-AES) with a Agilent Technologies 700 Series system. Samples were incubated overnight in 0.5 mL of concentrated $HNO_3$, diluted with MilliQ water, then analyzed by ICP-AES.

#### *2.5.4.2 Nanoparticles*

NPs were from repository list of JRC from NANOREG
NM300K: Ag NPs, with nominal size of 106 nm (DLS measured) and nominal charge of -11 mV.
NM 200: Si NPs, with nominal size of 207.8 nm (DLS measured) and nominal charge of -47.5 mV.
NM110: ZnO NPs, with nominal size of 275 nm (DLS measured) and nominal charge of 24.3 mV.

All NPs were dispersed according to NANOGENOTOX protocol upon probe sonicator. This protocol produces a highly dispersed stock solution of any NP, by ethanol pre-wetting followed by dispersion in sterile-filtered 0.05% w/v BSA-water at a fixed concentration of 2.56 mg/mL according to the SOP provided by NANOREG.

#### *2.5.4.3 Chemicals*

**Protein components**: Amylase (#A6380), BSA (#A2153), Pepsin (#P7000), Pancreatin (#P7545), Lipase (#L3126), Bile (#B3883) were purchased from Sigma-Aldrich. Mucin (#8494.1) was purchased from Roth.

**Organic solutions**: Urea, Glucose, Glucuronic Acid and Glucosaminehydrochloride were donated by RIKILT. Uric Acid (#U0881) was purchased from Sigma-Aldrich.

**Inorganic solutions**: KCl, KSCN, $NaH_2PO_4 \cdot H_2O$, $Na_2SO_4$, $NaHCO_3$, NaCl,$CaCl_2$, $NH_4Cl$, $KH_2PO_4$ batch solutions were kindly donated from RIKILT

Ultrapure grade water with a resistivity of 18.2 MΩ ·cm at 25°C, was used in all experiments (MilliQ).

### 2.5.5. Result spreadsheets

**NPs size profile in biological cell media (DMEM and RPMI)**

NPs were dispersed according to Nanogenotox protocol. Afterwards they were dispersed in DMEM and RPMI supplemented with 10% of FBS at the final concentration of 6.8 µg/mL. Size changes were detected at 0, 24 and 48 hours of incubation by DLS following the DLS SOP provided by NANOREG (see technical details).

**NM300K**

At time 0, DLS spectra indicate the presence of 3 species peaking around 10 (Peak 2), 100 – 200 (Peak 1), and 4000 – 5000 nm (Peak 3), respectively. Peak numeration refers to DLS software assignation according to the signal intensity (a representative image is reported below). The nominal size of NM300K is 106 nm, hence Peak 1 is reasonably the peak related to the primary NPs. Peak 2 is reasonably due to protein components of cell culture media, whereas Peak 3 represents aggregates of NPs.

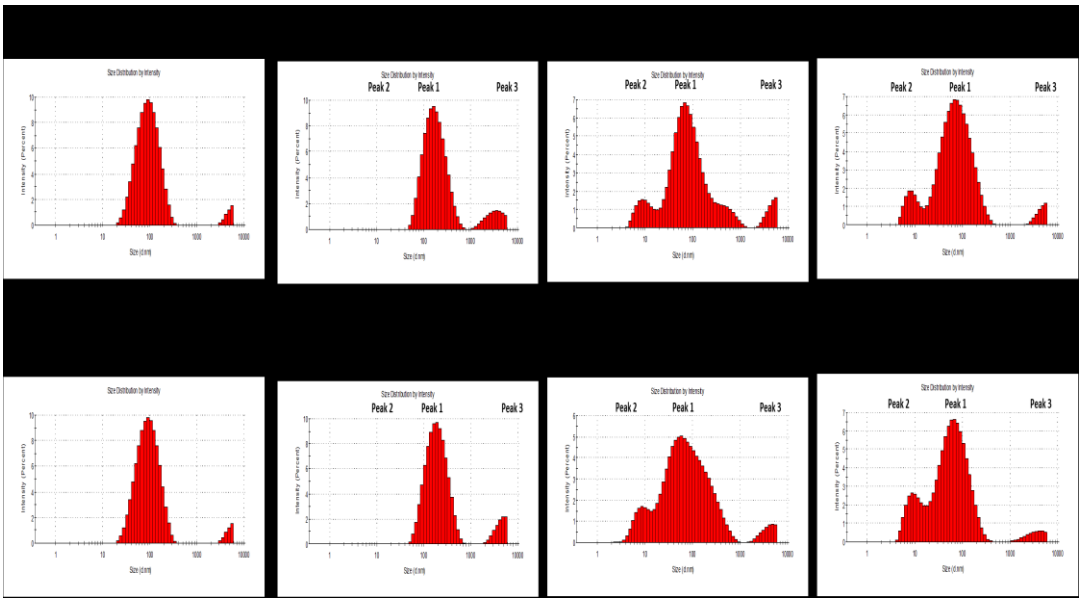


*Figure 25. DLS representative spectra of NM300K in biological cell media (DMEM and RPMI*

From the size plot of Peak 1 over time, it is possible observing that size profile, and relative kinetic, of NPs appear different in the two media. These changes in size may strongly impact on the biological outcome and must be taken into account when a specific effect may be derived and related to the NP size. Size reduction over time is monitored and possibly explained by dissolution phenomena or precipitation phenomena.

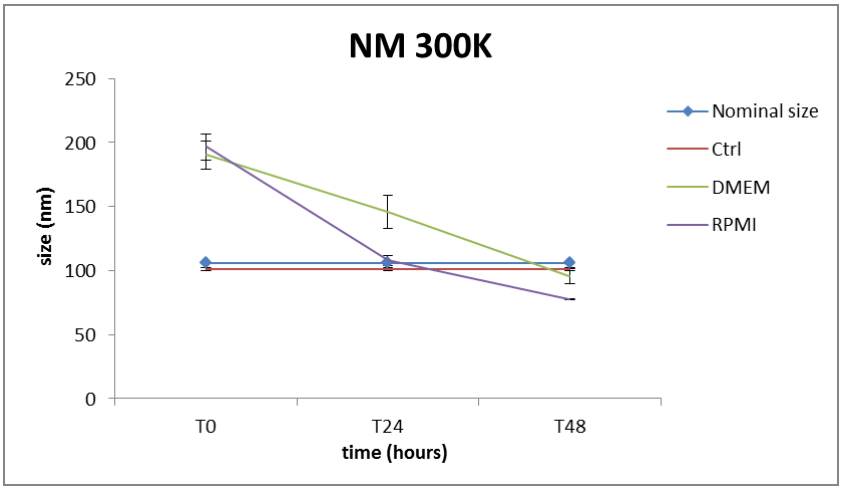


*Figure 26. NM300K size profile. The plot reports the size trend of Peak 1 over time (the deviation standard bars are relative to 10 runs)*

**NM200**

DLS analysis (see graphs below), indicated the presences of 4 species, distributed along spectrum according to their intensity. Peak 2 and Peak 1 were registered around 10 nm and 40 nm, respectively. Also in this case it was monitored the Peak of about 4000 – 5000 nm (Peak 4) corresponding to aggregates. The Peak 3, ranging from 400 nm to 800 nm was related to the primary NPs that partly aggregated over the incubation.

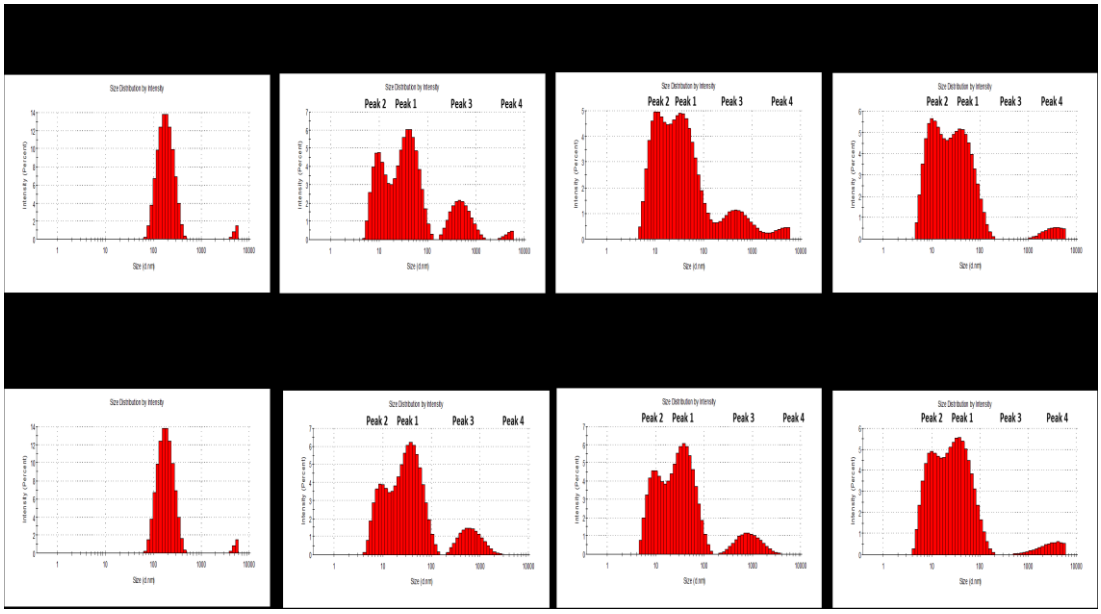


*Figure 27. DLS representative spectra of NM200 in biological cell media (DMEM and RPMI)*

Size plot of Peak 3 indicates the formation of protein shells around NPs and or soluble protein/NP aggregates in the time frame of 24 hours. After 48 hours, aggregation or degradation phenomena affect the DLS measurements and no NP signal was detected in both media.

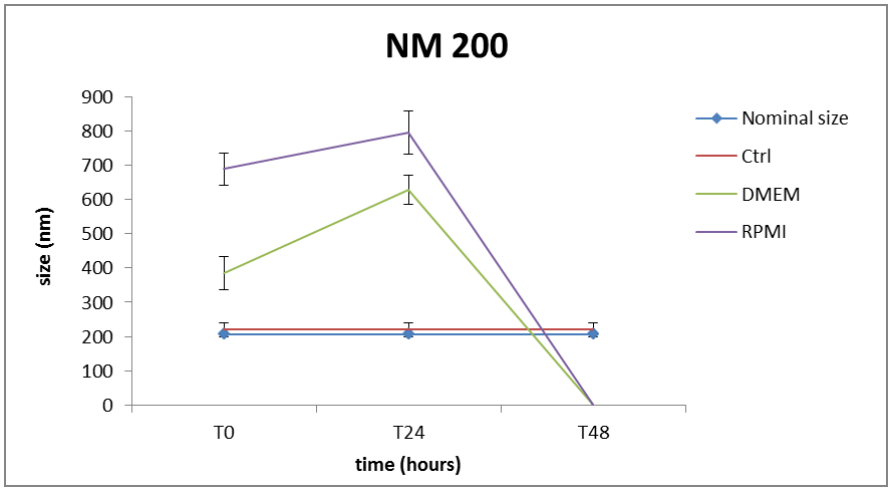


*Figure 28. NM200 size profile. The plot reports the size trend of Peak 3 (error bar are relative to 10 runs).*

**NM110**

NM110 DLS spectra reported the presence of 4 species, alternatively distributed during the time assay. As for the NM200, we monitored two peaks around 10 nn and 40 nm, which aggregate in a single peak during

the incubation. Primary NPs aggregated consistently already at time 0 and are possibly represented by Peak 3 (800 – 1200 nm). This peak disappears after 24 hours in both media possibly due to precipitation phenomena. Peak of about 4000 – 500 nm (Peak 4) are also detected.

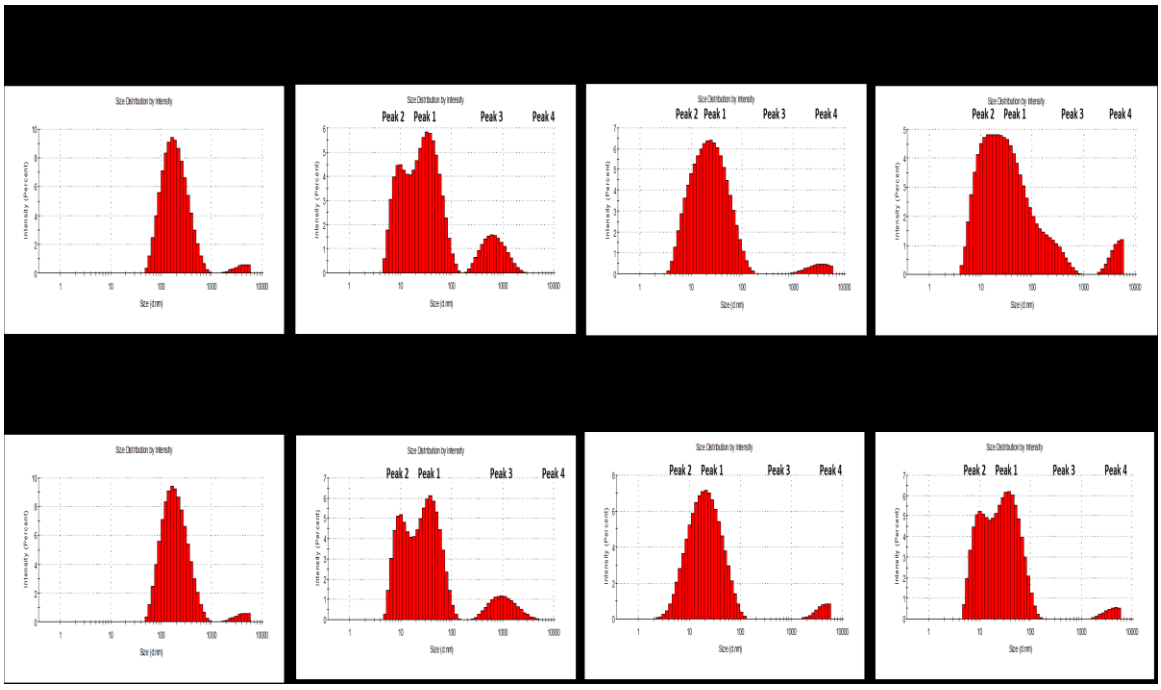


*Figure 29. DLS representative spectra of NM110 in biological cell media (DMEM and RPMI)*

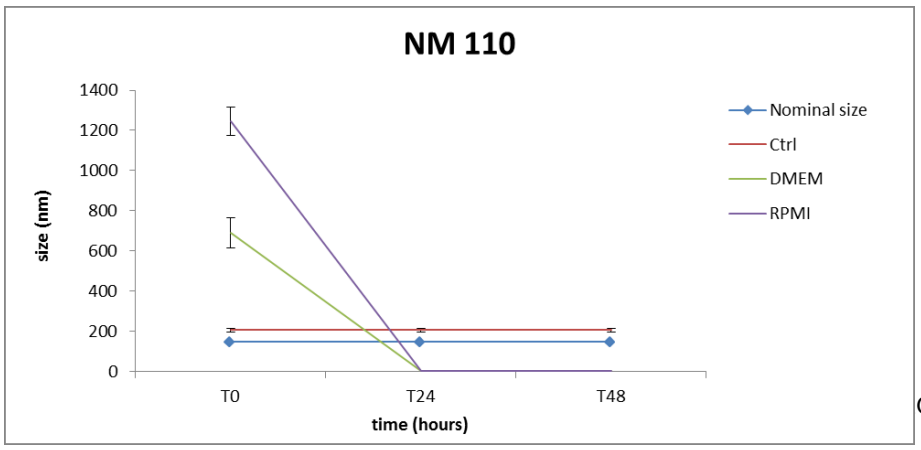

*Figure 30. NM110 size profile. The plot reports the size trend of Peak 3 (error bar are relative to 10 runs).*

**Zeta-potential analysis of NPs in biological cell media (DMEM and RPMI)**
Zeta-potential measurements were taken after 1 hour of incubation. Nominal charges are reported in the table below, and represent the surface charge of NMs dissolved in ultrapure water (as declared in the manufactures' data sheets).

NPs were dispersed using the Nanogenotox protocol (that employs 0.05% BSA as dispersing agent). As it is possible observing form the results, the original surface charges of NPs tend to peak around negative values in the range of -20/-29 mV. This "charge normalization" effect is possibly due to the presence of proteins corona in both Ctrl (albumin) and biological media (FBS).

*Table 18. Surface charge of NPs in the biological media, DMEM and RPMI.*

| | Nominal Charge (mV) | CTRL charge (mV) | DMEM (mV) | RPMI (mV) |
|---|---|---|---|---|
| **NM 300K** | -11.0 | -24.4 | -28.2 | -29.4 |
| **NM 200** | -47.5 | -28.0 | -26.0 | -27.5 |
| **NM 110** | -24.3 | -20.6 | -28.2 | -27.2 |

**Dissolution of NPs in the biological media**
NPs were dispersed in DMEM and RPMI (10% of serum protein) and the released ion were measured by UF/ICPAES. Dissolution profile of NPs indicated that only NM200 dissolved in the media whereas silver and zinc NPs appeared quite stable at the experimental conditions used (neutral pH). Note that amount of released ion, the relative abundance and kinetics may be strongly affected by many experimental parameters (such as starting concentration, media, techniques, filters, chemical coating of NPs, etc.) hence interlaboratory data comparison as well as application of more than 1 technique to follow the process is recommended for data validation.

*Table 19.*

| | | 6h | 24h | 48h |
|---|---|---|---|---|
| NM 300k | DMEM | n.d. | n.d. | n.d. |
| | RPMI | n.d. | n.d. | n.d. |
| NM 200 | DMEM | 48 uM | 77 uM | 82 uM |
| | RPMI | 10 uM | 42 uM | 73uM |
| NM 110 | DMEM | n.d. | n.d. | n.d. |
| | RPMI | n.d. | n.d. | n.d. |

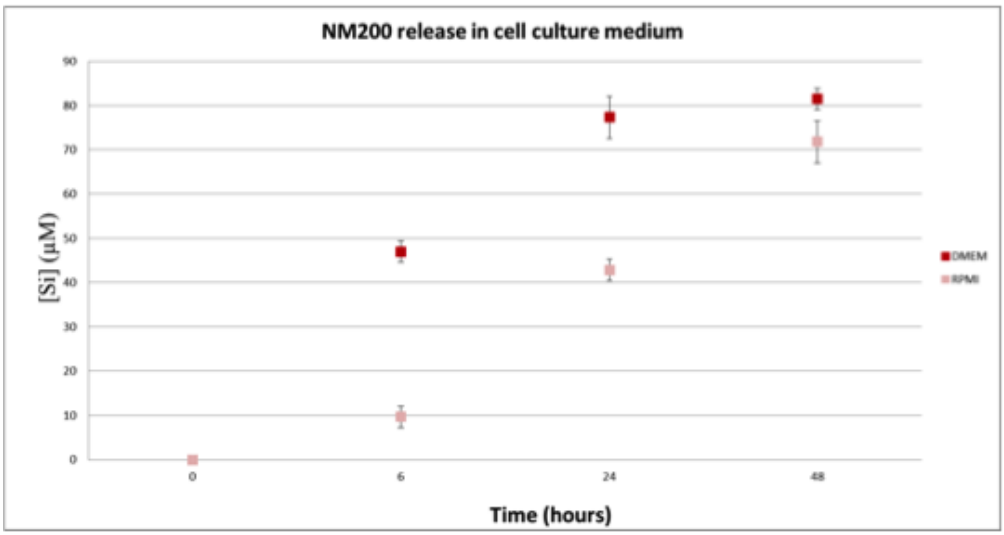


*Figure 31.*

**DLS analysis of NPs in the human digestive compartments**
Two values of starting NPs concentration were considered for this test: 45 ug/mL and 950 ug/mL. “Nominal size” refers to value of NP radius reported in the technical datasheet samples. “Ctrl” refers to NP size after the application of the Nanogenotox dispersion protocol. Treated samples are NP size when they are immersed in synthetic human digestion compartments at temporal points simulating digestion according to *Walczak et al, 2013*.

The size plots indicate that while all NPs in the saliva fluid maintained similar size profile with respect to the Ctrl, a progressive aggregation occurred in the stomach and intestine compartments. NM 110 showed a particular behaviour possibly due to its tendency to precipitate and aggregate already after the application of the dispersion protocol. These results are confirmed by TEM analyses (see below). Furthermore, NPs were subjected to dissolution (see data reported in Chapter 2.4 also) in these matrices.

In general, as these are very complex matrices, DLS data interpretation may result challenging so that we recommend the application of more than one complementary technique to follow the NP dissolution in the human in vitro digestive matrices (*e.g.*, DLS, TEM and ICP or others).

*This project has received funding from the European Union*
*Seventh Framework Programme (FP7/2007-2013)*
*under grant agreement no 310584*

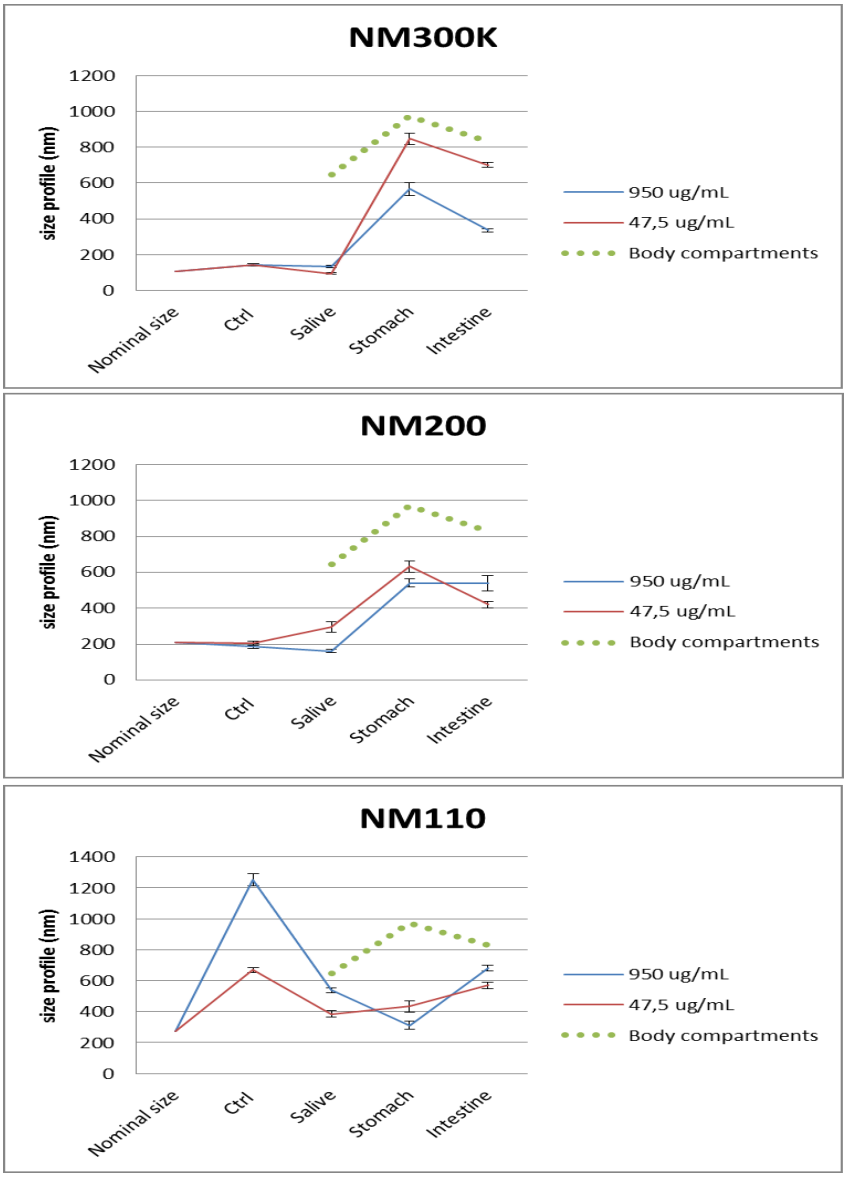


*Figure 32. NPs size profile in the human digestive juices. The plots report the size trend of DLS Peak 1 possibly related to primary NPs (deviation standard bars are relative to 10 runs).Body compartments are the size signals detected for inorganic/organic/protein components of the in vitro human digestive compartments.*

*This project has received funding from the European Union*
*Seventh Framework Programme (FP7/2007-2013)*
*under grant agreement no 310584*

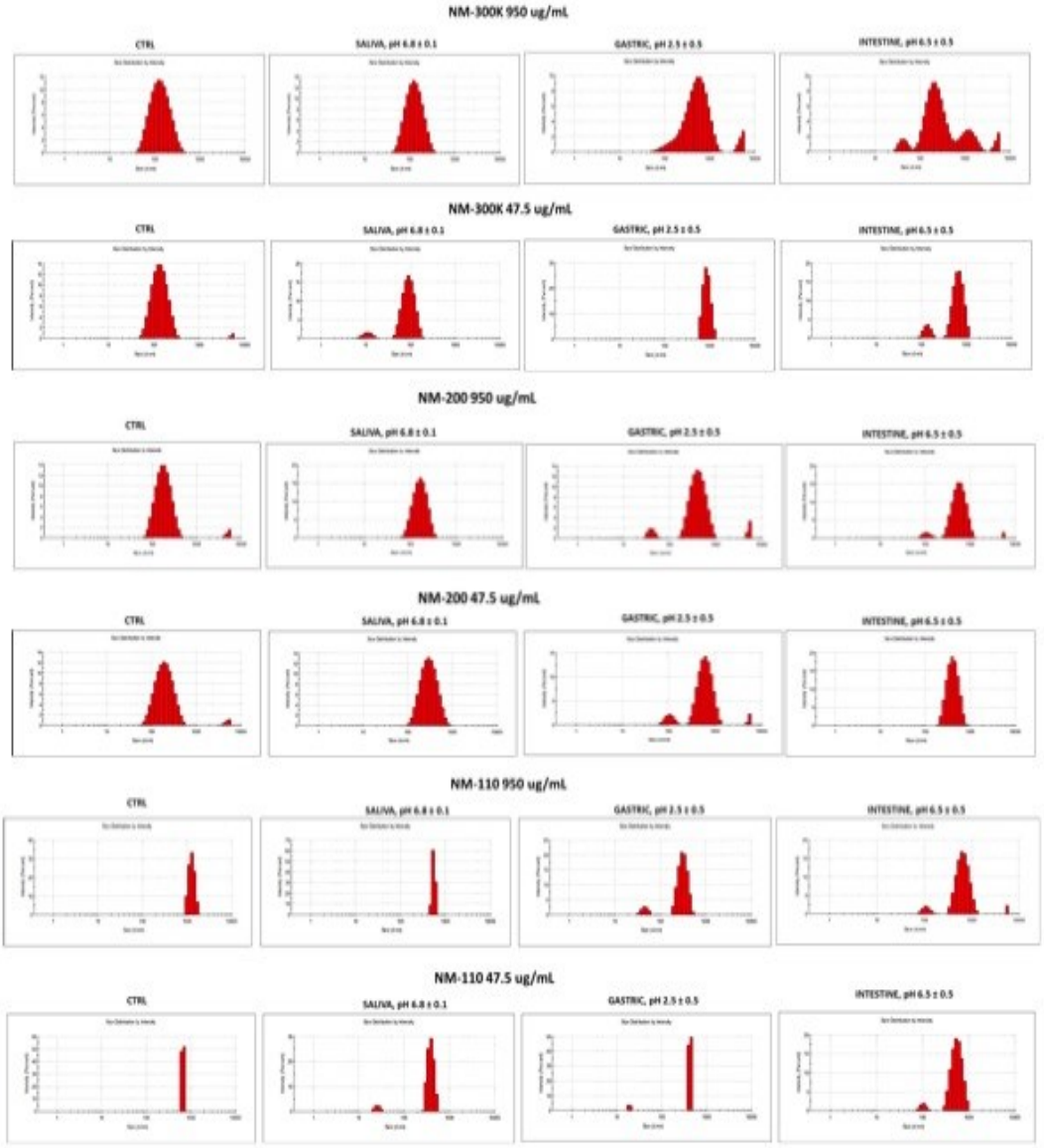


*Figure 33. DLS representative spectra of NM300K, NM200 and NM110 in human digestive compartments*

**Zeta-potential analysis of NPs in human digestive compartments**

The final NPs concentration was 6.8 µg/mL. Measurements were taken after 1 hour of incubation. The general trend observed was a more negative surface charges in saliva and intestine with respect to the Ctrl (NPs dispersed in 0.05% of BSA) and a tendency to charge neutralization in the stomach, possibly due to the increased concentration of hydrogen ions (pH 2,5). This method is under validation in WP2 Task 2.3.

*Table 20. NP charges in the human in vitro digestive compartments.*

| | Nominal Charge (mV) | CTRL charge (mV) | Saliva (mV) | Stomach (mV) | Intestine (mV) |
|---|---|---|---|---|---|
| **NM 300K** | -11.0 | -24.4 | -35.0 | -3.0 | -32.0 |
| **NM 200** | -47.5 | -28.0 | -30.0 | -10.0 | -39.0 |
| **NM 110** | -24.3 | -20.6 | -36.0 | -9.0 | -35.0 |

**TEM representative images of NPs in human digestive compartments**

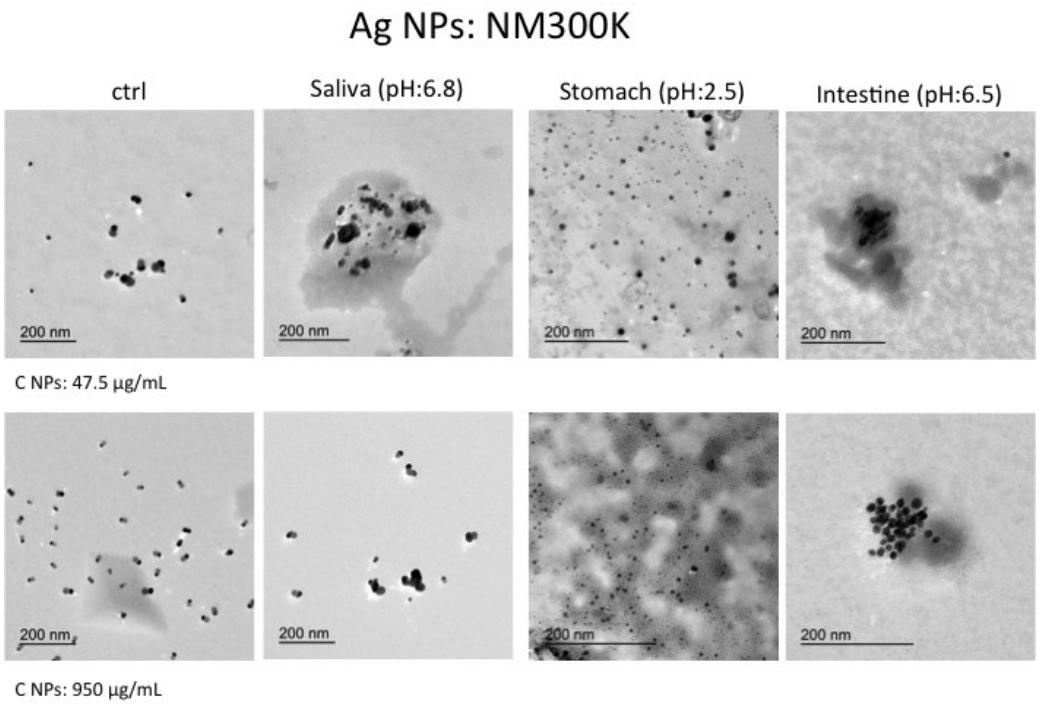


*Figure 34. TEM images show NP dissolution in the stomach and a partial re-aggregation in the intestine-bile compartments.*

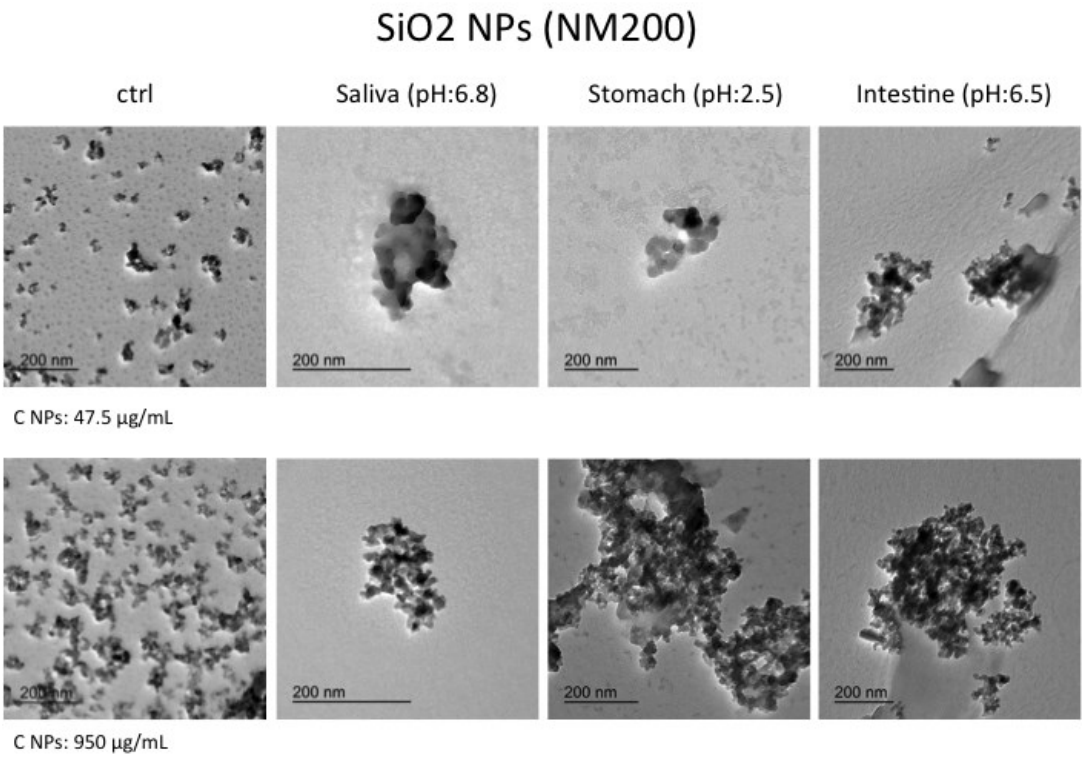


*Figure 35. TEM images show a progressive aggregation of NM200 in the different human digestive compartments.*

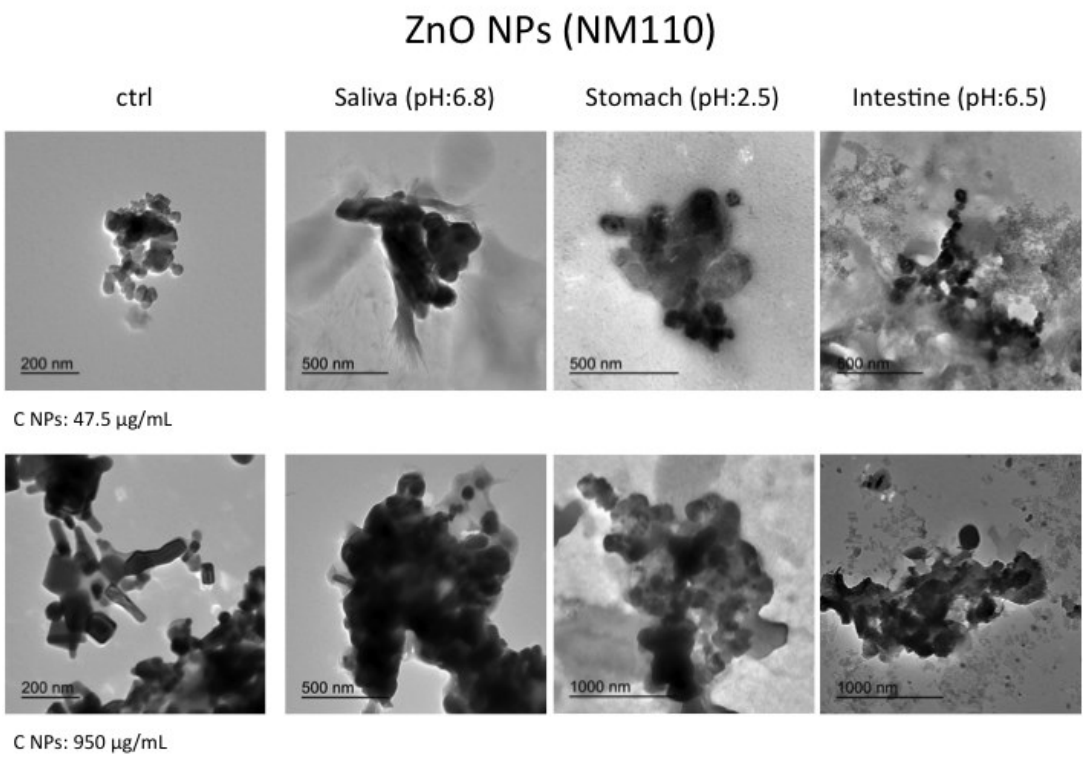


*Figure 36. TEM images show a progressive aggregation of NM110 in the different human digestive compartments.*

### 2.5.6. Conclusion and recommendations

Knowledge of physical-chemical properties of NMs under relevant exposure conditions (as for instance size, surface charge and dissolution) in biological matrices may be informative of the colloidal stability of NMs as well as of their fate in the dispersant medium.

In this Chapter, we applied a combination of techniques such as DLS, zeta potential analysis, TEM and dissolution measurements to monitor key NP physical properties using complex matrices with relevance for exposure. The relative methods are explained in this Chapter and in part validated in the WP2.

We recommend performing the characterization of NPs under relevant exposure conditions in order to provide at least a panel of information relative to size, surface change and dissolution profile of NPs as these parameters are relevant for risk assessment.

Size profile monitoring in complex matrices is challenging by using only DLS so that we recommend a combination of techniques. Results may be influenced by experimental parameters as matrices compositions, filter, techniques used, chemical coating, etc.

Size profile information must be combined with information relative to surface charge and dissolution in the complex matrices so to be able to correlate the in vitro effect to the NP properties.

*In vitro* studies (cell culture based or dissolution studies) should be supported by an accurate physical chemical characterization of NPs to provide a pattern of key properties (such as size, surface charge and dissolution) under relevant exposure conditions and using matrices relevant for exposure. The use (or the creation) of European characterization facilities are recommended also in accordance to similar proposals by other EU projects (*e.g.*, Q-Nano).

## 2.6 Conclusions and recommendations for suitable rapid solubility testing procedures

*In vitro* studies should be supported by an accurate physical chemical characterization of NPs under relevant exposure conditions. Evaluation of the dissolution properties of nanomaterials is one of the key properties that should be evaluated when performing *in vitro* studies. A review on the “state of the art” concerning dissolution identified all possible methods for dissolution measurements. From this review it was concluded that there is currently no universal method to determine nanomaterial solubility. The choice of method will heavily depend on many factors.

Biological media, which are considered complex matrices, complicate evaluation of dissolution due to interactions of the media with the nanomaterials. However, when performing experimental studies, measurement in complex matrices is crucial. In the NANoREG framework the goal of Task 5.2 was to determine the applicability of several solubility measurement methods in complex media and to devise a suitable rapid solubility testing procedure. *In vitro* digestion juices and cell culture media were used as complex media model systems and a selection of NANoREG materials was made.

Several ICP-MS/AES based methods were assessed mostly combined with a separation technique like UF or UC. Ultrafiltration appeared to be a robust technique although interactions of the nanomaterial with the matrix and/or filter are limiting the technique. If these interactions occur, the measurement will result in an underestimation of the “total” amount of dissolved material, as only the free dissolved species are measured. Clearly, in-depth knowledge of the nanomaterial and the matrix is essential when selecting this technique. UC was shown applicable, although the supernatant should always be tested for remnants of materials, as it was shown that not all material could always be properly pelleted. Furthermore, also for this technique in-depth knowledge on the material and the matrix is of importance as ions that have complexed or interacted with matrix compounds could be pelleted as well, again leading to an underestimation of the “total” amount of dissolution. Finally, SP-ICP-MS enables evaluation of the “total” amount of dissolution of nanomaterials in complex media, even when the nanomaterials interact with the matrix. This makes this a very promising technique, but presently the size detection limit is the limiting factor of this technique. Future research is currently focussing on lowering the size detection limits of SP-ICP-MS. AGNES and colorimetry methods are cheaper than ICP-MS/AES based methods and work well with certain metals. However, the choice of materials that work well with this techniques is limiting and complex matrices can interfere with the technique.

Dissolution measurement in a complex matrix appeared to be highly challenging and a single robust, rapid test method for types of materials in all types of matrices could not be developed. Knowledge of physical-chemical properties of the nanomaterials is crucial for selection of the best suitable method and it is recommended to use a combination of techniques. Furthermore, the sonication protocol, pre-analytical processing protocols, and the elemental detection method were shown to affect the measurement results. It is therefore recommended to further standardize these procedures and the protocol to measure solubility must be reported in detail, including all experimental conditions in which the data were collected. Finally, to obtain good quality data, techniques must be validated by conducting appropriate round robin studies and suitable reference materials should be available.

# 3 References


1. R. Tantra *et al.*, Suitability of analytical methods to measure solubility for the purpose of nanoregulation. *Nanotoxicology*, 1-12 (2015).
2. OECD, *Test No. 105: Water Solubility*. (OECD Publishing, 1995).
3. ISO. (2012).
4. European Chemicals Agency, "ECHA-12-G-03-EN. Appendix R7-1 Recommendations for nanomaterials applicable to Chapter R7a Endpoint specific guidance " *Guidance on information requirements and chemical safety assessment* (2012).
5. S. W. Bian, I. A. Mudunkotuwa, T. Rupasinghe, V. H. Grassian, Aggregation and Dissolution of 4 nm ZnO Nanoparticles in Aqueous Environments: Influence of pH, Ionic Strength, Size, and Adsorption of Humic Acid. *Langmuir* **27**, 6059-6068 (2011).
6. R. B. Reed, D. A. Ladner, C. P. Higgins, P. Westerhoff, J. F. Ranville, Solubility of nano-zinc oxide in environmentally and biologically important matricies. *Environmental Toxicology and Chemistry* **31**, 93-99 (2012).
7. Y. Zhang, M. Muhammed, Critical evaluation of thermodynamics of complex formation of metal ions in aqueous solutions VI. Hydrolysis and hydroxo-complexes of Zn2+ at 298.15 K. *Hydrometallurgy* **60**, 215-236 (2001).
8. R. A. Reichle, K. G. McCurdy, L. G. Hepler, Zinc Hydroxide: Solubility Product and Hydroxy-complex Stability Constants from 12.5 - 75 degrees C. *Canadian Journal of Chemistry* **53**, 3841-3845 (1975).
9. A. Degen, M. Kosec, Effect of pH and impurities on the surface charge of zinc oxide in aqueous solution. *J. Eur. Ceram. Soc.* **20**, 667-673 (2000).
10. A. Ivask, S. George, O. Bondarenko, A. Kahru, in *Nano-Antimicrobials,* N. Cioffi, M. Rai, Eds. (Springer Berlin Heidelberg, 2012), chap. 9, pp. 253-290.
11. S. Niyogi, C. M. Wood, Biotic Ligand Model, a Flexible Tool for Developing Site-Specific Water Quality Guidelines for Metals. *Environ. Sci. Technol.* **38**, 6177-6192 (2004).
12. M. E. Pettitt, J. R. Lead, Minimum physicochemical characterisation requirements for nanomaterial regulation. *Environ. Int.* **52**, 41-50 (2013).
13. A. L. Fabricius, L. Duester, B. Meermann, T. A. Ternes, ICP-MS-based characterization of inorganic nanoparticles-sample preparation and off- line fractionation strategies. *Anal. Bioanal. Chem.* **406**, 467-479 (2014).
14. R. Tantra, Boyd, R, Cackett, A, Fry, A T, Gohil, D D, Goldberg. S, Lee, J L S, Minelli, C, Peck, R, Quincey, P, Smith, S, Snowden, J, Spencer, S, Tompkins, J, Wang, J, Yang, L, "Final Report on the physico-chemical characterisation of PROSPEcT engineered nanomaterials.," (National Physical Laboratory, 2012).
15. M. Xu *et al.*, Challenge to assess the toxic contribution of metal cation released from nanomaterials for nanotoxicology–the case of ZnO nanoparticles. *Nanoscale* **5**, 4763-4769 (2013).
16. J. Fabrega *et al.*, Sequestration of Zinc from Zinc Oxide Nanoparticles and Life Cycle Effects in the Sediment Dweller Amphipod Corophium volutator. *Environ. Sci. Technol.* **46**, 1128-1135 (2012).
17. M. Cheryan, Ultrafiltration and Microfiltration Handbook. (1998).
18. J. Liu, J. Katahara, G. Li, S. Coe-Sullivan, R. H. Hurt, Degradation products from consumer nanocomposites: a case study on quantum dot lighting. *Environ. Sci. Technol.* **46**, 3220-3227 (2012).
19. E. Navarro *et al.*, Toxicity of Silver Nanoparticles to Chlamydomonas reinhardtii. *Environ. Sci. Technol.* **42**, 8959-8964 (2008).
20. A. M. El Badawy *et al.*, Surface charge-dependent toxicity of silver nanoparticles. *Environ. Sci. Technol.* **45**, 283-287 (2011).
21. M. Hadioui, S. Leclerc, K. J. Wilkinson, Multimethod quantification of Ag+ release from nanosilver. *Talanta* **105**, 15-19 (2013).
22. G. Cornelis, J. Kirby, D. Beak, D. Chittleborough, A method for determination of retention of silver and cerium oxide manufactured nanoparticles in soils. *Environ. Chem.* **7**, 298-308 (2010).
23. Y. Sivry *et al.*, Behavior and fate of industrial zinc oxide nanoparticles in a carbonate-rich river water. *Chemosphere* **95**, 519-526 (2014).
24. I. A. Mudunkotuwa, T. Rupasinghe, C. M. Wu, V. H. Grassian, Dissolution of ZnO Nanoparticles at Circumneutral pH: A Study of Size Effects in the Presence and Absence of Citric Acid. *Langmuir* **28**, 396-403 (2012).
25. G. Cornelis *et al.*, Solubility and batch retention of CeO2 nanoparticles in soils. *Environ. Sci. Technol.* **45**, 2777-2782 (2011).
26. Z. Wang *et al.*, CuO nanoparticle interaction with human epithelial cells: cellular uptake, location, export, and genotoxicity. *Chemical research in toxicology* **25**, 1512-1521 (2012).

27. M. Pesavento, G. Alberti, R. Biesuz, Analytical methods for determination of free metal ion concentration, labile species fraction and metal complexation capacity of environmental waters: A review. *Anal. Chim. Acta* **631**, 129-141 (2009).
28. C. Fortin, P. G. Campbell, An Ion-Exchange Technique for Free-Metal Ion Measurements (Cd2+ Zn2+): Applications to Complex Aqueous Media. *International Journal of Environmental Analytical Chemistry* **72**, 173-194 (1998).
29. G. Alberti *et al.*, A comparison between the determination of free Pb(II) by two techniques: Absence of gradients and Nernstian equilibrium stripping and resin titration. *Anal. Chim. Acta* **599**, 41-50 (2007).
30. M. Pesavento, R. Biesuz, Simultaneous Determination of Total and Free Metal-Ion Concentration in Solution by Sorption on Iminodiacetate Resin. *Anal. Chem.* **67**, 3558-3563 (1995).
31. M. Hadioui, C. Peyrot, K. J. Wilkinson, Improvements to single particle ICPMS by the online coupling of ion exchange resins. *Anal. Chem.* **86**, 4668-4674 (2014).
32. H. Zhang, W. Davison, Performance-Characteristics of Diffusion Gradients in Thin-Films for the in-Situ Measurement of Trace-Metals in Aqueous-Solution. *Anal. Chem.* **67**, 3391-3400 (1995).
33. W. Davison, H. Zhang, Progress in understanding the use of diffusive gradients in thin films (DGT) – back to basics. *Environ. Chem.* **9**, 1-13 (2012).
34. R. Uribe *et al.*, Contribution of Partially Labile Complexes to the DGT Metal Flux. *Environ. Sci. Technol.* **45**, 5317-5322 (2011).
35. S. Mongin *et al.*, Limits of the Linear Accumulation Regime of DGT Sensors. *Environ. Sci. Technol.* **47**, 10438-10445 (2013).
36. K. Schlich, T. Klawonn, K. Terytze, K. Hund-Rinke, Effects of silver nanoparticles and silver nitrate in the earthworm reproduction test. *Environmental Toxicology and Chemistry* **32**, 181-188 (2013).
37. N. Odzak, D. Kistler, R. Behra, L. Sigg, Dissolution of metal and metal oxide nanoparticles in aqueous media. *Environmental Pollution* **191**, 132-138 (2014).
38. T. Kunniger *et al.*, Release and environmental impact of silver nanoparticles and conventional organic biocides from coated wooden facades. *Environmental Pollution* **184**, 464-471 (2014).
39. P.-E. Buffet *et al.*, Biochemical and behavioural responses of the endobenthic bivalve Scrobicularia plana to silver nanoparticles in seawater and microalgal food. *Ecotoxicology and Environmental Safety* **89**, 117-124 (2013).
40. P. E. Buffet *et al.*, A marine mesocosm study on the environmental fate of silver nanoparticles and toxicity effects on two endobenthic species: The ragworm Hediste diversicolor and the bivalve mollusc Scrobicularia plana. *Sci. Total Environ.* **470-471**, 1151-1159 (2014).
41. P. E. Buffet *et al.*, Behavioural and biochemical responses of two marine invertebrates Scrobicularia plana and Hediste diversicolor to copper oxide nanoparticles. *Chemosphere* **84**, 166-174 (2011).
42. P.-E. Buffet *et al.*, A Mesocosm Study of Fate and Effects of CuO Nanoparticles on Endobenthic Species (Scrobicularia plana, Hediste diversicolor). *Environ. Sci. Technol.* **47**, 1620-1628 (2012).
43. Y. Song, V. Jimenez, C. McKinney, R. Donkers, R. W. Murray, Estimation of size for 1-2 nm nanoparticles using an HPLC electrochemical detector of double layer charging. *Anal. Chem.* **75**, 5088-5096 (2003).
44. T. Baati *et al.*, The prolongation of the lifespan of rats by repeated oral administration of [60]fullerene. *Biomaterials* **33**, 4936-4946 (2012).
45. T. Braun, L. Mark, R. Ohmacht, U. Sharma, Olive oil as a biocompatible solvent for pristine C60. *Fullerenes Nanotubes Carbon Nanostructure* **15**, 311-314 (2007).
46. M. A. Rodriguez, D. W. Armstrong, Separation and analysis of colloidal/nano-particles including microorganisms by capillary electrophoresis: a fundamental review. *Journal of Chromatography B-Analytical Technologies in the Biomedical and Life Sciences* **800**, 7-25 (2004).
47. S. Muralidharan, K. Du, P. Amaratunga, Fundamental characterization of nanoparticles and their interactions by capillary electrophoresis. *Abstr. Pap. Am. Chem. Soc.* **233**, (2007).
48. R. A. Keeney, M. R. Ivanov, A. J. Haes, Nanoparticle synthesis for separation optimization with capillary electrophoresis. *Abstr. Pap. Am. Chem. Soc.* **237**, (2009).
49. W. M. Hwang, C. Y. Lee, D. W. Boo, J. G. Choi, Separation of nanoparticles in different sizes and compositions by capillary electrophoresis. *Bull. Korean Chem. Soc.* **24**, 684-686 (2003).
50. K. H. Lin, T. C. Chu, F. K. Liu, On-line enhancement and separation of nanoparticles using capillary electrophoresis. *J Chromatogr A* **1161**, 314-321 (2007).
51. Y. Xue, H. Y. Yang, Y. T. Yang, Determination of size distribution of nano-particles by capillary zone electrophoresis. *Chin. Chem. Lett.* **16**, 67-70 (2005).
52. N. Li, S. Zeng, L. He, W. Zhong, Probing nanoparticle− protein interaction by capillary electrophoresis. *Anal. Chem.* **82**, 7460-7466 (2010).
53. W. W. Zhong, Capillary electrophoresis in the study of nanoparticle-protein interactions. *Abstr. Pap. Am. Chem. Soc.* **243**, (2012).

54. M. Y. Xie, Z. P. Guo, Y. Chen, Inspection into the Interaction of Bovine Serum Albumin with Gold Nanoparticles by Capillary Electrophoresis. *Chem. J. Chin. Univ.-Chin.* **31**, 2162-2166 (2010).
55. R. Tantra, J. Jarman, in *Journal of Physics: Conference Series*. (IOP Publishing, 2013), vol. 429, pp. 012011.
56. J. C. Giddings, Field-flow fractionation: analysis of macromolecular, colloidal, and particulate materials. *Science* **260**, 1456-1465 (1993).
57. M. Hassellov, J. W. Readman, J. F. Ranville, K. Tiede, Nanoparticle analysis and characterization methodologies in environmental risk assessment of engineered nanoparticles. *Ecotoxicology* **17**, 344-361 (2008).
58. S. K. Williams, J. R. Runyon, A. A. Ashames, Field-flow fractionation: addressing the nano challenge. *Anal. Chem.* **83**, 634-642 (2011).
59. F. von der Kammer *et al.*, Analysis of engineered nanomaterials in complex matrices (environment and biota): general considerations and conceptual case studies. *Environmental Toxicology and Chemistry* **31**, 32-49 (2012).
60. B. Schmidt *et al.*, Quantitative characterization of gold nanoparticles by field-flow fractionation coupled online with light scattering detection and inductively coupled plasma mass spectrometry. *Anal. Chem.* **83**, 2461-2468 (2011).
61. W. Sermsri, P. Jarujamrus, J. Shiowatana, A. Siripinyanond, Flow field-flow fractionation: a versatile approach for size characterization of alpha-tocopherol-induced enlargement of gold nanoparticles. *Anal Bioanal Chem* **396**, 3079-3085 (2010).
62. L. Calzolai, D. Gilliland, C. P. Garcia, F. Rossi, Separation and characterization of gold nanoparticle mixtures by flow-field-flow fractionation. *Journal of chromatography. A* **1218**, 4234-4239 (2011).
63. T. J. Cho, V. A. Hackley, Fractionation and characterization of gold nanoparticles in aqueous solution: asymmetric-flow field flow fractionation with MALS, DLS, and UV-Vis detection. *Anal Bioanal Chem* **398**, 2003-2018 (2010).
64. C. Contado, R. Argazzi, Size sorting of citrate reduced gold nanoparticles by sedimentation field-flow fractionation. *Journal of chromatography. A* **1216**, 9088-9098 (2009).
65. A. R. Poda *et al.*, Characterization of silver nanoparticles using flow-field flow fractionation interfaced to inductively coupled plasma mass spectrometry. *J Chromatogr A* **1218**, 4219-4225 (2011).
66. S. A. Cumberland, J. R. Lead, Particle size distributions of silver nanoparticles at environmentally relevant conditions. *J Chromatogr A* **1216**, 9099-9105 (2009).
67. E. Bolea, J. Jimenez-Lamana, F. Laborda, J. R. Castillo, Size characterization and quantification of silver nanoparticles by asymmetric flow field-flow fractionation coupled with inductively coupled plasma mass spectrometry. *Anal Bioanal Chem* **401**, 2723-2732 (2011).
68. D. M. Mitrano *et al.*, Silver nanoparticle characterization using single particle ICP-MS (SP-ICP-MS) and asymmetrical flow field flow fractionation ICP-MS (AF4-ICP-MS). *J Anal Atom Spectrom* **27**, 1131-1142 (2012).
69. H. Hagendorfer *et al.*, Characterization of Silver Nanoparticle Products Using Asymmetric Flow Field Flow Fractionation with a Multidetector Approach - a Comparison to Transmission Electron Microscopy and Batch Dynamic Light Scattering. *Anal. Chem.* **84**, 2678-2685 (2012).
70. S. Tadjiki, S. Assemi, C. E. Deering, J. M. Veranth, J. D. Miller, Detection, separation, and quantification of unlabeled silica nanoparticles in biological media using sedimentation field-flow fractionation. *J. Nanopart. Res.* **11**, 981-988 (2009).
71. C. Contado, A. Pagnoni, TiO2 in commercial sunscreen lotion: Flow field-flow fractionation and ICP-AES together for size analysis. *Anal. Chem.* **80**, 7594-7608 (2008).
72. C. Contado, A. Pagnoni, TiO2 nano- and micro-particles in commercial foundation creams: Field Flow-Fractionation techniques together with ICP-AES and SQW Voltammetry for their characterization. *Anal Methods-Uk* **2**, 1112-1124 (2010).
73. B. L. Chen, J. P. Selegue, Separation and characterization of single-walled and multiwalled carbon nanotubes by using flow field-flow fractionation. *Anal. Chem.* **74**, 4774-4780 (2002).
74. J. Chun, J. A. Fagan, E. K. Hobbie, B. J. Bauer, Size separation of single-wall carbon nanotubes by flow-field flow fractionation. *Anal. Chem.* **80**, 2514-2523 (2008).
75. H. Q. Peng, N. T. Alvarez, C. Kittrell, R. H. Hauge, H. K. Schmidt, Dielectrophoresis field flow fractionation of single-walled carbon nanotubes. *J. Am. Chem. Soc.* **128**, 8396-8397 (2006).
76. N. Tagmatarchis, A. Zattoni, P. Reschiglian, M. Prato, Separation and purification of functionalised water-soluble rnulti-walled carbon nanotubes by flow field-flow fractionation. *Carbon* **43**, 1984-1989 (2005).
77. J. Kanzer *et al.*, In situ formation of nanoparticles upon dispersion of melt extrudate formulations in aqueous medium assessed by asymmetrical flow field-flow fractionation. *J Pharmaceut Biomed* **53**, 359-365 (2010).

78. M. Y. Thompson, D. Brandes, A. D. Kney, Using electronic conductivity and hardness data for rapid assessment of stream water quality. *Journal of Environmental Management* **104**, 152-157 (2012).
79. A. D. Kney, D. Brandes, A graphical screening method for assessing stream water quality using specific conductivity and alkalinity data. *Journal of Environmental Management* **82**, 519-528 (2007).
80. A. J. Bard, L. R. Faulkner, *Electrochemical methods : fundamentals and applications*. (Wiley, New York, ed. 2nd, 2001), pp. xxi, 833 p.
81. P. L. Bailey, *Analysis with ion-selective electrodes*. Heyden international topics in science (Heyden, London ; Philadelphia, ed. 2nd, 1980), pp. xv, 247 p.
82. J. Wang, *Analytical electrochemistry*. (Wiley-VCH, New York, ed. 2nd, 2000), pp. xvi, 209 p.
83. M. Koch, S. Kiefer, C. Cavelius, A. Kraegeloh, Use of a silver ion selective electrode to assess mechanisms responsible for biological effects of silver nanoparticles. *J. Nanopart. Res.* **14**, (2012).
84. R. Benoit, K. J. Wilkinson, S. Sauvé, Partitioning of silver and chemical speciation of free Ag in soils amended with nanoparticles. *Chemistry Central Journal* **7**, (2013).
85. Y. Umezawa, P. Buhlmann, K. Umezawa, K. Tohda, S. Amemiya, Potentiometric selectivity coefficients of ion-selective electrodes Part I. Inorganic cations - (Technical report). *Pure Appl. Chem.* **72**, 1851-2082 (2000).
86. T. M. Benn, P. Westerhoff, Nanoparticle silver released into water from commercially available sock fabrics. *Environ. Sci. Technol.* **42**, 4133-4139 (2008).
87. G. A. Sotiriou, S. E. Pratsinis, Antibacterial Activity of Nanosilver Ions and Particles. *Environ. Sci. Technol.* **44**, 5649-5654 (2010).
88. G. A. Sotiriou, A. Meyer, J. T. N. Knijnenburg, S. Panke, S. E. Pratsinis, Quantifying the Origin of Released Ag+ Ions from Nanosilver. *Langmuir* **28**, 15929-15936 (2012).
89. A. Kakinen, O. Bondarenko, A. Ivask, A. Kahru, The Effect of Composition of Different Ecotoxicological Test Media on Free and Bioavailable Copper from CuSO4 and CuO Nanoparticles: Comparative Evidence from a Cu-Selective Electrode and a Cu-Biosensor. *Sensors-Basel* **11**, 10502-10521 (2011).
90. C. M. van den Berg, Potentials and potentialities of cathodic stripping voltammetry of trace elements in natural waters. *Anal. Chim. Acta* **250**, 265-276 (1991).
91. J. Galceran, E. Companys, J. Puy, J. Cecilia, J. L. Garces, AGNES: a new electroanalytical technique for measuring free metal ion concentration. *J. Electroanal. Chem.* **566**, 95-109 (2004).
92. J. Galceran *et al.*, The impact of high Zn degrees concentrations on the application of AGNES to determine free Zn(II) concentration. *J. Electroanal. Chem.* **638**, 131-142 (2010).
93. C. Parat *et al.*, Determination of Free Metal Ion Concentrations Using Screen-Printed Electrodes and AGNES with the Charge as Response Function. *Electroanalysis* **23**, 619-627 (2011).
94. C. Kokkinos, A. Economou, P. S. Petrou, S. E. Kakabakos, Microfabricated Tin-Film Electrodes for Protein and DNA Sensing Based on Stripping Voltammetric Detection of Cd(II) Released from Quantum Dots Labels. *Anal. Chem.* **85**, 10686-10691 (2013).
95. M. Szymanski, A. P. F. Turner, R. Porter, Electrochemical Dissolution of Silver Nanoparticles and Its Application in Metalloimmunoassay. *Electroanalysis* **22**, 191-198 (2010).
96. J. R. Morones *et al.*, The bactericidal effect of silver nanoparticles. *Nanotechnology* **16**, 2346-2353 (2005).
97. S. Pinijsuwan, P. Rijiravanich, M. Somasundrum, W. Surareungchai, Sub-femtomolar electrochemical detection of DNA hybridization based on latex/gold nanoparticle-assisted signal amplification. *Anal. Chem.* **80**, 6779-6784 (2008).
98. J. Schmidt, W. Vogelsberger, Dissolution kinetics of titanium dioxide nanoparticles: The observation of an unusual kinetic size effect. *J. Phys. Chem. B* **110**, 3955-3963 (2006).
99. J. Schmidt, W. Vogelsberger, Aqueous Long-Term Solubility of Titania Nanoparticles and Titanium(IV) Hydrolysis in a Sodium Chloride System Studied by Adsorptive Stripping Voltammetry. *Journal of Solution Chemistry* **38**, 1267-1282 (2009).
100. R. F. Domingos *et al.*, Comparison of AGNES (absence of gradients and Nernstian equilibrium stripping) and SSCP (scanned stripping chronopotentiometry) for trace metal speciation analysis. *J. Electroanal. Chem.* **617**, 141-148 (2008).
101. C. A. David *et al.*, Dissolution Kinetics and Solubility of ZnO Nanoparticles Followed by AGNES. *J. Phys. Chem. C* **116**, 11758-11767 (2012).
102. N. Adam *et al.*, The chronic toxicity of ZnO nanoparticles and ZnCl2 to Daphnia magna and the use of different methods to assess nanoparticle aggregation and dissolution. *Nanotoxicology* **8**, 709-717 (2014).
103. Q. Mu *et al.*, Systematic Investigation of the Physicochemical Factors That Contribute to the Toxicity of ZnO Nanoparticles. *Chemical Research in Toxicology* **27**, 558-567 (2014).
104. J. Galceran *et al.*, The impact of electrodic adsorption on Zn, Cd and Pb speciation measurements with AGNES. *J. Electroanal. Chem.* **722–723**, 110-118 (2014).

105. R. F. Domingos, C. Franco, J. P. Pinheiro, Stability of core/shell quantum dots-role of pH and small organic ligands. *Environmental Science and Pollution Research* **20**, 4872-4880 (2013).
106. E. Rotureau, Analysis of metal speciation dynamics in clay minerals dispersion by stripping chronopotentiometry techniques. *Colloid Surf. A-Physicochem. Eng. Asp.* **441**, 291-297 (2014).
107. S. S. Crouch, Douglas A; West, Donald M; Holler, F. James. (1969), chap. 29.
108. A. Vogel, *Vogel's Textbook of Quantitative Inorganic Analysis, Including Elementary Instrumental Analysis*. (1980).
109. C. E. Säbel, J. M. Neureuther, S. Siemann, A spectrophotometric method for the determination of zinc, copper, and cobalt ions in metalloproteins using Zincon. *Analytical biochemistry* **397**, 218-226 (2010).
110. T. Fujita, H. Hamasaki, C. Furukata, M. Nonobe, NEW ENZYMATIC ASSAY OF IRON IN SERUM. *Clinical Chemistry* **40**, 763-767 (1994).
111. *NM-Series of Representative Manufactured Nanomaterials – Zinc Oxide NM-110, NM-111, NM-112, NM-113 Characterisation and Test Item Preparation* (EUR 25066 EN, http://publications.jrc.ec.europa.eu/repository/bitstream/111111111/23031/1/lana25066enn.pdf).
112. R. J. B. Peters *et al.*, Development and validation of single particle ICP-MS for sizing and quantitative determination of nano-silver in chicken meat. *Anal Bioanal Chem* **406**, 3875-3885 (2014).
113. D. M. Mitrano *et al.*, Detecting nanoparticulate silver using single-particle inductively coupled plasma-mass spectrometry. *Environmental Toxicology and Chemistry* **31**, 115-121 (2012).
114. H. E. Pace *et al.*, Determining Transport Efficiency for the Purpose of Counting and Sizing Nanoparticles via Single Particle Inductively Coupled Plasma Mass Spectrometry (vol 83, pg 9361, 2011). *Anal. Chem.* **84**, 4633-4633 (2012).
115. F. Laborda, J. Jimenez-Lamana, E. Bolea, J. R. Castillo, Selective identification, characterization and determination of dissolved silver(I) and silver nanoparticles based on single particle detection by inductively coupled plasma mass spectrometry. *J Anal Atom Spectrom* **26**, 1362-1371 (2011).
116. S. Takenaka, E. Karg, W. Moller, C. Roth, A. Ziesenis, A morphologic study on the fate of ultrafine silver particles: Distribution pattern of phagocytized metallic silver in vitro and in vivo. *Inhal. Toxicol.* **12**, 291-299 (2000).
117. J. L. Tang *et al.*, Silver Nanoparticles Crossing Through and Distribution in the Blood-Brain Barrier In Vitro. *J. Nanosci. Nanotechnol.* **10**, 6313-6317 (2010).
118. H. Bouwmeester *et al.*, Characterization of Translocation of Silver Nanoparticles and Effects on Whole-Genome Gene Expression Using an In Vitro Intestinal Epithelium Coculture Model. *ACS Nano* **5**, 4091-4103 (2011).
119. W. Liu *et al.*, Impact of silver nanoparticles on human cells: Effect of particle size. *Nanotoxicology* **4**, 319-330 (2010).
120. A. M. Alkilany *et al.*, Cellular Uptake and Cytotoxicity of Gold Nanorods: Molecular Origin of Cytotoxicity and Surface Effects. *Small* **5**, 701-708 (2009).
121. M. van der Zande *et al.*, Sub-chronic toxicity study in rats orally exposed to nanostructured silica. *Particle and Fibre Toxicology* **11**, (2014).
122. K. Loeschner *et al.*, Distribution of silver in rats following 28 days of repeated oral exposure to silver nanoparticles or silver acetate. *Particle and Fibre Toxicology* **8**, (2011).
123. J. Liu, R. H. Hurt, Ion release kinetics and particle persistence in aqueous nano-silver colloids. *Environ. Sci. Technol.* **44**, 2169-2175 (2010).
124. J. Y. Liu, D. A. Sonshine, S. Shervani, R. H. Hurt, Controlled Release of Biologically Active Silver from Nanosilver Surfaces. *ACS Nano* **4**, 6903-6913 (2010).
125. Z. M. Xiu, Q. B. Zhang, H. L. Puppala, V. L. Colvin, P. J. J. Alvarez, Negligible Particle-Specific Antibacterial Activity of Silver Nanoparticles. *Nano Lett.* **12**, 4271-4275 (2012).
126. R. Behra *et al.*, Bioavailability of silver nanoparticles and ions: From a chemical and biochemical perspective. *Journal of the Royal Society Interface* **10**, (2013).
127. K. Loza *et al.*, The dissolution and biological effects of silver nanoparticles in biological media. *Journal of Materials Chemistry B* **2**, 1634-1643 (2014).
128. H. B. Ma, P. M. Bertsch, T. C. Glenn, N. J. Kabengi, P. L. Williams, Toxicity of Manufactured Zinc Oxide Nanoparticles in the Nematode Caenorhabditis Elegans. *Environmental Toxicology and Chemistry* **28**, 1324-1330 (2009).
129. S. Kittler, C. Greulich, J. Diendorf, M. Koller, M. Epple, Toxicity of Silver Nanoparticles Increases during Storage Because of Slow Dissolution under Release of Silver Ions. *Chem. Mat.* **22**, 4548-4554 (2010).
130. R. Ma *et al.*, Size-Controlled Dissolution of Organic-Coated Silver Nanoparticles. *Environ. Sci. Technol.* **46**, 752-759 (2012).

131. Y. J. Lee *et al.*, Ion-release kinetics and ecotoxicity effects of silver nanoparticles. *Environmental Toxicology and Chemistry* **31**, 155-159 (2012).
132. E. Farmen *et al.*, Acute and sub-lethal effects in juvenile Atlantic salmon exposed to low µg/L concentrations of Ag nanoparticles. *Aquatic Toxicology* **108**, 78-84 (2012).
133. W. Huang *et al.*, Dissolution and nanoparticle generation behavior of Be-associated materials in synthetic lung fluid using inductively coupled plasma mass spectroscopy and flow field-flow fractionation. *J Chromatogr A* **1218**, 4149-4159 (2011).
134. K. Loeschner *et al.*, Detection and characterization of silver nanoparticles in chicken meat by asymmetric flow field flow fractionation with detection by conventional or single particle ICP-MS. *Anal. Bioanal. Chem.* **405**, 8185-8195 (2013).
135. M. Prach, V. Stone, L. Proudfoot, Zinc oxide nanoparticles and monocytes: Impact of size, charge and solubility on activation status. *Toxicol. Appl. Pharmacol.* **266**, 19-26 (2013).
136. J. Y. Liu, R. H. Hurt, Ion Release Kinetics and Particle Persistence in Aqueous Nano-Silver Colloids. *Environ. Sci. Technol.* **44**, 2169-2175 (2010).
137. M. van der Zande *et al.*, Distribution, Elimination, and Toxicity of Silver Nanoparticles and Silver Ions in Rats after 28-Day Oral Exposure. *ACS Nano* **6**, 7427-7442 (2012).
138. A. P. Walczak *et al.*, Behaviour of silver nanoparticles and silver ions in an in vitro human gastrointestinal digestion model. *Nanotoxicology* **7**, 1198-1210 (2013).
139. A. M. Striegel, A. K. Brewer, Hydrodynamic chromatography. *Annual review of analytical chemistry* **5**, 15-34 (2012).
140. J. W. Robinson, Atomic Absorption Spectroscopy. *Anal. Chem.* **32**, A17-& (1960).
141. J. P. Gustafsson. (2013).
142. G. S. Z. Plumlee, T.L., The Medical Geochemistry of Dusts, Soils, and Other Earth Materials. *Treatise on Geochemistry* **9-9**, 61 (2003).
143. C. Levard, E. M. Hotze, G. V. Lowry, G. E. Brown, Environmental Transformations of Silver Nanoparticles: Impact on Stability and Toxicity. *Environ. Sci. Technol.* **46**, 6900-6914 (2012).
144. J. Masuoka, J. Hegenauer, B. R. Vandyke, P. Saltman, Intrinsic Stoichiometric Equilibrium-Constants for the Binding of Zinc(Ii) and Copper(Ii) to the High-Affinity Site of Serum-Albumin. *J Biol Chem* **268**, 21533-21537 (1993).
145. D. Gleeson, G. M. Murphy, R. H. Dowling, Calcium-Binding by Bile-Acids - Invitro Studies Using a Calcium-Ion Electrode. *J Lipid Res* **31**, 781-791 (1990).
146. X. C. Zhao, R. T. Liu, Y. Teng, X. F. Liu, The interaction between Ag+ and bovine serum albumin: A spectroscopic investigation. *Sci. Total Environ.* **409**, 892-897 (2011).
147. S. P.-M. Janeck J. Scott-Fordsmand, L. Tran, K. Aschberger, S. Sabella, U. Vogel, C. Poland, D. Balharry, T. Fernandes, S. Gottardo, S. Hankin, M.G.J. Hartl, N.B. Hartmann, D. Hristozov, K. Hund-Rinke, H. Johnston, A. Marcomini, O. Panzer, D. Roncato, A.T. Saber, H. Wallin, V. Stone, A unified framework for nanosafety is needed. *NanoToday* **9**, 4 (2014).
148. V. Stone *et al.*, ITS-NANO--prioritising nanosafety research to develop a stakeholder driven intelligent testing strategy. *Part Fibre Toxicol* **11**, 9 (2014).
149. K. A. Dawson, S. Anguissola, I. Lynch, The need for in situ characterisation in nanosafety assessment: funded transnational access via the QNano research infrastructure. *Nanotoxicology* **7**, 346-349 (2013).
150. S. Sabella *et al.*, A general mechanism for intracellular toxicity of metal-containing nanoparticles. *Nanoscale* **6**, 7052-7061 (2014).
151. M. Lundqvist, Stigler, J., Elia, G., Lynch, I., Cedervall, T., Dawson, K. A., Nanoparticle size and surface properties determine the protein corona with possible implications for biological impacts. *Proc. Natl. Acad. Sci. U. S. A.* **105**, 14265-14270 (2008).
152. A. E. Nel *et al.*, Understanding biophysicochemical interactions at the nano-bio interface. *Nat. Mater.* **8**, 543-557 (2009).
153. G. Maiorano *et al.*, Effects of Cell Culture Media on the Dynamic Formation of Protein-Nanoparticle Complexes and Influence on the Cellular Response. *ACS Nano* **4**, 7481-7491 (2010).
154. M. A. Malvindi *et al.*, SiO2 nanoparticles biocompatibility and their potential for gene delivery and silencing. *Nanoscale* **4**, 486-495 (2012).

# 4 List of abbreviations

EC (European Commission)

OECD (Organisation for Economic Co-operation and Development)

ISO (International Organization for Standardization)

REACH (Registration, Evaluation, Authorisation and Restriction of CHemicals)

ECHA (European Chemicals Agency)

BLM (Biotic Ligand Model)

Free Ion Activity Model (FIAM)

Ultrafiltration (UF)

Ion exchange technology (IET),

Diffusion Gradients in Thin Films (DGT)

High Performance Liquid Chromatography (HPLC)

Capillary zone electrophoresis (CZE).

Electroosmotic flow (EOF)

Field Flow Fractionation (FFF).

Asymmetrical flow FFF (AF4)

Multiangle light scattering (MALS)

Inductively coupled plasma mass spectroscopy (ICP-MS)

Optical emission spectrometry (OES)

Ion selective electrodes (ISE) measurement

Absence of gradients and Nernstian equilibrium stripping (AGNES)

Anodic stripping voltammetry (ASV)

Pulse waveform (such as the Differential Pulse mode, DPASV)

Cathodic stripping voltammetry (AdCSV),

Nitroso-PSAP

Atomic Absorption Spectrometry (AAS)

Graphite furnace atomic absorption spectrometry (GF-AAS)

CTRL: sample control

DLS: Dynamic Light Scattering

TEM: Transmission Electron Microscopy

UF-ICPAES: Ultrafiltration - Inductively Coupled Plasma Atomic Emission Spectroscopy

DMEM: Dulbecco's Modified Eagle's Medium

RPMI: Roswell Park Memorial Institute Medium

FBS: Fetal Bovine Serum

NM/NMs: nanomaterial/s

NP/NPs: nanoparticle/s

R.T.: Room Temperature

$R_i$: Refractive index

$R_{abs}$: Adsorption index